DSB clusters impair the efficiency of both homologous recombination and c-NHEJ and initiate Rad52 dependent error prone processing

Inaugural-Dissertation

zur

Erlangung des Doktorgrades

Dr. rer. nat.

der Fakultät für Biologie

an der

Universität Duisburg-Essen

vorgelegt von

Shipra Chaudhary

Jaipur (Rajasthan), INDIA

Februar 2020

Die der vorliegenden Arbeit zugrunde liegenden Experimente wurden am Institut für Medizinische Strahlenbiologie an der Universität Duisburg-Essen, Standort Essen, durchgeführt.

1. Gutachter: Prof. Dr. George Iliakis

2. Gutachter: Prof. Dr. Alexander Schramm

Vorsitzender des Prüfungsausschusses: Prof. Dr. Christian Johannes

Tag der mündlichen Prüfung: May 27th 2020

DOI: 10.17185/duepublico/71869
URN: urn:nbn:de:hbz:464-20200618-074544-7

प्रबिसि नगर कीजे सब काजा।
हृदयँ राखि कौसलपुर राजा।।

"Do all deeds remembering God
you will get success"

-Sunder Kand
Shloka Number 5

"A little more persistence, a little more effort, and what seemed hopeless failure may turn to glorious success".

- Elbert Hubbard

Contents

Contents

Contents

List of Figures

List of figures and tables

List of figures and tables

List of Tables

List of figures and tables

List of Abbreviations

%	percent
°C	Degree Celsius
53BP1	p53 binding protein
Ab	Antibody
ADP	Adenosine diphosphate
alt-EJ	Alternative end joining
ATM	Ataxia-telangiectasia-mutated
ATR	Ataxia-telangiectasia and rad3 related
BER	Base excision repair
B-NHEJ	Backup pathway of non homologous end joining
bp	Base pair
BRCA1	Breast cancer susceptibility protein 1
BRCA2	Breast cancer susceptibility protein 2
BRCT	Breast cancer C-terminal
BSA	Bovine serum albumin
CHO	Chinese hamster ovary
c-NHEJ	Canonical- non-homologous end joining
Cpm	Counts per minute
CSR	Class switch recombination

List of abbreviations

CtIP	C-terminal binding protein interacting protein
DAPI	4',6-diamidino-2-phenylindole
DDR	DNA damage response
D-MEM	Dulbecco's modified eagle's medium
DMSO	Dimethyl sulfoxide
DNA	Deoxyribonucleic acid
DNA-PK	DNA dependent protein kinase
DNA-PKcs	Catalytic subunit of the protein DNA-PK
Ds	Double stranded
DSB	DNA double strand break
e.g.	exempli gratia
EDTA	Ethylene diamine tetraacetic acid
EGFP	Enhanced green fluorescent protein
et al.	et alii (and others)
eV	Electron volt
Exo1	Exonuclease 1
FACS	Fluorescence activated cell sorting
FBS	Fetal bovine serum
FHA	Fork head-associated
G1	Cell cycle phase gap 1

List of abbreviations

G2	Cell cycle phase gap 2
Gy	Gray
H	Histidine
Hr	Hour
HE	Homing endonuclease
HEPES	4-(2-Hydroxyl)-1-piperazineethanesulfonic acid
HRR	Homologous recombination repair
HST	Histogram
IR	Ionizing radiation
IR/DR	Inverted/directed repeat
IRIF	Ionizing radiation induced foci
K	Lysine
kDa	Kilo-dalton
keV	Kilo electron volt
LET	Linear energy transfer
LIF	Leica image format
Lig	Ligase
LMDS	Locally multiply damaged site
LSB	Low salt buffer
Mab	Monoclonal antibody
MDC1	Mediator of the mammalian DNA damage

List of abbreviations

	Checkpoint
MEM	Minimal essential medium
MI	Mitotic index
Min	Minute
MMEJ	Microhomology-mediated end joining
MMR	DNA mismatch repair
M-phase	Cell cycle phase mitosis
MQ	Milli-Q
MRE11	Meiotic recombination 11
MRN complex	Mre11-Rad50-Nbs1 complex
MW	Molecular weight
NBS1	Nijmegen breakage syndrome1
NE	Nuclear extract
ng	Nanogram
NHEJ	Non-homologous end joining
NLS	Nuclear localization signal
Pab	Polyclonal antibody
PAGE	Polyacrylamide gel electrophoresis
PARP	Poly (ADP-ribose) polymerase
PBS	Phosphate buffer saline
PBST	PBS with Tween 20

List of abbreviations

PCC	Premature chromosome condensation
PFGE	Pulsed field gel electrophoresis
PI	Propidium iodide
PIKK	Phosphoinositide-3-kinase-related protein kinase
PMSF	Phenylmethylsulfonylfluoride
PMT	Photomultipliers
RAP80	Receptor-associated protein 80
RBE	Relative biological effectiveness
RE	Restriction endonuclease
RNAse	Ribonuclease
RNF8/168	Ring finger protein 8/168
ROS	Reactive oxygen species
RPA	Replication protein factor A
rpm	Revolution per minute
RS	Recombination signal
RT	Room temperature
SB	Sleeping beauty
SDS	Sodium dodecyl sulfate
SDSA	Synthesis dependent strand annealing
Sec	Second

List of abbreviations

Ser	Serine
SMC	Structural maintenance of chromosome
S-Phase	Cell cycle synthesis phase
ss	Single stranded
SSA	Single strand annealing
SSB	Single strand break
SUMO	Small ubiquitin-like modifier
Thr	Threonine
Tris	Tris-(hydroxymethyl)-aminomethane
Tyr	Tyrosine
Ub	Ubiquitylation
UIM	Ubiquitin interacting motive
UV	Ultraviolet light
V(D)J	Variable (diversity) joining
WCE	Whole cell extract
wt	Wild type
XRCC	X-ray cross complementation group
ɣ-H2AX	Phosphorylated form of histone H2AX at Ser- 139

List of abbreviations

Introduction

1.1 DNA double strand breaks (DSBs)

When both ends of the DNA double helix structure are severed, it results in the formation of a double-strand DNA break (DSB). DSBs arise from exogenous sources that include ionizing radiation and topoisomerase II inhibitors, and endogenous sources, which include V(D)J recombination and class switch recombination. If left unrepaired, DSBs induced from exogenous sources like ionizing radiation pose a major threat to cellular homeostasis. They are particularly deleterious as their mis-repair can promote potentially lethal chromosomal rearrangements [1]. DSBs arise when both strands of the DNA are broken through cleavage of phosphodiester bonds in the backbone of the DNA [2, 3]. They might also occur when two single strand breaks (SSBs) arise in close proximity of each other (within 10 bp), or when the DNA-replication apparatus encounters a SSB. While DSBs do not occur as frequently as the other DNA lesions, they are difficult to repair and are extremely toxic [2]. If left unrepaired, DSBs may also lead to cell death. That is why it is very crucial for the cells to rapidly detect the presence of these cytotoxic lesions, and repair them through proper signaling events and repair pathways. Indeed, DSBs elicit a cascade of highly coordinated transductive events collectively termed as DDR, integrating homologous recombination (HRR), classical non-homologous end joining (c-NHEJ), alternative end joining (alt-EJ), and single strand annealing (SSA) with signaling, cell cycle arrest, and/or apoptosis (Figure 1) [3, 4].

DNA-DSBs can arise, either by exogenous DNA-damaging agents like ionizing radiation (IR), restriction endonuclease-like enzymes and chemotherapeutic agents (radiomimetic drugs, topoisomerase inhibitors), or by endogenous physiological cellular processes, such as generation of reactive oxygen species (ROS), V(D)J recombination and class switch recombination (CSR) during maturation of B- and T-lymphocytes, as well as during DNA replication.

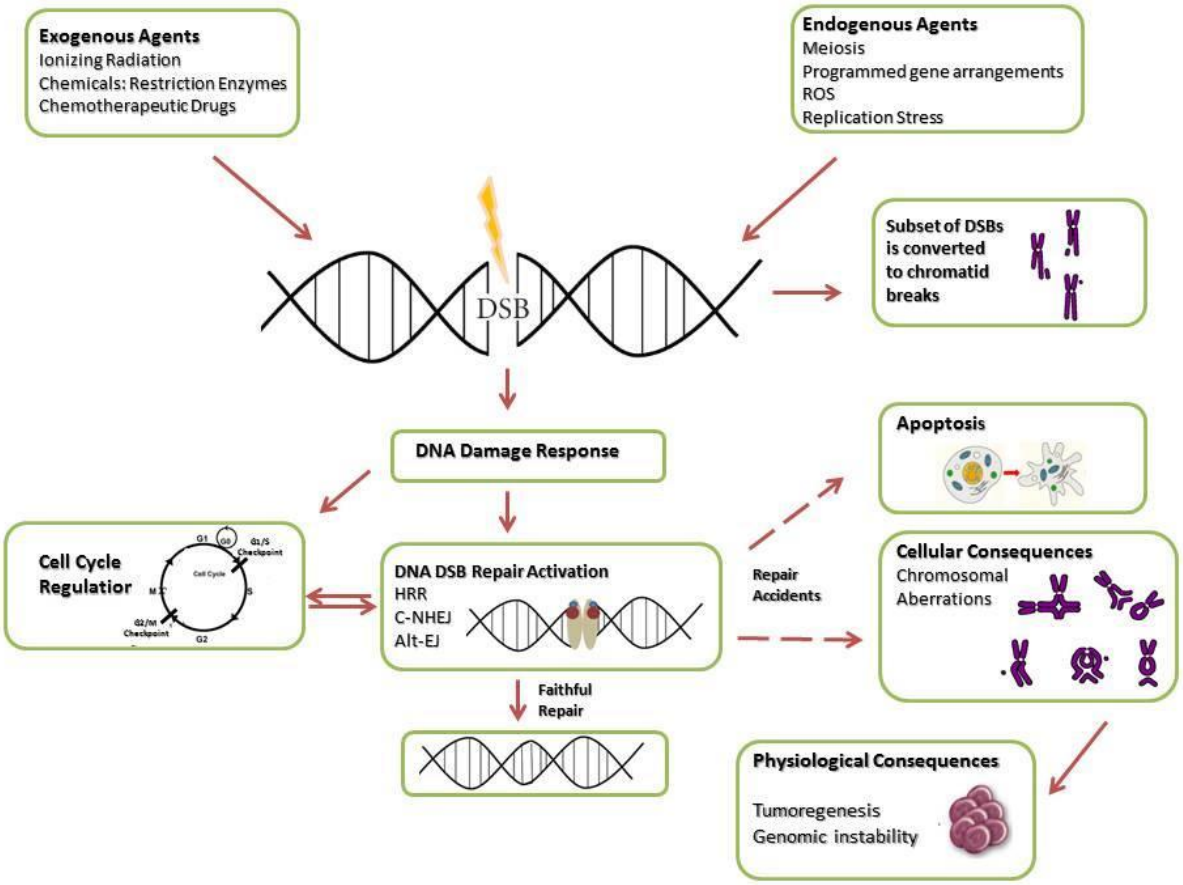

Figure 1: *DNA damage induction and its consequences.*

Upon induction of DDR the cell cycle regulation is altered via activation of G1/M or G2/S checkpoints, as well as the activation of DSB repair pathways. A small proportion of DSBs are converted into chromatid breaks. Following unfaithful repair due to any kind of error in repair pathways, repair accidents may occur that may result in cellular apoptosis or formation of chromosomal aberrations. Physiological consequences of chromosomal aberrations contribute to genomic instability and tumorigenesis.

1.1.1.DSBs – Physiologically Induced

Even though DSBs are considered to be extremely consequential for the cell, still certain important biological processes employ DSBs in programmed and well-controlled manner. Physiologically induced DSBs function either as Genomic Shufflers (in genetic recombination) or act as Genomic Sculptors (to manipulate DNA topology). As genomic shufflers DSBs result in genomic diversification in lymphocytes and germ cells [3]. As far as their role in the manipulation of DNA topology is concerned DSBs act as genomic "sculptors" that result in

manipulation of DNA structure that aids in DNA replication and transcription [3], the regulation of gene expression and which also results in alterations of chromatin state [3]. Refer to Figure 2 for schematic summarization for diverse roles of physiologically induced DSBs.

V(D)J - recombination

V(D)J recombination is initiated in progenitor B lymphocytes by recombinase-activating 1 (RAG-1) and RAG-2 proteins, which introduce DNA double-strand breaks (DSBs) precisely between target recombination signal sequences (RSSs) and flanking V, D or J coding segments [5]. B and T lymphocytes recognize foreign antigen through specialized receptors: the immunoglobulins and the T cell receptor (TCR), respectively. These receptors have antigen-recognition regions that are composed of variable (V), diversity (D), and joining (J) gene segments that undergo somatic rearrangement prior to their expression by a mechanism known as V(D)J recombination [6]. Joining of coding sequences to the target regions is carried out by NHEJ proteins [6]. Three of these proteins are sub-units of the DNA-dependent protein kinase (DNA-PK), which is comprised of the Ku70 and Ku80 DNA end-binding complex (Ku), and the catalytic subunit (DNA-PKcs) of DNA-PK. Two additional NHEJ proteins, DNA ligase IV (Lig4) and XRCC4 are involved in the ligation step.

Class switch recombination CSR

Class switch recombination (CSR) results in alteration of the heavy chain on immunoglobulins [7]. It is a process by which proliferating B cells rearrange the constant region genes in the immunoglobulin heavy chain locus to switch from expressing one class of immunoglobulin (such as IgM) to another (such as IgG). This produces an antibody with different effector properties, without altering its antigen specificity [8].

Meiotic Recombination

Meiosis takes place in sexually reproducing organisms to generate haploid gametes. One round of DNA replication is followed by two successive rounds of cell division resulting in cells with half the amount of genome. Meiotic Recombination involves the formation and repair of DSBs that are induced in programmed manner to allow exchange of genetic information between

homologous paternal and maternal chromosome pairs. DSBs in meiotic recombination are generated by SPO-1 [8].

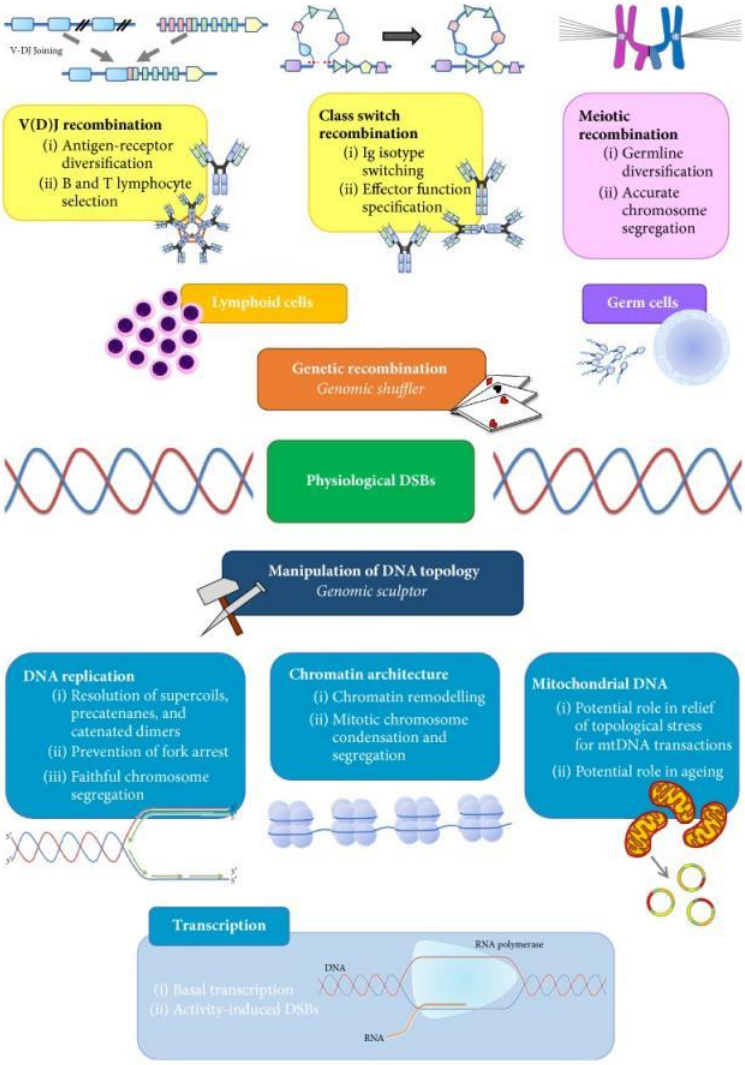

Figure 2: *Schematic representation of the diverse roles of physiological DSBs in biological processes.*

For detailed description refer to section above [figure taken from Farhaan A. Khan, Syed O. Ali (2017) [9]]

Introduction

1.1.2.Ionizing radiation (IR) and IR induced DSBs:

IR is extensively used in the clinics for diagnostic and therapeutic purposes. IR is also used increasingly in scientific research due to its property to induce random DSBs. This is especially interesting as it provides a perfect platform to investigate DNA damage response mechanisms.

IR deposits its energy along the particle tracks in the matter it traverses producing numerous ionizations and a few highly consequential ionization clusters. It is therefore up to 1000 times more effective at cell killing compared to other types of DNA damaging agents that give rise to randomly distributed radicals. The dose of radiation deposited to biological material is defined in terms of the amount of energy absorbed per unit mass. 1 Gy is equivalent to 1 J/kg. DNA damage by IR is formed either as direct action with the particle- tracks hitting the DNA, or as indirect action with the particle tracks hitting other molecules to generate radicals, which in-turn hit the DNA by radical diffusion at around 4 nm. Indirect action is mainly mediated by the radiolysis of water.

The biological effects of IR are therefore the end product of the initial physical events, comprising of ionizations and excitations of atoms and molecules along the tracks of the ionizing particles. The interaction of IR with matter is largely determined by the physical properties of IR, which in-turn cause the observed biological effects.

Physical properties of IR

From a physical point of view “IR is defined as energy, deposited to matter that is large enough to eject one or more orbital electrons from an atom, leaving an electrically charged atom behind”. IR could be sub-classified as electromagnetic radiation or particulate radiation. Gamma-rays and X-rays are examples of electromagnetic radiation; particulate radiation comprises all elementary particles (electrons, protons, neutrons) and nuclei up to heavy ions.

X-rays are produced by electrical devices that accelerate electrons to a high speed and which are abruptly stopped in the anode to produce photons. X-rays, if compared to ordinary light, have shorter wavelength, greater frequency and higher photon energy. They fall into a higher segment of the electromagnetic spectrum [10]. In short “X-rays can penetrate through materials that ordinary light waves can't because they're much more energetic”.

Depending on the energy of photons and the matter they pass through, X-rays can have two different modes of absorption:

- **Compton process (for higher energy x-rays)**
- **Photoelectric process (for lower energy x-rays)**

In **Compton process** the higher energy photon interacts with the loosely bound electrons in the outermost shell. Through this interaction a part of photon energy is transferred to the electron as kinetic energy which then proceeds further to ionize other atoms. The loss of photon energy results in photon continuing further in a different direction i.e. it becomes scattered. The overall process breaks chemical bonds leaving ionized atoms behind.

In case of lower energy X-rays the **photoelectric process** dominates; the photon interacts with an electron that is strongly bound in the inner shell of the absorbing atom. Photon then transfers its entire energy to this electron, which results in its release from the atom. This released electron is called as photoelectron. In this process the entire photon is absorbed, and this kind of effect is considered as the primary reason for the attenuation of the X-ray beam [10, 11].

Ionization events are not just randomly distributed in the space but, they tend to localize along radiation tracks. Different radiation modalities have different rates at which they deposit their energy to the material through which they travel. The amount of energy that IR deposits to the material it travels through per unit distance is called linear energy transfer (LET) [12, 13]. "LET is the amount of energy deposited by an ionizing particle over the length of its track" [14]. Depending on the value of this parameter a type of radiation can either be **high LET** or **low LET**.

High LET radiation includes particles such as alpha particles (a helium nucleus), which deposit a large amount of energy over a small distance thereby producing more ionizations in the matter they traverse per unit track length. High LET radiation, owing to the higher density of the ionizations it produces, generates more severe damage in biological molecules including the DNA [15, 16].

Low LET radiation comprises of X-rays and gamma rays; they are indirectly ionizing in the sense that their biological effects are mainly elicited by the secondary electrons they generate through Compton scattering or the photo-effect (see above).

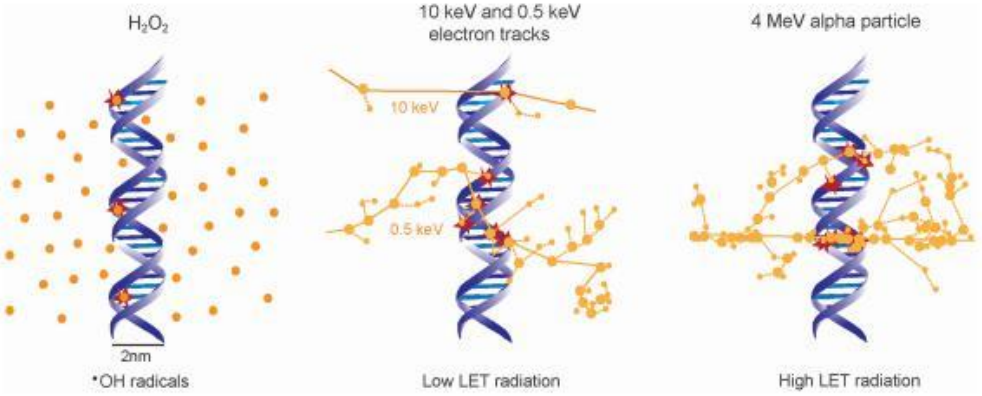

Figure 3: *Distribution of DNA damage induced after exposure to H_2O_2, low and high LET IR.*

H_2O_2 induce evenly distribute DNA damage as the radicals that are produced are evenly distributed in space and time. IR induces ionization along particle tracks and therefore induces clustered damage. With increasing LET the clustering increases. Large dots in Figure 3 represent ionizations and small dots represent excitations along the radiation track. (Schipler and Iliakis 2013) [12].

DSBs – Induced by IR

IR induced DSBs result in decreased cell survival because they might remain unrepaired or be repaired in an erroneous manner. The types of lesions produced via exposure to IR resemble chemical lesions formed by the formation of reactive oxygen species (ROS). In numbers, low LET IR induces around 850 pyrimidine lesions, 450 purine lesions, 1000 SSB and 20-40 DSB per cell per Gy [17]. Daily, owing to various insults inflicted on one's DNA, around 50,000 DNA lesions are produced by ROS [15]. This number is higher than the number of DNA lesions produced by a therapeutic dose of 2 Gy IR. A fundamental question then arises as to what makes Radiation damage more effective in terms of cell killing?

Majority of the lesions induced by IR are confined to one DNA strand and are majorly repaired by base excision repair (BER), nucleotide excision repair (NER) or mismatch repair (MMR) [18]. The most toxic of all lesions arising after radiation exposure is the DSBs. DSBs are induced by the direct disruption of the sugar phosphate backbone in both DNA strands. They can also be induced through the generation of two SSBs in opposite strands in close proximity

(approximately 10 bp apart). Since the second strand is also not intact, DSBs require a more coordinated and complex machinery to be repaired. The repair pathways will be discussed in more detail in later sections in the work. Clustered sites of damage in DNA are a hallmark of radiation induced damage (especially for high LET radiation) and this also includes the generation of DSBs. Such clustered DNA lesions may also comprise sugar and base damages [19, 20]. Moreover only a small number of DSBs (10%–20%), are transformed to chromatid breaks (CBs) and can therefore be visualized via classical cytogenetic approaches [21].

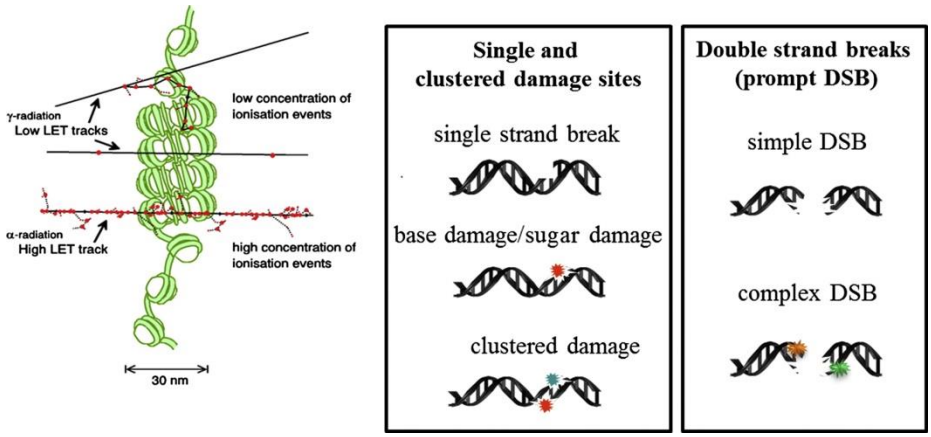

Figure 4: *An overview of the lesions induced by ionizing radiation.*

Ionizing radiation produces a plethora of different lesions including for example single strand breaks, base- or sugar damages and the highly toxic DSB (Figure adapted from (Lomax 2013) [15]).

Complex DNA lesions induced by low LET vs high LET radiation

Complex lesions are a cluster of closely spaced DNA lesions (lying within 10bp of distance) including SSBs, oxidized base lesions and AP sites on same or opposite strand; they are considered a hallmark of high LET radiation [12, 22]. Clustered lesions are resistant to processing by glycosylases and endonucleases and persist in the genome over a longer period of time. They are considered highly mutagenic and result in high number of chromosomal aberrations [23].

Clustering of DNA lesions depends except on LET also on chromatin structure in its vicinity [24, 25] (Figure 4). For low LET radiations, as compared to high LET radiations, clustering occurs less frequently on the DNA molecule and the nucleosomes. For high LET radiation this clustering

is on a much larger scale and more frequent and shows more dependence on chromatin structure [26] (Figure 5).

Various theories have been proposed to describe the differences in the effects on cell survival as a function of the LET of the radiation tested. These theories include the generation of **Locally Multiply Damaged Sites (LMDS)** [27] or **Regionally Multiply Damaged Sites (RMDS)** [28] [29]. According to the LMDS theory, IR ionization clusters in form of blobs and spurs damage the DNA. These structures have dimensions similar to the DNA double helix. With the increase of LET the number of blobs that are created is increased resulting in increased damage complexity and thus in increased cell lethality.

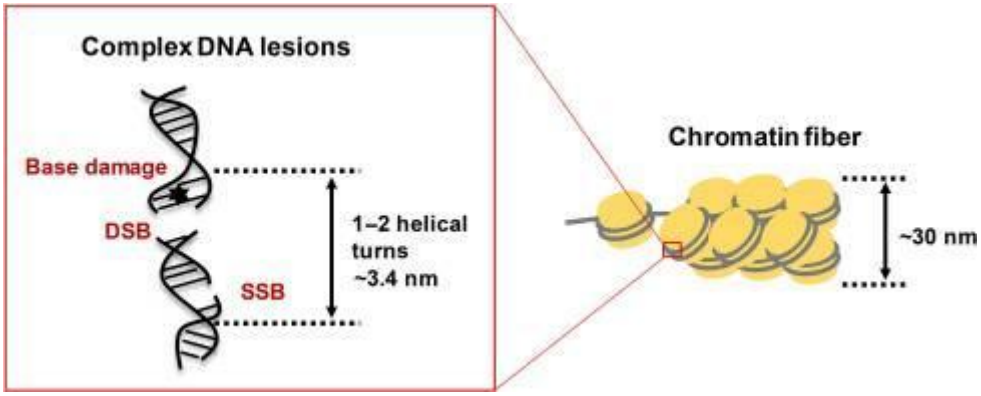

Figure 5 : *Scale diagrams of high LET induced DNA damage.*

The scale diagrams of low and high LET induced simple and complex DNA lesions in the chromatin fiber. IR causes simple DNA lesions or complex DNA lesions, which contain DSBs and SSBs and/or base damage within 1–2 helical turns of the DNA. The scale of a chromatin fiber is ~30 nm. [30]

RMDS theory puts emphasis on the 30-nm chromatin fiber that serves as the target for ionizing particles. Experiments showed a linear increase in the numbers of DNA fragments formed with increasing LET in the size range of 0.1-2.0 kb. For high LET radiation, a substantial fraction of DNA fragments in a given size range, 20-90% of DSBs were accompanied by one additional DSB [28].

Differences between low LET and high LET induced DNA damage reflects different levels of structural organization of the DNA as follows:

Introduction

1. Clustering of damage at the level of the DNA helix, or in higher-order DNA structures such as nucleosomes (theory of Multiple damaged sites or (MDS) [31];
2. Spatial orientation of separate points of damage such as across a chromatin fiber, or between adjacent chromatids [32];
3. The simultaneous induction (in <10-12 s) of the overall burden of damage to the cell nucleus, such as the ~200 DNA single-strand breaks (SSB) and ~20 DSB from the traversal of a single α-particle.

From various works that have been done in the past it has been revealed that a high proportion of the DSBs that are generated, have additional associated damages, such as base damage and additional strand breaks within the same very short segment of DNA [33]. This clustered damage at the DNA level is a feature of virtually all different ionizing radiations, although its frequency and severity depend on the radiation quality (high or low LET) (Figure 4, Figure 5).

Cell lethality in relation to complex lesions

Complexity of lesions, along with their distribution and position in chromatin, influences DNA repair. Protein levels of repair enzymes and accessibility of the damaged site also play an important role in DNA repair. The increased propensity towards mis-repair or no repair plays a critical role in the formation of chromosomal aberrations and the decreased clonogenic cell survival. One of the suggested models for decreased clonogenic survival suggests a “paired" DSB mechanism. Here it is hypothesized that potentially lethal damages (PLD) are produced when IR results in the production of two DSBs along a single track separated at relatively large distances [34]. This model shows consistency with the dependence of cell lethality on linear energy transfer (LET).

One more model based on Poisson distribution has been proposed that speculates about the induction of DSBs from the elution of DNA from residual nuclear structures. According to this model elution of DNA fragment from nucleoids could occur only if two or more DSBs are induced within a single looped domain. Multiple DSBs within these structures allows release of the segment of non-matrix-bound DNA which is precisely bordered by two DSBs, thus allowing its elution [34-36].

1.1.3.Chemically induced DSBs

Restriction Enzymes:

Restriction enzymes (RE) are originally described as a part of the defense mechanism of prokaryotic organisms like bacteria and archaea that provides protection against invading genomic DNA (bacteriophage). In prokaryotes, the invading foreign DNA is disrupted by RE that generates either blunt or staggered DSB ends. In all the cases 5' phosphate and 3' OH are retained on both the strands. RE in molecular biology are used also to mimic and model the clastogenic effects of IR. The major advantage of using RE in the experimental scenario is that it induces DSBs with specific end-structures. On the other hand radiation induces several types of DNA lesions that range from SSBs, DSBs to base-damage, inter-strand cross-links and DNA-protein cross-links. Thus, in the absence of IR, treatment with RE produces DSB of specific types at specific base recognition sequences in DNA [37].

Based on their enzymatic properties there are four types of RE. The most frequently applied RE in molecular biology are type II RE. These are homodimers and recognize a 4-8 bp palindromic DNA sequence. Cleavage of these palindromic sites results in blunt ends or in ends with 5' or 3' overhanging segments [38]. Homing endonucleases (HEs) are a set of endonucleases that are encoded as freestanding genes within introns. They might also exist as fusion products with host proteins or as inteins [39]. They catalyze the hydrolysis of genomic DNA within the host cells at very few specifically coded locations. When the repair of the host DNA occurs, the gene encoding HE also gets copied in the cleavage site, hence increasing allele frequency by transmitting their genes horizontally within a host population,

HE recognition sites are 18bp long and are extremely rare. They occur once in every $7x10^{10}$ of random sequence [40]. They bind to long DNA targets despite having a small size (less than 40kDa) and this ensures a high specificity and low toxicity associated with excessive cleavage of a host genome [41].

In this thesis, the major focus will be on I-SceI (Figure 6) HE; it is used as a tool to study DSB repair. It originates from the mitochondria of *Saccharomyces cerevisiae* with an 18 bp non-

palindromic recognition sequence. I-SceI recognition sites (Figure 7) are not present in the human genome [42] and have to be inserted in the genome for I-SceI based studies. The enzymatic properties of I-SceI meganuclease/endonuclease make it a potent tool that is extensively used to generate DSBs in a controlled manner at designated sites where the I-SceI recognition sites are artificially inserted.

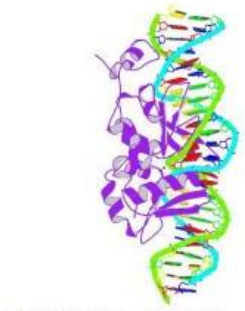

Figure 6: *I-SceI bound to DNA* (taken from 1R7M protein bank) [43]

Various fluorescence based reporter assays have been developed allowing functional analysis of specific repair pathways after site specific induction of DSBs by I-SceI. These reporter assays are based on the fluorescence restoration of different fluorescent proteins, after accurate restitution of the gene cassettes, encoding these proteins. DSBs are either generated by transient transfection of I-SceI expressing vectors, or by a controlled translocation of constitutively expressed I-SceI from the cytoplasm into the nucleus. To measure HRR in the living cells a recombinational reporter system termed as direct repeat green fluorescent protein (DR-GFP) assay is widely used. In this system a chromosomally integrated construct harbors the I-SceI recognition site in a way that disrupts the GFP gene ORF. A truncated GFP gene fragment with the correct ORF sequence has been placed downstream in the construct. Repair of the cleaved I-SceI site by HRR using the downstream fragment gives rise to a functional GFP gene and GFP fluorescence can be measured by flow cytometry. GFP-based chromosomal reporters have been developed to measure c-NHEJ as well. In this system two I-SceI sites flank an intervening sequence that separates the promoter from the GFP coding cassette. Simultaneous cleavage of both the sites leads to the loss of the intervening sequence resulting in GFP expression upon successful rejoining of the two nearby I-SceI-induced DSBs. Bindra et al. have developed an assay to measure mutagenic non-homologous end-joining (alt-NHEJ, termed here mut-NHEJ) repair combined with a homologous recombination (HRR) assay enabling the simultaneous monitoring of both pathways in living cells[42, 44].

Introduction

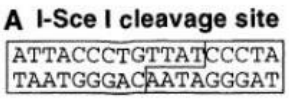

Figure 7: *I-SceI recognition cleavage site* [45]

1.2 Types of DSBs based on their complexity

"Although the DNA double-strand break (DSB) is defined as a rupture in the double-stranded DNA molecule that can occur without chemical modification in any of the constituent building blocks, it is recognized that this form is restricted to enzyme induced DSBs"[12]. DSBs generated by IR or other exogenous agents (physical and chemical) can include at the break site different base lesions. The nature and number of such chemical alterations define the complexity of the DSB and are generally considered to be the determinants for repair pathway choice. As the pathways engaged in DSB processing show distinct and frequently inherent propensities for errors, pathway choice defines the error-levels cells opt to accept [12]. In the current section the classification of DSBs on the basis of increasing complexity is discussed and is extensively reviewed in the review article from Schipler and Iliakis; 2013 [12]

Type 1 (T1) DSBs: the simplest form

These are considered as the simplest form of DSBs that are generated by restriction endonucleases. As described above, RE-induced DSBs retain a 5' phosphate and 3'OH groups at both strand ends. Blunt ends, length of the protruding ends, or also the type of ends i.e. 3' or 5' affects the processing of DSBs. DSBs with protruding overlapping ends are easier to repair than the ones with blunt ends [12].

Type 2 (T2), DSBs: complexity deriving from modified ends

In contrast to RE, type 2 DSBs are generated by physical or chemical agents (IR or radiomimetic drugs). IR generated DSBs differ from those induced by RE because they frequently comprise a 3' damaged sugar in the form of phosphor-glycolate and a 5' OH. Therefore, the T2-DSBs are categorized as simple DSBs where the complexity derives from modified ends.

This form of ends necessitates end-processing as a step before ligation. In contrast to RE, IR induces a wide spectrum of lesions through the formation of free radicals resulting in oxidative damage, including sugar and base damages each of which outnumbers DSBs by approx. 20:1 [12]. Certain forms of sugar damage disrupt the phosphodiester backbone of the DNA molecule resulting in formation of SSBs. So, IR-induced DSBs can be classified as a more complex type of breaks which are distinguished from RE induced type 1 DSBs. As IR induced DSBs are generated by coincidence of two SSBs (<10 bp apart); blunt ends, or ends with protruding single strands similar to those described for RE can be generated [12].

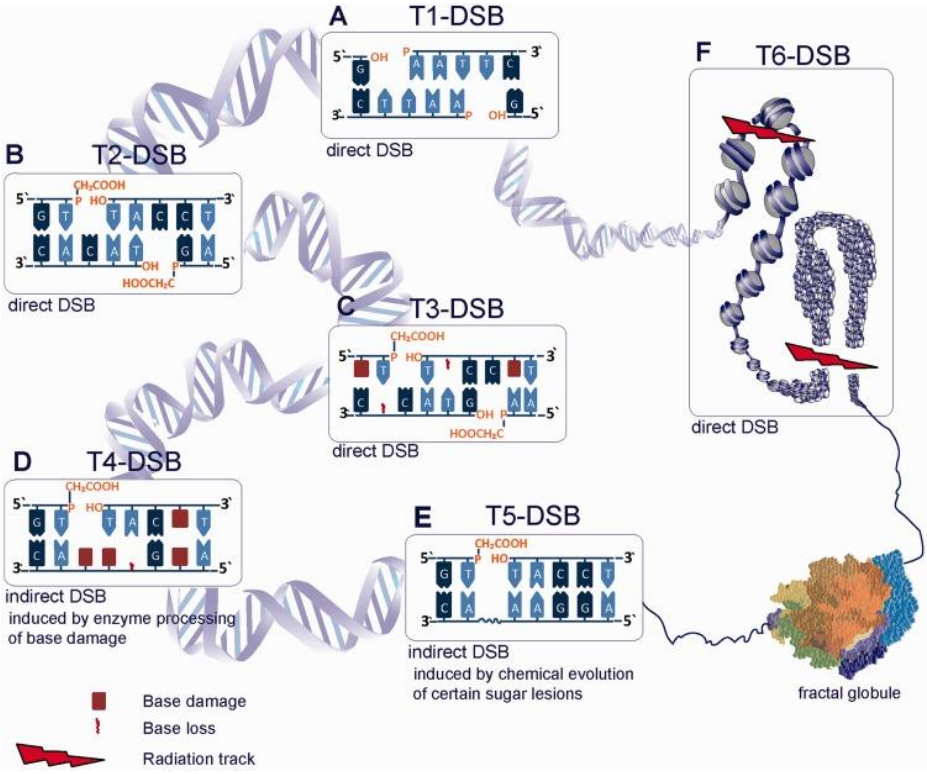

Figure 8: *Diagram showing different types of DSBs. Types 1-6.*

A: T1-DSBs are direct DSBs induced by RE with a 5` phosphate and a 3` OH group. B: T2-DSBs are induced by IR and frequently comprise a 3` phosphoglycolate and a 5'-OH. C: T3-DSB comprises also other types of lesions like base damages or base loss in close proximity to the DSB. D: T4-DSB represents a non-DSB cluster that can convert to DSBs by subsequent enzyme processing. E: T5-DSBs represent a non-DSB cluster that can convert to DSBs by chemical processing. F: T6-DSBs are composed of clustered DSBs. Two conditions are shown. On top left of the inset a single radiation track induces two DSBs in the linker regions of a nucleosome leading to nucleosomal loss. On the right, packaged nucleosomes are illustrated forming a loop that is also hit by a single radiation track that can

Introduction

lead to chromatin destabilization. In the right lower corner, chromatin compacted as a fractal globule is illustrated (Schipler and Iliakis 2013) [12].

Type 3 (T3), DSBs: complexity deriving from the presence of DNA lesions in the vicinity of the break

The presence of two or more DNA lesions on opposing strands within one helical turn of the DNA constitutes clustered DNA damage that potentially has more severe biological consequences than the T2-DSBs described above. These clustered lesions are classified as Type 3 DSBs. IR, both low LET and high LET, damage DNA along their particle tracks. There might be more than one or two lesions per helical turn of DNA. These multiple damaged sites are referred to as clustered damage sites (CDS). The prevailing hypothesis is that high-LET modalities induce increased number of clustered lesions, resulting in higher RBE (relative biological effectiveness). RBE is defined as "The ratio of physical doses between two different types of radiation required to produce the same biological endpoint" [46]. The simultaneous presence of DSBs and other forms of DNA damage within a clustered damage site generates higher complexity, classified as T3 DSB. In T3-DSBs cellular repair may be compromised and two or more repair pathways may work simultaneously to process lesions in close proximity [12].

Type 4 (T4) DSBs: indirect form, arising from base damage processing within a non–DSB-CDS

"In addition to DNA damage clusters that generate DSBs right at the outset, IR also generates clusters of base damage, possibly including SSBs, which do not form DSBs immediately (non-DSB clusters). DSBs can subsequently form through the processing of a base lesion opposite an unrepaired SSB, or through the parallel processing on both DNA strands of base damage" [12]. Experimental evidence shows that this form of clustered DNA damage outnumbers T2/T3-DSBs after exposure to low-LET radiation by nearly 4:1 [47] [12] "DSBs formed by the simultaneous disruption of the phosphodiester bond at base damage sites in opposite strands, or with the combination of BER opposing an SSB, form yet another level of complexity that integrates the parameter time in the induction process and is termed therefore T4-DSB" [47] . Although BER and SSB repair pathways may remove individual lesions within non-DSB clusters, repair

attempts may also fail. Composition, spacing and polarity of the lesions comprising the non-DSB cluster determine the reparability of the lesion [48]. Altered nuclease activity and/or reduced glycosylase activity may result in unrepaired non-DSB clusters. Post irradiation repair of sugar and base residues might also result in delayed formation of DSBs [12, 49].

T5-DSBs: Indirect DSBs induced by chemical processing

IR besides generating sugar damage within clustered damage sites promptly (prompt DSBs) also generates breaks after temperature dependent chemical processing (delayed DSBs). These thermally labile sugar lesions form radiation-induced labile sites which include diverse forms of sugar damage, abasic sites and forms of base damage affecting sugar stability. Chemical processing of such lesions can generate additional DSBs [12].

T6-DSBs: Clustered DSBs

Nucleosomal instability may arise due to multiple DSBs occurring in close proximity and may result in deletions and exchange type aberrations. Nucleosomes are the fundamental units of chromatin organization. A nucleosome core particle consists of approximately 146 bps of DNA wrapped in 1.67 left handed super-helical turns around an octameric histone core. Core particles are connected by stretches of "linker DNA", which are about 80 bp long. It is considered that the nucleosome filament is packed as a chromatin fiber of approximately 30 nm length. 6-7 nucleosomes exist per 10 nm length of fiber. DSB clusters at 100-1000 bp distances destabilize chromatin and this, results in the loss of the fragment (Figure 9). The structure of chromatin dictates the process of destabilization, as well as the linear distance between interacting DNA damages. Thus, DSBs Mbp apart can interact. These forms of interactions are naturally occurring in a cell during the process of V(D)J and class-switch recombination [50].

T6-DSBs represent a form of highly local chromothripsis. Chromothripsis can result in tens to hundreds of chromosomal rearrangements that occur as a consequence of a single event of cellular crisis [51]. Several investigations using mathematical modeling by Monte Carlo Calculations, PFGE and atomic force microscopy (AFM) after high and low LET irradiation describe the potential of clustered DSBs after exposure to IR, particularly high LET IR [12]. Monte Carlo simulations for DSB induction on higher order DNA structures by radiations of

different LET show regional DSB clustering with fragmentation peaks appearing at 85 bp (revolution period about nucleosome) and broader peaks at 1000 bp (one turn around solenoid) [33, 52]. Results obtained after low LET irradiation of pUC19 plasmid DNA (2864 bp) show that 35% of the generated fragments are 0-50 nm in size (bp); this proportion increases to 70% after exposure to high LET argon irradiation. Thus, the generation of short DNA fragments by T6-DSBs points to their high risk potential for severe biological consequences. Yet, to this date a biological system enabling the investigation of clustered DSBs does not exist.

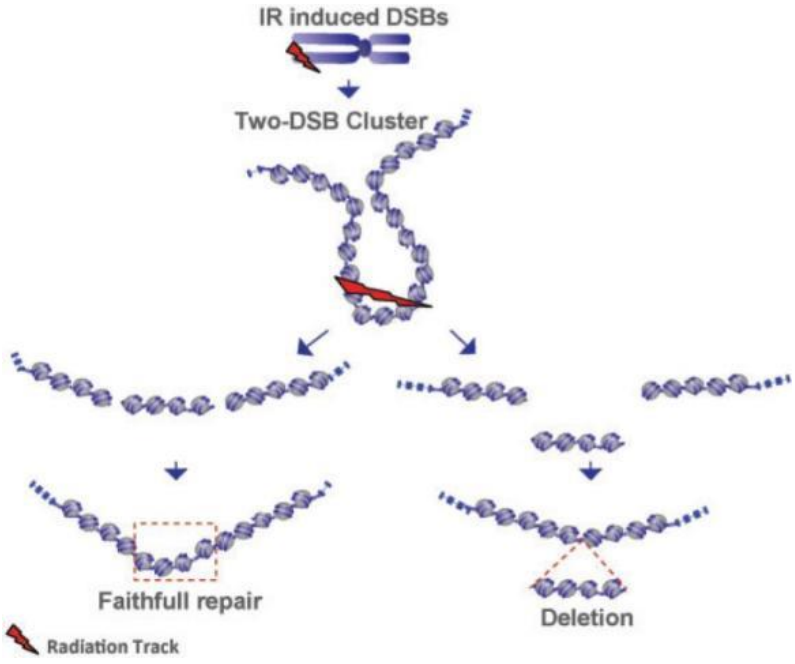

Figure 9: *Nucleosomal loss due to clusters of DSBs.*

Two different situations may arise post repairing that may lead to complete restoration of sequence (left) or to a deletion causing nucleosomal loss (right) ([12]).

1.3 DNA damage Response

Upon induction of DSBs a cascade of events is initiated to prevent the adverse consequences of DSB formation. These events feature a coordinated cascade of events that range from activation of cell cycle checkpoints, the transcriptional and post-transcriptional activation of a subset of genes including those associated with DNA repair, enhancement of DNA repair pathways or initiation of apoptosis, when the level of damage is severe [53]. All of these processes are

carefully coordinated so that the genetic material is faithfully maintained, duplicated, and segregated within the cell.

Within seconds of DNA damage induction DDR response gets activated. As shown in Figure 10 DDR comprise of a network that consists of sensors, mediators and effectors. A sensor protein senses the DNA damage and transmits the signal to effectors through a series of transduction events. Effectors then activate mechanisms, which are important in the coordination of:

(1) Cell cycle checkpoints to avoid replication and/or accumulation of damaged DNA;

(2) DNA damage repair;

(3) Apoptotic processes for irreparable DNA damage.

(4) The transcriptional and post-transcriptional activation of a subset of genes including those associated with DNA repair [53, 54].

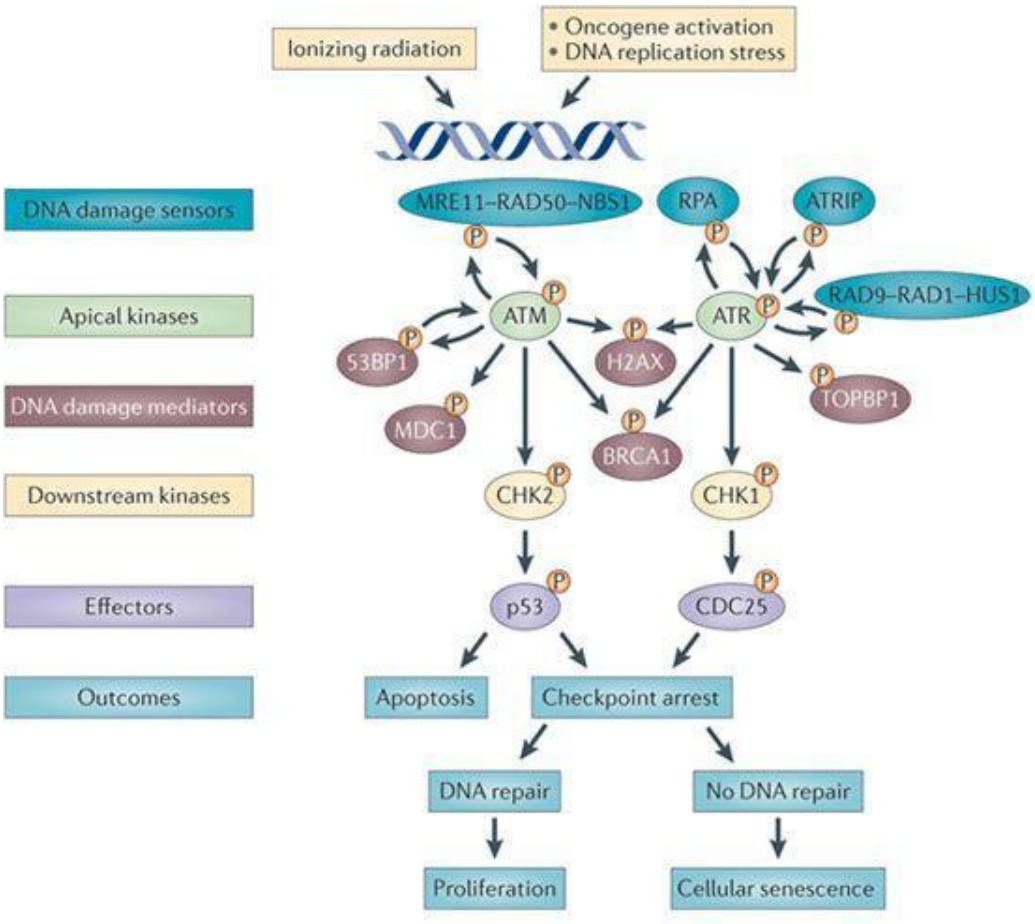

Figure 10: *Schematic representation of DDR signaling.*

Introduction

Sensor proteins recognize the DNA damage and the mediator proteins amplify the signaling. The transducers transmit the generated signal to effector proteins for appropriate cellular responses Taken from *(Sulli et al. 2012).* [55].

1.3.1 DNA damage Response (Sensing and Signaling)

DDR signaling forms a network that is essential for the maintenance of genomic stability, initiation and coordination of DNA repair mechanisms with appropriate cell cycle arrest checkpoints [2, 56]. Briefly, a typical DDR cascade (Figure 11) begins with MRN complex (MRE-11, Rad-51 and NBS-1 proteins) sensing the breaks that leads to the recruitment and activation of ATM (ataxia-telangiectasia mutated) to DNA double-strand breaks (DSBs). This is followed by the local phosphorylation of multiple ATM substrates in the chromatin surrounding the DNA lesion, and almost always the histone variant H2AX on Ser-139 [57, 58] (phospho-H2AX or gamma-H2AX). These local chromatin modifications result in recruitment of additional DDR mediators at the break, including MDC1 (mediator of DNA damage checkpoint protein 1). MDC 1 in turn interacts with Mre11 to tether the MRN complex and ATM to the DSB site. Recruitment of these proteins amplifies chromatin modifications over mega-base pairs of DNA and can be visualized microscopically in mammalian nuclei as macroscopic structures called DNA damage foci (DDF) [57, 59]. MDC 1 also initiates the recruitment of the E3 ubiquitin ligases RNF8 and RNF168. RNF8 assists in recruitment of p53 binding protein (53BP1) as well as BRCA1; by ubiqutinylating the histone proteins at the site of the DSB, RNF8 and RNF168 generate a histone mark that facilitates the recruitment of 53BP1 protein. Both these molecules assist in the activation of DSB repair [60, 61]. After DSB sensing, ATM and ATR trigger further processes that includes a series of events promoting cell cycle checkpoints and the activation of p53 [62]. This cell cycle arrest is transient in case of repairable damage but, when DNA lesions are severe they trigger prolonged DDR signaling, resulting in apoptosis or senescence [63].

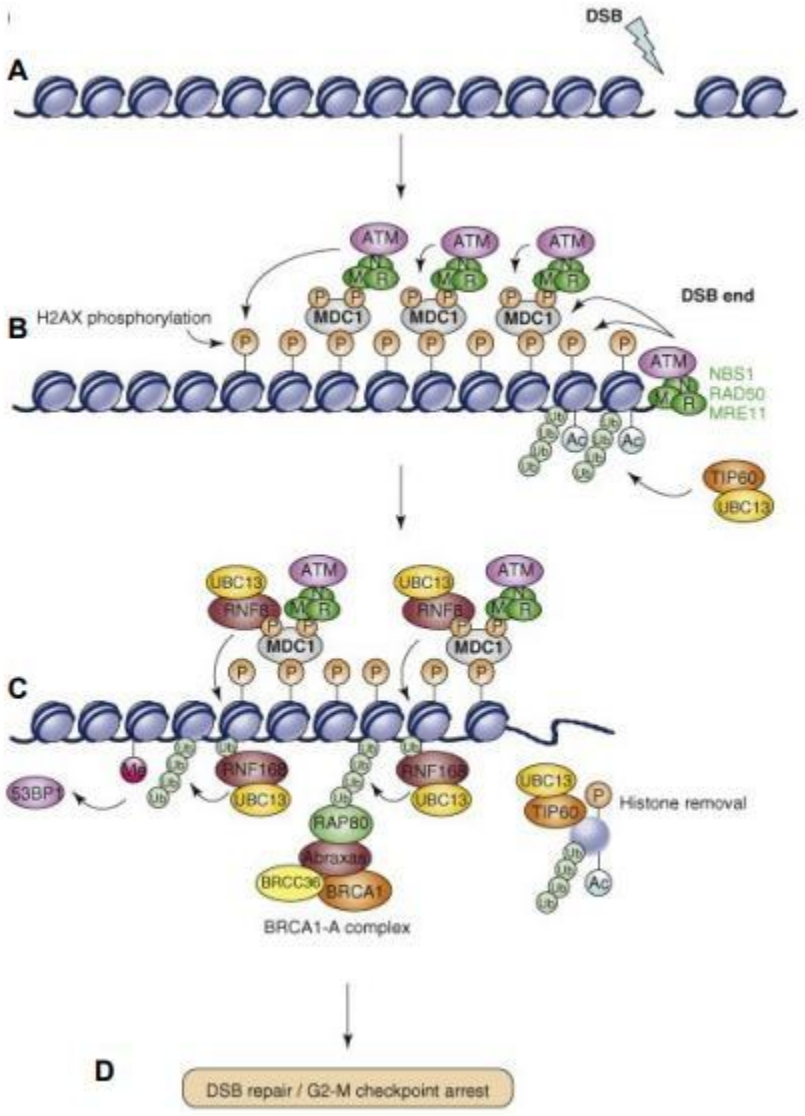

Figure 11: *Model for the function of ɣ-H2AX at DSB in mammals*

A: IR induces DSB. **B:** The MRN complex binds to the DSB ends and recruits ATM, which phosphorylates H2AX to ɣ-H2AX. MDC1 is then recruited and it binds to ɣ-H2AX. Phosphorylation of MDC1 recruits more MRN-ATM and more ɣ-H2AX. TIP60 acetylates (Ac) ɣ-H2AX and associates itself with the E2 ubiquitin-conjugating enzyme UBC13 to regulate polyubiquitylation (Ub) of acetylated ɣ-H2AX. **C:** Polyubiquitylated and acetylated ɣ-H2AX is removed from chromatin. ATM phosphorylates MDC1 to recruit an RNF8–UBC13 complex that regulates ubiquitylation of histone H2AX and H2A. RNF168 binds to these ubiquitylated histones and these polyubiquitylated histones recruit the BRCA1-A complex and 53BP1. 53BP1 binds to methylated (Me) histones after RNF8–RNF168–UBC13-mediated polyubiquitylation. **D:** This sequence of events facilitates DSB checkpoint arrest and repair. Figure taken from (van AttiKum and Gasser 2009) [64].

Introduction

1.3.2 Activation of DNA damage induced cell cycle checkpoints

DDR activates cell cycle checkpoints upon induction of DNA damage in a synchronized manner. Cell cycle checkpoints are controlled mechanisms in eukaryotic cells which ensure proper cell division. At each checkpoint the cell is assessed and is allowed to progress through the various phases of the cell cycle only when favorable conditions are met. The timing and order is a key feature and the foremost priority during activation of checkpoints so that cell cycle progression is paused to ensure completion of one cellular event prior to commencement of another. This regulated pause in cell cycle progression also ensures that damaged cells have ample amount of time to repair faithfully or to avoid duplication and segregation of damaged DNA. The key regulators of the checkpoint pathways in the mammalian DNA damage response are the members of the phosphatidylinositol-3 kinase-related kinases (PIKK) family namely the ATM (ataxia telangiectasia, mutated) and ATR (ATM and Rad3-related) protein kinases in response to DSBs and ssDNA, respectively [65].

The main targets in cell cycle checkpoint activation are cyclins and cyclin-dependent kinases (Cdks) forming cyclin/Cdk complexes [66]. “The cell cycle is controlled by the interplay between cyclins, whose concentrations vary throughout the cell cycle and the cyclin dependent protein kinases” [67].

Upon DNA damage induction in the G1 phase, cells activate G1/S – checkpoint. The entry into S phase is regulated by the cyclin D/Cdk4/6 and cyclin E-Cdk2 complexes. The G1/S – checkpoint is regulated by inactivation of these complexes. Two mechanisms have been described [68]. The rapid mechanism is initiated via checkpoint kinase 2 Chk2, which phosphorylates Cdc25A at Serine-123 leading to ubiquitination of Cdc25A followed by proteasomal mediated degradation. This reduces the abundance of Cdc25A blocking cdk2-Clyclin E in an inactive state and thereby, stopping the progression of cells to the S-phase [68]. In addition the second slowly activated mechanism requires ATM dependent phosphorylation resulting in stabilization of p53. Stabilized p53 activates the transcription of the cdk inhibitor p21, which binds to the cdk2 – Cyclin E kinase complex, thus maintaining the cells in G1-phase [68, 69].

During S-phase stalled replication forks results in ATR activation, and subsequent Chk1 phosphorylation and Cdc25A degradation. This delays replication and stops cells in S-phase.

Upon induction of damage in G2 phase cells can halt the cell cycle at the G2/M border. The principal target in the G2/M checkpoint is the cdk1–Cyclin B complex, which is essential for the progression towards mitosis. DSBs in G2 phase can activate ATM and indirectly ATR through generating single stranded DNA by end resection. The mechanisms that prevent the cell from entering into mitosis after induction of DNA damage in G2 cells are similar to those triggered during the G1/S checkpoint activation. A rapid signal transduction involving phosphorylation of effector kinases Chk2 and Chk1 results in phosphorylation of Cdc25a and its subsequent degradation, which inhibits the interaction with Cdk1/cyclin B. Furthermore an increase of Wee1, mediated by negative regulation of Plk1 (pololike kinase 1) by ATM and ATR, reduces Cdk1 activity to attain a strong G2 arrest, which prevents entry to mitosis [70, 71].

Cell cycle remains halted until the DNA damage is repaired; in case of DSBs by one of the following repair pathways.

1.3.3 DSB repair pathways

DSBs are one of the most toxic lesions encountered by a cell and to eliminate them higher eukaryotes have evolved highly coordinated mechanisms. It has already been mentioned that mis-repaired DSBs can cause chromosomal aberrations, of which translocations are the most consequential. To avoid these genomic alterations the DSB repair machinery needs to ensure first that the right DNA ends are put together and joined together, thus avoiding mis-joining of two incongruent DNA ends. Second, the DSB repair machinery should ensure restoration of sequence around the broken ends to prevent mutations and loss of genetic information.

Higher eukaryotes have evolved two major DSB repair pathways that differ in almost every aspect of their molecular set-up, in their efficiency to process DSB ends, in their speed and their activity through-out the cell cycle. These two main DSB repair pathways are: HRR (error-free) and c-NHEJ (fast and error-prone).

If either of the two major pathways is genetically or chemically compromised then a back-up pathway referred to as alternative-end joining seems to be functional that has extremely high propensity towards errors and chromosomal translocation formation. Fourth error prone homology dependent repair pathway termed as single strand annealing (SSA) also remove the break from the genome, but can cause mutations, deletions, and translocations. All these repair pathways will be discussed in the following sections.

a. c-NHEJ: Classical DNA-PKcs dependent non-homologous end joining

In 1996 Moore and Haber coined the term non homologous end joining for the DNA damage repair pathway that just required the direct ligation of broken DNA ends to repair the break. NHEJ is a dominant double strand break repair pathway in mammalian cells and it is evolutionarily conserved throughout all kingdoms of life.

NHEJ has a fast repair kinetics (with half times of 15-30 minutes) [72] [73] and therefore is one of the primary repair pathways that promotes genomic stability but, since it includes direct end ligation its fidelity is compromised. It is active in all three cell cycle phases and includes the following steps: [74]

-DSB recognition by Ku

-Synaptic end bridging

-Processing of DNA ends

-Ligation of the break

-Ku removal from the break

Ku dependent DSB recognition

In eukaryotic cells, the Ku protein is abundant (500,000 molecules per cell) and is the key detector of DSB (detects DSB within 5 seconds) [74]. The Ku70/80 heterodimer is important to hold the two broken DNA ends together. Once the Ku heterodimer has encircled the DSB ends it forms a scaffold for other NHEJ factors. Many DDR response factors form foci that are visible clearly and distinctly, but, only recently have techniques been developed using super resolution microscopy that demonstrate that only two Ku molecules are present at a DSB presumably one at each DSB end [74, 75].

The processing of DSB ends

The mismatched overhangs or covalently modified DNA ends require the recruitment of specific enzymes to clean and fill nucleotides prior to ligation. Once Ku-DNA complex is formed DNA-PKcs [76], XRCC4, XLF, PAXX and Lig4 comes into action [74].

DNA-PKcs kinase belongs to the PI3K family and has an extremely important role in c-NHEJ. In its inactive state DNA-PKcs remains un-phosphorylated; but, once Ku forms a complex with the DNA ends, activation of DNA-PKcs occurs through N and C-terminal residues of Ku80 [74]. Upon activation, DNA-PKcs is able to phosphorylate more down-stream proteins that ensure the completion of repair. Proteins phosphorylated by DNA-PKcs include Ku, XRCC4, XLF, and Lig4; but also proteins like WRN and Artemis [74]. Thus, DNA-PKcs might function as a molecular switch that coordinates end processing and end ligation at the DNA ends [77].

Artemis has been shown to carry out hairpin opening in order to remove ssDNA overhangs containing damaged nucleotides [78]. After DSB end processing the final step of c-NHEJ is the ligation of DSB ends, carried out by the coordinated action of the DNA XRCC4 – Lig4 and XLF complex.

DSB ligation

Once the DSBs are ready for ligation, XRCC4-XLF forms a complex with Ligase 4. XRCC4 is anchored to the DNA-PK complex bound to the DNA ends. XRCC4 majorly acts as a bridge for DNA ligase 4 that acts to seal the broken ends. In contrast to the role of XRCC4, the role of XLF in promoting c-NHEJ is less clear [78]. Refer to Figure 12 for schematic representation.

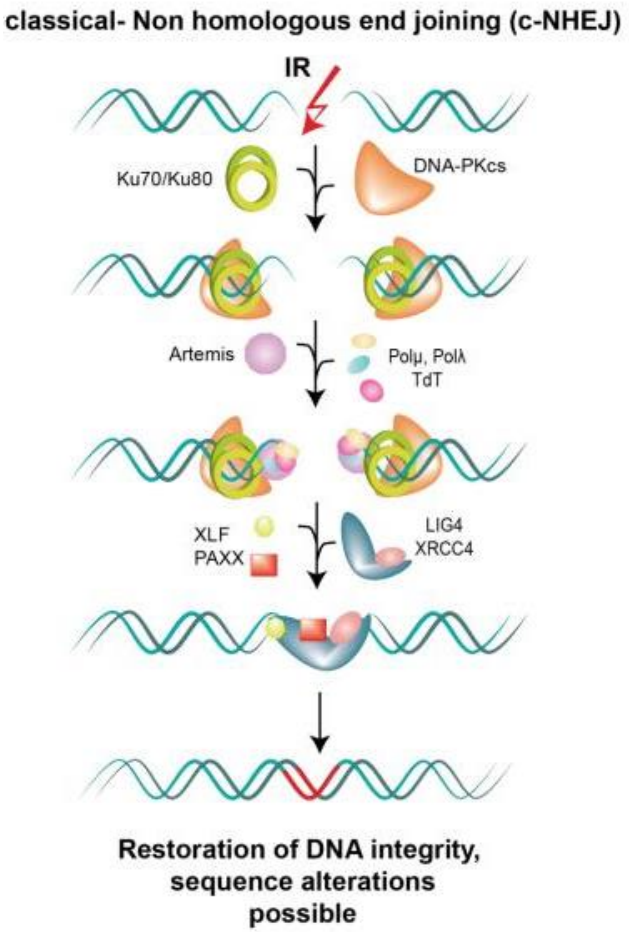

Figure 12: *Schematic representation of c-NHEJ*

Main steps involved in c-NHEJ include the binding of the Ku70/80 heterodimer to the DSB ends, followed by the recruitment of DNA-PKcs. End processing enzymes help in cleaning up the DSB ends to make them ligatable. Ligation is carried out by the Lig4/XRCC4/XLF complex. c-NHEJ is potentially error prone and may therefore, result in small scale alterations (taken from (Iliakis, et al. 2015b) [18])

c-NHEJ is a comparatively less complicated process than HRR and it is able to restore chromosome continuity, but, it **does not ensure** that **a)**.the correct DSB ends are ligated and **b)**.the sequence around the break side is reestablished. This renders c-NHEJ a potentially error prone pathway that can contribute to translocation formation.

DNA End Resection dependent Rejoining of DSBs by HRR, alt-EJ and SSA

The ends of DSBs that are not removed from the genome by c-NHEJ are prepared for processing by three alternative pathways (HRR, alt-EJ and SSA). All of these pathways begin with DNA-end resection. In DNA-end resection the exonucleolytic degradation of the 5′-strands of each DNA end generates 3′-single-stranded DNA (ssDNA) [79]. Although DSBs can be induced in any phase of the cell cycle, the process of DNA end resection has specific cell cycle requirements and DSBs get resected mainly in the S and G2 phases [80]. DNA-end resection process can be considered as a two-step process involving: (Figure 13)

- resection initiation, and
- resection extension

Resection initiation is stimulated by Snf2-related CREB-binding protein (CREBBP) activator protein (SRCAP), CtIP, and the MRN complex. Sartori et al. first reported about the DNA end resection catalyzed by CtBP-Interacting Protein (CtIP) [81]. CtIP plays two distinguishing roles in the process of DNA end resection based on involvement of its catalytic activity or not. Briefly, the resection of DSBs with clean broken ends produced by restriction endonuclease requires CtIP protein without its nuclease activity. In contrast, endonuclease activity of CtIP makes it absolutely essential for repair of more complex DNA lesions created by IR or topoisomerase [80].

EXO1 and BLM/DNA2 cooperate with other chromatin remodeling factors to promote resection extension. EXO1 belongs to the xeroderma pigmentosum complementation group G (XPG) family of nucleases and it exhibits 5’ to 3’ dsDNA exonuclease and 5’ flap endonuclease activities in vitro. BLM is a member of the RecQ family of helicases that unwinds DNA (Sgs1 is its ortholog in Saccharomyces cerevisiae). DNA2, which is related to the bacterial RecB proteins, exhibits both helicase and nuclease activities. Previous findings suggest that EXO1 and DNA2–BLM/Sgs1 function in parallel at the second step of end resection [80].

In summary, DNA end resection machinery (MRN complex, CtIP, Exonuclease 1 (EXO1), DNA replication helicase/nuclease 2 (DNA2), and the Bloom's syndrome (BLM) helicase) generates ssDNA with 3′-overhangs that is stabilized by Replication Protein A (RPA). This structure subsequently initiates HRR, SSA, or alt-EJ [79].

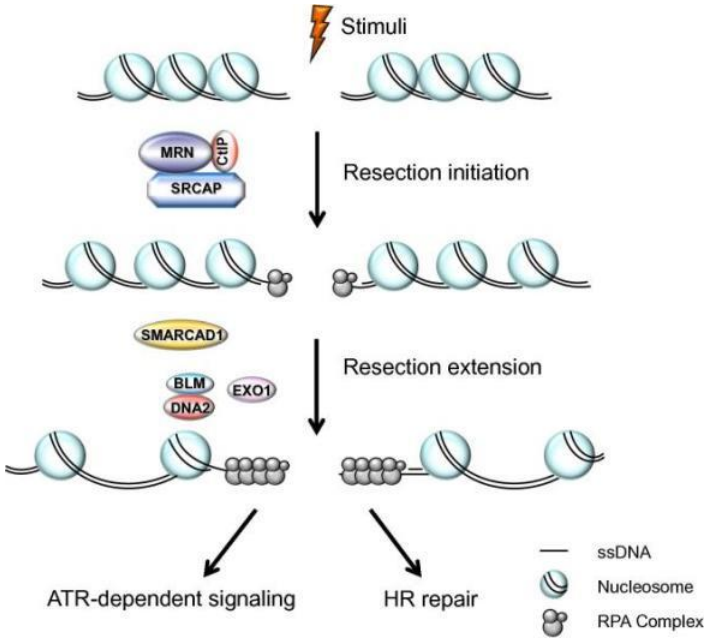

Figure 13: *Schematic representation of DNA end resection*

A two-step model has been suggested for DSB processing as MRE11 lacks the 5' to 3' exonuclease activity required to produce long 3' ssDNA overhangs essential for loading of replication protein A (RPA). In this model, the MRN complex and CtIP remove the first 50–100 nucleotides from the 5' end of the damaged DNA, followed by EXO1 mediated generation of long 3' ssDNA tails. This model is also supported by the finding from in vivo experiments that CtIP is required for the accumulation of EXO1 at DSB sites (figure taken form [80]).

b. HRR (Homologous Recombination repair)

HRR is a high fidelity and efficiency pathway that engages the undamaged sister chromatid or the homologous chromosome to repair the DSB. It is widely accepted that HRR accounts for the repair of 25% of all DSBs in higher eukaryotes. Owing to its more complicated mechanism, HRR is a relatively slower repair process confined to late S and G2 phase of cell cycle [82]. Refer to Figure 14 for schematic representation.

The most salient feature of HRR in vertebrates is that it requires a homologous template in the form of the sister chromatid [79]. The ends of DSBs that are not removed from the genome by c-NHEJ are prepared for HRR by DNA end resection. During HRR, end resection removes a few thousand base pairs to generate equally long 3' ssDNA strands that are stabilized by RPA [79].
As has been discussed above end resection involves the recognition of DSBs by the MRN (Mre11-Rad50-Nbs1) complex. Together with CtIP; the MRN complex regulates short range resection. Long-range resection is carried out by Exo1, Dna2 and BLM. This activity results in the generation of 3' ssDNA overhangs that gets coated by RPA. RPA coating of ssDNA strands stabilizes them, eliminates secondary structures and prepares the formation of a Rad51 nucleoprotein filament. Mediator proteins that are involved in the formation of Rad51 filament include the Rad51 paralogs (Rad51B, Rad51C, Rad51D, XRCC2, and XRCC3) and BRCA2 [83].

The RAD51 nucleoprotein filament subsequently invades (resulting in formation of displacement loop or D-loop) and anneals to the homologous region in the sister chromatid to form a Holliday junction [79]. Holliday Junctions are intermediates of homologous recombination in which two homologous DNA duplexes are joined by the interchange of a pair of (nearly) identical single strands [84]. Further chromatin remodeling and DNA synthesis associated with branch migration is carried out by Rad54 after Rad51is dissociated from the hetero-duplex DNA [85, 86].

Mainly two subpathways are involved in the repair of DSBs by HRR, and either can be engaged. Predominantly, synthesis-dependent strand annealing (SDSA) occurs. Briefly it occurs by resolving of D-loop and annealing with the second resected and extended 3' single stranded DNA. The process culminates with gap filling via DNA polymerases and the ligation of the annealed DNA ends.

In the second type of the process, called as double strand break repair (DSBR), two 3' single stranded DNA overhangs participate. This results in formation of two intermediate Holliday junctions. This process can yield either crossover or non-crossover products after gap filling and ligation [87].

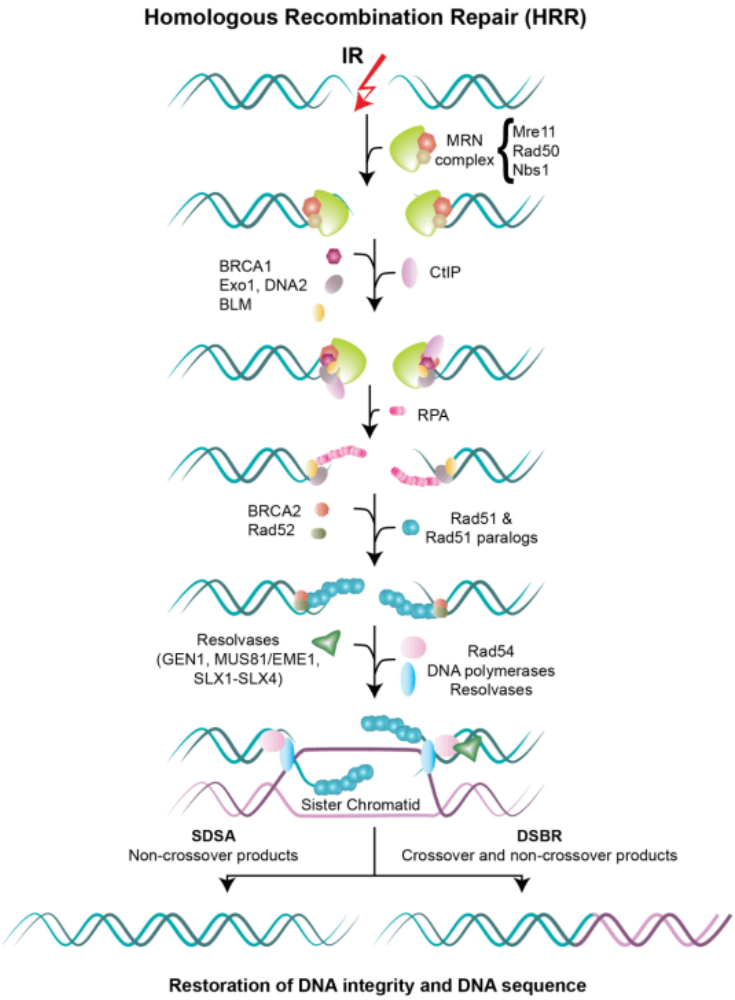

Figure 14: *Schematic representation of HRR*

Initial steps involved in HRR include the recognition of the DSB ends by the MRN complex followed by DSB end resection controlled by molecules such as CtIP, Exo1, BLM, BRCA1 and Dna2, to produce 3' prime DNA overhangs, which are swiftly coated with RPA. In the latter steps Rad51 engages in homology search and strand invasion with the aid of its paralogs. Resolution of the DSBs is then either carried out by synthesis dependent strand annealing (SSA) or double strand break repair (DSBR) with the help of resolvases and Rad54 to restore the original sequence of DNA molecule (taken from (Iliakis, et al. 2015a) [18].

c. Alternative end joining (alt-EJ)

When either c-NHEJ or HRR is genetically or chemically compromised a third pathway termed as alternative end-joining pathway (alt-EJ) can engage to eliminate DSBs. It was discovered over two decades back when Ku80 mutant cells showed residual DSB repair activity and the repair products showed strong dependence on short homologous sequences at the junctions. alt-EJ is

known to be highly mutagenic and results in translocations that are also found in many hematological cancers. Refer to Figure 15 for schematic representation.

alt-EJ has three main characteristic features:

1. Very low fidelity resulting in translocations.
2. Slower kinetics when compared to c-NHEJ (30 minutes – 20hours).
3. It operates throughout the cell cycle but it is enhanced in G2 and suppressed when the cell enters G0/quiescence.

Two forms of alt-EJ have been described. One form utilizes micro-homology, i.e. it benefits from the presence of short patches of homology ranging from 5-25 nucleotides distant from the DSB ends. Since it uses such micro-homologous sequences (5-25 base pairs), there is increased chance of nucleotide loss at the regions surrounding the break, resulting in deletions owing to resection and end processing. alt-EJ is thus, a completely distinguished pathway than c-NHEJ and has activity independently of Ku, DNA-PK or Lig IV.

Even though alt-EJ benefits from microhomologies at the DSB junctions, it can also operate in the absence of microhomology. alt-EJ benefits from the enzymatic activities of Poly (ADP-ribose) polymerase 1 (Parp1) and DNA Ligase III (Lig3)/XrCC1 [88] or DNA Ligase 1 (Lig1). Other proteins that are involved in alt-EJ are H1 (Histone 1), end resection proteins like CtIP and Mre11 [18, 89].

Parp1 is involved in alt-EJ but also has many additional functions in the cell. A rather dedicated newcomer protein to alt-EJ is Polθ, an A family DNA polymerase, encoded by the POLQ gene [79]. It has been shown that it facilitates end – joining of DNA ends that contain micro-homologies [90, 91]. The final ligation step of alt-EJ is mediated by DNA ligases I and III (LIG1 and LIG3), while the linker histone H1 may serve as an alignment factor [79]. By using RNAi screening of known DNA damage response factors, additional genes associated with Alt-EJ have been identified. They include: FAAP24, NTHL1, RAD53B, POLA1, SOD1, RUVBL2, GEN1, TIP60, DNA2, SH6, FANCA and PRP19/PS04 [92].

Similarly to c-NHEJ, alt-EJ joins any DNA ends independently of origin. However, because it operates with slower kinetics than c-NHEJ and is carried out by a much less coordinated apparatus, a drifting apart of the DNA ends is more likely and as a consequence also the probability of translocation formation [79]. alt-EJ has also no built-in mechanisms to restore DNA sequence at the DSB junction. This fact, together with the often-required DNA-end resection, increases the frequency of deletions and other sequence alterations at the junction [79].

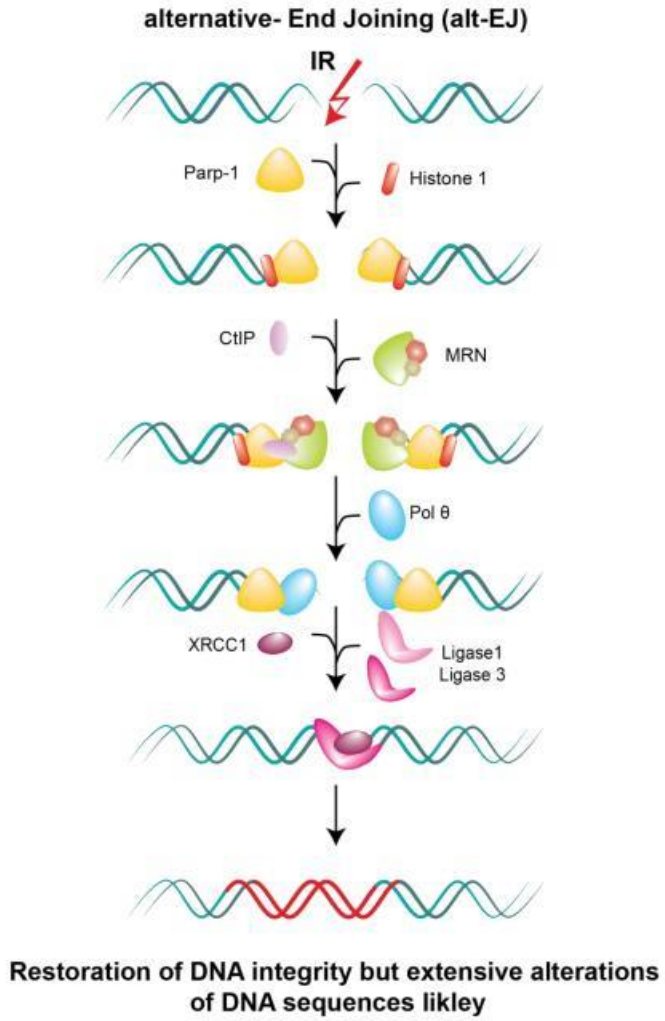

Figure 15: *Schematic representation of Alternative End-Joining*

alt-EJ is utilized in the repair of DSBs when either c-NHEJ or HRR are compromised. It results in large number of translocations and thus, is highly mutagenic. Factors utilized in alt-EJ include Parp1, which binds to the DSB ends. alt-EJ benefits from DNA end resection. Hence, proteins involved in initiation of DNA end resection (Mre11 and CtIP) have also been shown to play a role. Ligation is carried out by Ligase 3 or Ligase 1 (taken from [18]).

d. Single Strand Annealing (SSA)

SSA is a homology dependent pathway of DSB processing. It involves annealing of homologous repeat sequences that flank a single DSB. SSA involving repeats that flank a single DSB causes a deletion rearrangement between the repeat and hence is mutagenic [93]. In contrast to HRR that relies exclusively on homology found in the sister chromatid, SSA normally utilizes homologous regions present in the same DNA molecule [79]. SSA involves extensive use of end resection and during SSA, resection of DNA ends may extend even further than after HRR, depending on the distance between the flanking homologies [79].

In contrast to HRR, SSA does not require RAD51 but instead uses the strand annealing protein RAD52 to anneal the DSB-flanking homologous DNA sequences, as they become exposed after DNA-end resection [79]. SSA activation mostly causes deletion of the DNA segment between the utilized regions of homology. As a consequence, it also requires the removal of the ssDNA flaps formed after annealing of the homologous regions [79]. XPF–ERCC1 and MSH2–MSH3 complexes are involved in the removal of ssDNA flaps and are followed by DNA ligation to restore integrity in the DNA molecule.

SSA is highly error prone owing to the large deletions it generates and can be promiscuous in partner selection, thus forming translocations [79]. The requirement for resection makes it cell cycle dependent with maximum activity during S- and G2-phase [79]. It has been previously suggested that SSA is strongly suppressed by HRR and vice-versa since SSA activity is enhanced upon loss of Rad51, Rad54 or BRCA2. This kind of regulation suggests a back-up role for SSA to HRR [94] [95] [96]. Refer to Figure 16 for schematic representation.

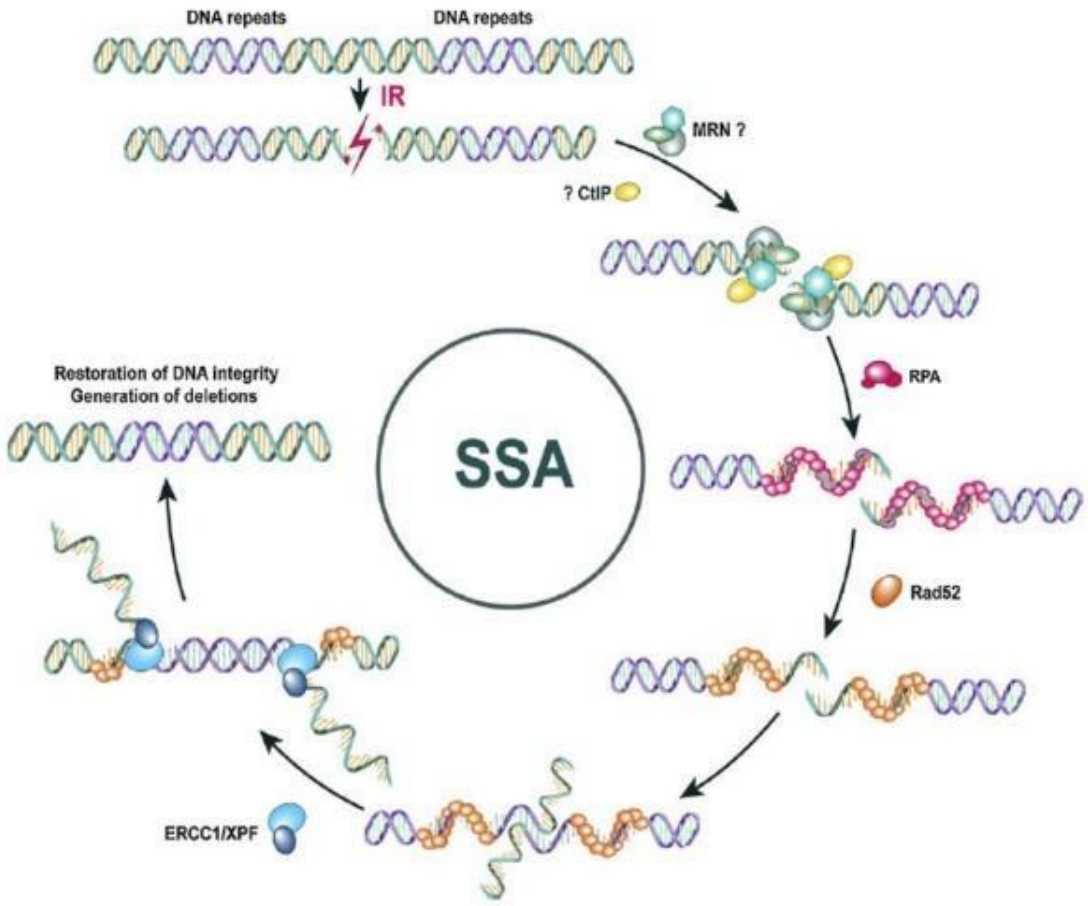

Figure 16: *Schematic representation of SSA*

SSA is a highly error-prone repair pathway as long stretches of DNA are deleted and may also cause translocations. It seems to function as a bacKup mechanism for HRR (figure taken from [94].

1.3.4. DSB repair pathways in high LET induced DSBs

In mammalian cells DSBs are mainly repaired by c-NHEJ or HRR [61]. Recent studies have showed that approximately 70% of DSBs induced by low LET are repaired by c-NHEJ in mammalian cells, even in G2 phase [30]. In comparison to low LET, DSBs induced by high LET radiation, are also repaired rather extensively by HRR [30]. However, this cannot explain the increased incidence of chromosome aberrations after exposure to high LET radiation. Cytogenetic data suggests that some DSBs arising from high LET radiation are likely repaired after resection in G2 phase by error-prone repair pathways, such as single-strand annealing (SSA) or alternative-EJ (alt-EJ) [97], [30], [98], [99]. Refer to Figure 17.

Following high LET irradiation, RPA foci can be detected in G1 cells, which are not detectable after low LET irradiation, as the length of resection is not long enough for detection [30]. It follows that in comparison to DSBs induced in G1 cells after low LET irradiation, DSBs induced by high LET irradiation undergo greater end resection in G1 cells [100]. Although resection occurs in G1 cells after exposure to high LET irradiation, HRR cannot be utilized due to the unavailability of the sister chromatid [30]. Therefore, DSBs undergoing resection in G1 cells are repaired with high probability by the non-HR pathway. After inhibiting DNA-PKcs in G1 cells exposed to high LET irradiation, a strong defect in DSB repair is observed and Parp inhibition generates a modest DSB repair defect. Thus, c-NHEJ is also repairing DSBs following high LET irradiation [101].

More studies are required to precisely understand the molecular mechanisms of DSB repair following high LET irradiation.

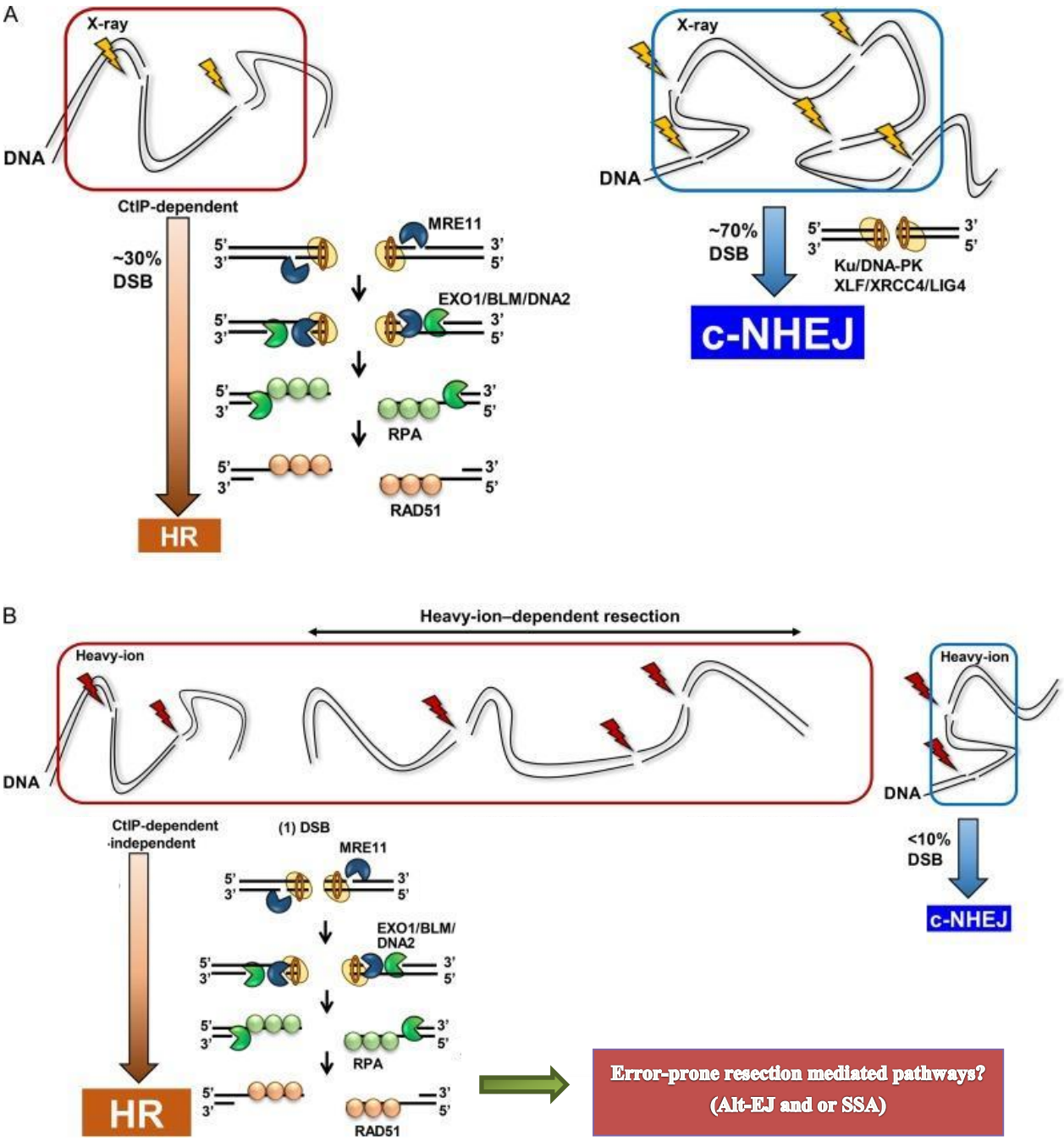

Figure 17: *Repair pathways involved in repair of DSB clusters after exposure to low and high LET IR.*

Figure adapted from Hagiwara. Y. et al; Journal of Radiation Research; 2019 [30]. DSB repair pathway following low and high LET radiation. (A) The model of DSB repair in G2 cells following low LET X-ray irradiation. Recent studies in human G2 cells have demonstrated that ~70% of DSBs are repaired by c-NHEJ, whereas ~30% of DSBs in G2 are repaired by HRR. (B) The model of DSB-repair following high LET irradiation. A high proportion of DSBs induced by high LET irradiation are repaired by resection dependent pathway, i.e. mainly HRR. DSBs repaired with slower kinetics after high-LET irradiation than that after low LET irradiation [102]. This

Introduction

implies that DSB end complexity does influence the speed of DSB repair. One of the models proposes that in G2 phase, c-NHEJ factors initially binds to DSB ends; however, when rapid c-NHEJ fails, then DSB end resection and HRR occur [61, 102],. Thus, when DSB clusters and complex lesions occur after exposure to high LET radiation, DSBs showing delayed repair are repaired by HRR. “At DSB ends induced by high-LET irradiation, the resection can be CtIP-dependent or independent” [30, 101]. MRE11 endonuclease initiates resection with CtIP. After the incision, EXO1/BLM/DNA2 promotes extension of resection as described above. Afterwards, the generated nick may trigger EXO1/BLM/DNA2-dependent extension of resection without MRE11/CtIP-dependent endonuclease activity. EXO1/BLM exonucleases may readily promote resection” [30].It remains to be investigated whether after exposure to high LET radiation all resected DSBs are repaired by HRR or other error prone pathways, e.g. alt-NHEJ, SSA or other repair pathways.

Aim of the Work

DSBs are the most deleterious lesions for the integrity of the cellular genome. Often their repair can lead to the formation of chromosomal translocations, which underlies cell death or carcinogenesis. To counteract the detrimental effects of DSBs, cells have evolved multiple DSB repair pathways: error-free homologous recombination repair (HRR), and potentially error-prone, classical non-homologous end-joining(c-NHEJ), which is orchestrated by DNA-PKcs activity. It is now widely accepted that in absence of c-NHEJ and/or HRR, an alternative form of end-joining (alt-EJ) is engaged in the repair of DSBs. alt-EJ has speed and fidelity markedly lower than c-NHEJ, which increases the probability for chromosome-translocations. Abrogation of error-free DSB repair pathways also result in shunting towards yet another highly mutagenic pathway termed as single strand annealing (SSA). Like alt-EJ which results increased probability towards formation of translocations, SSA can also result in large deletions and may result in formation of translocations. Therefore chromosome-translocations result from accidents that compromise c-NHEJ or HRR, allowing the operation of error-prone alt-EJ or SSA. One of the sources for such accidents is DSB-complexity, which is typically defined by the nature and the number of chemical alterations that accompany a DSB in close vicinity to the break site. We investigated DSB-clusters as a form of DSB complexity and examined the DSB-repair pathways involved in their processing.

DSB-clustering as a cause of irreversible-radiation effects has been mainly tested using mathematical modeling in the past. To overcome this limitation, we introduced a restriction endonuclease (RE)-based system involving the generation of DSBs by I-SceI endonuclease. To carry out this work we have utilized the Chinese Hamster Ovarian (CHO) cell lines harboring multiple copies of constructs in their genome with multiple I-SceI recognition sites engineered at specific-distances in different orientations to generate clusters of DSBs. The DNA damage was introduced into the CHO genome by transfecting I-SceI endonuclease enzyme. Depending on the numbers of constructs that were integrated into the genome of CHO cells DSBs were generated ranging from simple DSBs to DSB pairs and DSB quadruplets; and depending on the orientation of I-SceI constructs DSBs were generated with compatible apical ends or incompatible apical

ends. DSBs/clusters having compatible ends don't require DNA end processing before ligation and DSBs/clusters with incompatible ends require DNA end processing before ligation.

Previously published work shows a significant correlation between cell killing and the formation of chromosomal-aberrations with increasing DSB-clustering. Translocation-formation from DSB-clusters utilizes alt-EJ and shows a strong Parp1-dependence. Immunofluorescence experiments show ɣ-H2AX foci formation by both single-DSBs and DSB-clusters, suggesting similar activation of early DNA damage response (DDR).

In this thesis in order to investigate the contribution of different repair pathways in repair of simple and clustered DSBs we have utilized in addition to wt CHO cells the following HRR and c-NHEJ mutants: irs1 SF with defect in XRCC3, xrs6 defective in Ku80, and XR-C1-3 defective in DNA-PKcs. To study the outcome of generation of simple DSBs and DSB clusters by I-SceI endonuclease, we essentially designed experiments to investigate three separate end points to base our conclusions on. We examined killing potential of simple DSBs and DSB clusters in CHO wt and mutant clonal cells by clonogenic survival assay and the mis-repair accidents resulting in survival defects were studied using classical cytogenetics approach. To investigate the consequence of generation of DSB clusters on cell signaling, we utilized indirect immunofluorescence method. For this we specifically looked at recruitment of ɣ-H2AX and/or 53BP1 foci (as a marker for DSBs); and Rad51 foci (as a marker for functional HRR).

We also investigated the role of DSB end processing in the repair of DSB clusters. It has already been discussed above that in our CHO based biological system I-SceI constructs are engineered in different orientations resulting in compatible and incompatible DSB ends upon I-SceI transfection; in the presence of directly ligatable DSB ends ("D clone"), DNA end processing is not required and in the presence of incompatible DSB ends ("R clone") it is essential. To confirm the observations made in CHO "D and R" clones we used two distinct approaches, in first we used I-SceI-TREX plasmid to generate DSB pairs with blunt ends; and in second we knocked down CtIP in the CHO clones resulting in single DSBs and DSB clusters (pairs and quadruplets).

Furthermore, we confirmed the observations made in the CHO mutant clones by both chemically inhibiting and knocking down major DSB repair proteins. To chemically inhibit c-NHEJ, HRR,

Aim of the Work

alt-EJ and SSA we used specific inhibitors against DNA-PKcs (NU7441), Rad51 (BO2), ATR (VE-821), Rad52 (6-OH DOPA) and Parp1 (PJ34). To genetically deplete the DSB repair proteins in CHO wild type and DNA-PKcs mutant clones, we knocked down Rad51 to inhibit HRR; Ku80 to inhibit c-NHEJ; and Rad52 to inhibit SSA. We designed the experiments similar to the ones mentioned above and measured the effect of abrogated DSB repair pathways in repair of single DSBs and DSB clusters by scoring surviving cell colonies and translocations (chromosomal and chromatid type) formation.

Aim of the Work

Materials and Methods

Materials

1. Laboratory apparatus

Beckman Tabletop GS-6R centrifuge	Beckman Coulter, USA
BioFuge (Fresco)	Thermo Scientific, Germany
Cell culture “Herasafe” hood	Thermo Scientific, Germany
CO2 Incubator	Sanyo, Japan
Confocal laser scanning microscope	Leica Microsystems, Germany
Coulter Counter	Beckman Coulter, USA
Express Pipet-Aid	BD Falcon, USA
Flow Cytometer	Beckman Coulter, USA
Heating unit	Peter Oehman, Germany
Inverted Microscope	Olympus, Japan
Magnetic Stirrer	Heidolph, Germany
Nano-drop	Thermo Scientific, Germany

Materials and Methods

Nucleofactor	LonzaCologneGmbH, Germany
Overnight Culture Shaker	Infors, Germany
Pasteur pipette	BD Falcon, USA
Peristaltic pump	Ismatec, Switzerland
pH Meter	InoLab, Germany
Pipettes	Eppendorf, Germany
Rocky Shaker	Peter Oehmen, Germany
Scintillation Counter	Beckman Coulter, USA
Ultracentrifuge	Beckman Coulter, USA
Vortexer (Vortex-Genie 2)	Scientific Industries, USA
Water Bath	GFL Instruments, Germany
Weighing Balance	Sartorius (BP110 S)
X-ray machine	GE Pantak, Germany

2. Disposable elements

1.5 and 2 ml tubes	Eppendorf, Germany
15 & 50 ml Centrifuge Tubes	BD Falcon, USA

Cell Culture Dishes	Cell Star, USA
Flasks and beakers	Schott Duran, Germany
Parafilm	Lab Depot Inc. USA
Spinner Flask	Bellco, USA
Cuvettes	Hellma, Germny

3. Chemical reagents

Albumin Bovine	Sigma-Aldrich, USA
Bromophenol Blue	Sigma-Aldrich, USA
EDTA	Roth, Germany
Ethanol	Roth, Germany
FCS/FBS	Gibco Life Sciences, USA
Glycerol	Roth, Germany
Glycine	Roth, Germany
Isopropanol	Roth, Germany
KCl	Roth, Germany
Luria Agar	USB Corp, USA

Luria Broth	USB Corp, USA
McCoy's 5A	Sigma-Aldrich, USA
Methanol	Sigma-Aldrich, USA
ProLong Gold Antifade solution	Invitrogen, USA.
Propidium Iodide	Sigma-Aldrich, USA
TRIS Base	Roth, Germany
Tris-HCL	Sigma-Aldrich, USA
Triton X-100	Roth, Germany
Trypsin	Biochrom, Germany
Tween 20	Roth, Germany

4. Cell Lines

Table 1: Cell Lines Used

Species	Name	Cell type	Description
Chinese hamster	CHO-10B4	Fibroblast	Repair proficient
Chinese hamster	irs1 SF	Fibroblast	Mutation in XRCC3
Chinese hamster	XR-C1-3	Fibroblast	Mutation in DNA-PKcs

Materials and Methods

Chinese hamster	xrs6	Fibroblast	Mutation in Ku 80

5. Plasmids

Table 2: Plasmids Used

Name	Description
pCMV 3xnls-I*Sce*I	I-SceI expressing plasmid (M. Jasin)
pGFP-53BP1	Expresses a 53BP1-GFP fusion protein
pEGFP-N1	Fuses EGFP to C-terminus of partner protein
pEGFP-KAP1	Expresses a KAP1-EGFP fusion protein
I-SceI-TREX-BFP	I-*Sce*I-TREX chimera plasmid (Bennardo, Cheng et.al. 2008)

6. Oligonucleotides sequences

Table 3: siRNA sequences used from Nicolas Mermod [103]

Name	Sequences
Rad51	GUGCCAAUGAUGUGAAGAA
	GGGAAUUAGUGAAGCCAAA
	GGCGUUCAGAAAUCAUACA
Rad52	CCCUGAAGACAACCUUGAA
	UGAGAUGUUUGGUUACAAU

	ACUGCAUUCUGGACAAAGA
Ku80	GAAACUGUCUAUUGCUUAA
	CCAUAGGGAAGAAGUUUGA
	GGAUUCCUAUGAGUGUUUA
CtIP	GUGCAAGGUUUACAAAUAA
	CAAAGUCCCUGCCAAACAA
	AGAAUACUCUCCAGGAAGA

7. Inhibitors

Table 4: List of Inhibitors used

Name	**Description**
PJ34	PARP 1 inhibitor
NU7441	DNA-PKcs inhibitor
VE-821	ATR inhibitor
BO2	Rad51 inhibitor
Colcemid	Arrest cells in metaphase
Rad52	6-Hydroxy-DL- DOPA

8. Antibodies

Table 5: Primary and Secondary Antibodies used

Method	Name	Provider
Immunofluorescence	***Primary Antibodies***	
	ɣ-H2AX (mAb)	Abcam plc
	53BP-1 (rPab)	Santa Cruz Bio
	Rad51 (mAb)	Genetex
	Secondary Antibodies	
	Alexa Fluor 488; 568 (mAb; rAb)	Invitrogen, Germany
Western Blot	***Primary Antibodies***	
	Rad51 (mAb)	Genetex
	Rad52 (rPAb)	Santa Cruz Bio
	Ku80 (rAb)	Cell Signaling
	CtIP (mAb)	Santa Cruz Bio
	Gapdh (mAb; rAb)	Millipore ;Santa Cruz Bio
	Secondary Antibodies	
	IRDye 680 (mAb; rAb)	Li-COR Bio.

9. Software

Table 6: Table of used Softwares

Name	Provider
Adobe Creative Suite® 5.5	Adobe Systems, USA
ImarisXT® 6.0	Bitplane AG, Switzerland
Kaluza®	Beckman Coulter, USA
Las AF®	Leica Microsystems, Germany

Metafer®	MetaSystems, Germany
SigmaPlot® 12	Systat Software Inc. USA
WincycleTM	Phoenix Flow Systems, USA

Methods

1. Tissue cell culture

Cells were cultivated in 100 mm tissue culture dishes with 15 ml McCoy's growth media supplemented with 5% fetal bovine (FBS) and kept in incubators (Sanyo) at 37 °C with 5% CO2. Exponentially growing cells were passaged every two (CHO) days keeping them at a maximum confluence of less than 80%. For passaging, media was removed and cells were washed once with 1 x PBS. 2 ml of 0.05% trypsin-EDTA was added and incubated for less than 5 min at 37 °C to detach the adhering cells. Trypsin was inactivated by adding 5ml growth media and cells were re-suspended with a Pasteur pipette to reduce cell clumping. Cells were counted with the Coulter Counter (Multisizer™, Beckman Coulter) and appropriate numbers of cells were plated for subculture. Cells were discarded after approx. 30 passages. When frozen cells were thawed, they were passed three times before performing experiments with them.

2. X-ray irradiation

To induce DNA damage, cells were irradiated at various doses using an X-ray unit (Precision X-ray, North Branford, CT) operated at 320 kV and 10 mA. A 1.65 Al filter at a distance of either 50 cm (for irradiation of 60 mm dishes) or 100 cm (for irradiation of 100 mm dishes) was used at a dose rate of ~3.7 Gy/min or 1.68 Gy/min respectively.

3. Inhibitor treatments

Inhibitors were dissolved in dimethyl sulfoxide (DMSO) and were added to the culture medium 2 hours after transfection. Colcemid was added for 2 hours before collection of cells for cytogenetic analysis. To measure the contribution of different DSB repair pathways cells were treated with

various inhibitors. **Table 1** gives an overview of these inhibitors, their mode of action and the protocols of their application in experiments.

Table 7: List of inhibitors used in experiments

Inhibitors Name	Working Concentration	Administration
Colcemid	0.1µg/ml	24hrs after transfection for 2hrs
NU7441	5µM; and 10µM	2hrs after transfection
PJ34	5µM	2hrs after transfection
VE-821	5µM	2hrs after transfection
BO2	25µM	2hrs after transfection
6-Hydroxy-DL- DOPA	10µM	2hrs after transfection

4. Transfection by electroporation

The Amaxa Nucleofector device was used for transfection. $1x10^6$ to $5x10^6$ exponentially growing cells were transfected with 1000 ng plasmid/$1x10^6$ cells. The cells were trypsinized, centrifuged at 1500 rpm and dissolved in 100 µl transfection reagent HB buffer. The solution was mixed with calculated amount of plasmid and transferred to the electroporation cuvette. A transfection program of U-23 was used for CHO cells. After transfection the cells were transferred to growth media. Transfection efficiency, measured by FACS analysis of pEGFP-N1 or pGFP-53BP1/pEGFP-KAP1 transfected cells, varied between 85-95% for CHO cells.

5. Classical Cytogenetic Assay

For classical cytogenetics, $1x10^6$ I-*Sce*I transfected and $1x10^6$ mock transfected cells were plated for the 24 h time point. 24hours post I-SceI transfection metaphases were accumulated by adding colcemid 2h before collecting the time point. Working concentration for Colcemid used is 0.1µg/ml. Due to Colcemid treatment the cells accumulated at metaphase. At metaphase, cells

round up and detach, the rest can be trypsinized and collected. The cells were collected and centrifuged at 1500 rpm for 5 min. The media was removed leaving 1 ml behind to dissolve the pellet. 10 ml of hypotonic solution (75 mM of KCl) was added dropwise while slightly tapping the tube and incubated for 10 min at RT. After 7 min centrifugation at 1200 rpm the supernatant was removed, cells were resuspended and fixed in 10 ml fixative (3:1 methanol: glacial acetic acid) and kept at 4 °C overnight. After washing the cells twice in fixative, metaphase spreads were prepared and stained in 3% Giemsa stain, dissolved in 1 x Sörensen`s buffer for 15 min and washed with tap water. The slides were air dried at RT overnight and finally mounted with coverslips using Entellan® (Merck). Either the metaphase spreads were scored manually using Bright field microscopy (Olympus VANOX-T, Japan) or an automated imaging system (MetaSystems) was used to obtain high quality images of metaphase chromosomes. For searching metaphases the M-Search module of the Metafer software (MetaSystems) was employed, using the 10x objective of the Zeiss microscope. A classifier was used for M-Search that was specifically trained for the selected cell line. After performing M-Search, metaphases with good spreading were selected and captured at a higher magnification (63x oil immersion objective) using the AutoCapt setting of the Metafer software. Images were analyzed using the Metafer Software. For analysis approximately 100 metaphase spreads were scored in multiple experiments. The data shows the average of breaks or translocations in the multiple experiments with the error bars representing the standard deviation.

6. Immunofluorescence staining

For measuring ɣ–H2AX, 53BP1, and Rad51 foci formation using immunofluorescence staining, $0.5x10^6$ to $1.0x10^6$ transfected cells were plated in 35 mm dishes with 2 ml growth medium. 8h or 15h and 24h (depending on the experiment as mentioned in the result section) after transfection the growth media was removed, cells were washed with PBS and fixed in 2 ml 2% paraformaldehyde (PFA) containing 2% sucrose for 15 min. Cells were washed again 3 times for 5 min each in PBS and permeabilized in 2 ml P-solution (100 mM Tris, [pH 7.4], 50 mM EDTA, 0.5% Triton X-100) for 10 min. After washing, cells were blocked in PBG (0.2% gelatin, 0.5% BSA in PBS) at 4 °C overnight. The primary antibody was diluted accordingly (Table 8) in PBG and 90-100 µl dissolved antibody was pipetted on Parafilm. The cover slips were placed on the antibody solution and incubated for 2h at RT. After returning the cover slips into the dishes they

were washed with PBS (PBS) 3 x 5 min at RT. In the next step the cells were incubated for 1.5h at RT in the dark with the secondary antibody diluted 1:400 and washed 3 x 5 min each in PBS. The cells were then incubated with DAPI (50 ng/ml for 10 minutes at RT and finally washed again 3 x 5 minutes each with PBS. The coverslips were mounted with 15 µl ProLong Gold antifade mounting media (P-7481, Invitrogen), heated at 50ºC. Before scanning, slides were kept at 4 °C in dark. Scanning of the slides was carried out on a Confocal Laser Scanning Microscope (CLSM) from Leica Microsystems (DMI 6000 B).

Table 8: Working dilutions of Primary and Secondary Antibodies

Name	Dilution	Host species	Type	Provider
ɣ-H2AX	1/400	Mouse	Monoclonal	Abcam plc
53BP-1 (rPab)	1/400	Rabbit	Polyclonal	Santa Cruz Bio
Rad51 (mPab)	1/400	Mouse	Monoclonal	Genetex
Alexa Fluor 488; 568	1/400	Goat	Polyclonal	Invitrogen

7. Foci analysis by Imaris

The analysis of the LIF files (three dimensional data sets) that were generated after scanning was performed using the Imaris® software (Imaris 6.0; Bitplane). For foci scoring, images of timeframes ranging from 8 h or 15h and 24 h were loaded and foci of cells captured in 5-10 different fields were counted for each time point. Foci were defined as spots of higher intensity than the defined threshold and with minimum size of 0.5 or 0.7µm. The data was analyzed with Microsoft Excel and graphs were plotted with SigmaPlot® 12.0

8. Cell Cycle analysis by FACS

Fluorescence-activated cell sorting (FACS) is a specialized type of flow cytometry that allows cell sorting by assessing fluorescence intensity. Cell cycle distribution was evaluated by measuring the propidium iodide (PI) fluorescence intensity. The stoichiometry of PI binding to DNA is sequence independent, making it a convenient means of quantification. Cells were

washed with 1 x PBS, trypsinized at 37 °C for 5 min and re-suspended in growth media. $1x10^6$ non transfected or transfected cells were collected and centrifuged with 100 x g at 4 °C for 5 min. The media was removed, the cell pellets dissolved in cold 70% ethanol and stored at -20 °C overnight. Next the cells were centrifuged (100 x g, 5 min), the supernatant was removed and the cells were re-suspended in 800µl PI staining solution (40µg/ml PI, 62µg/ml RNaseA dissolved in PBS) per $1x10^6$ cells for 20 min. at 37 °C. The samples were measured in a flow cytometer (Coulter Epics XL, or Gallios™, Beckman Coulter) according to pre-established protocols that were optimized for each cell line. To obtain standard histograms 15000 events were counted, and gated. LMD data files were analyzed using the Kaluza® flow cytometry analysis software. Cell cycle distribution calculations were made by WinCycle® software using the generated HST files.

9. Colony forming assay

To assess the colony forming ability of CHO-clones after expression of I-SceI, 250–1000 cells were plated in duplicates after transfection with pCMV3xnlsI-SceI plasmid. Cells were grown for 7 days and stained with 1% crystal violet dissolved in 70% ethanol. Colonies were counted using a low magnification binocular microscope. Transfection with the GFP expressing plasmid GFP-53BP1/Kap1/pEGFP served as a control to estimate transfection efficiency. The transfection efficiency was estimated by flow cytometry measurement of the GFP fluorescence signal, 24 h after transfection.

10. siRNA knock down assay.

To assess the effect of depletion of specific proteins on formation of chromosomal translocations, the CHO clones were transfected first with specific siRNAs (cocktail of all the three oligonucleotides was prepared) on day 1 and were seeded in the 100 mm cell culture dishes. 5µl of the siRNA was used to deplete the specific protein in 3.5 million cells. 24 hours later the seeded cells were again transfected with specific siRNA and I-SceI expressing enzyme. The metaphase spreads were prepared to score chromosomal aberrations using classical cytogenetics, in a way similar to that described above. The list of oligonucleotides that were used are provided in the Materials section (refer to Table 3).

11. Preparation of whole cell lysate

Whole cell lysates were prepared using $2x10^6$ cells. After washing in 1 x PBS and pelleting, cells were dissolved in 100-200 µl RIPA buffer. 1x protease inhibitor cocktail (10µl for 1 ml) was added to the reaction mixture and incubated for 15 min on ice. The mixture was centrifuged at 12000 x g for 15 min at 4 °C and then was sonicated, kept on ice for 15 minutes and finally transferred to a new tube. The colorimetric Bradford assay was applied to measure protein concentration using a calibration curve generated with different amounts of BSA.

12. SDS-PAGE

Cell lysates were resolved on 10% polyacrylamide gels. For loading 50µg cell extract were mixed in a 1:1 ratio with 2x Laemmli Buffer, denatured for 5 min at 96 °C and centrifuged briefly at 12000 x g. SDS-PAGE mini gels were prepared using casting stand (Bio-Rad) according to the manufacturer's instructions. For electrophoresis a constant voltage of 130 V was set for 1.5 h.

Table 9: SDS-PAGE

	5 ml Stacking Gel (5%)	5 ml Resolving gel (10%)
Mon. Sol.	840 µl	1.7 ml
4 x SGB (0.125 M)	1.25 ml	-
4 x RGB (0.37 M)	-	1.25 ml
Milli-Q water	2.8 ml	1.9 ml
10% SDS	50 µl	50 µl
10% APS	50 µl	50 µl
TEMED	10 µl	5 µl

13. Western Blot

During Western blotting the proteins are transferred from the SDS-polyacrylamide gel onto a nitrocellulose membrane. Therefore blotting paper (GB004 Whatman), transfer sponge and nitrocellulose membrane of the desired size were prepared and equilibrated in cold 1 x transfer buffer (consisting of 25% 4 x electrode buffer at pH 8.3 (0.1 M Tris-HCl, 0.7 M glycine) and 20% methanol). All components were assembled together with the gel into the electro-transfer unit according to the instructions of the manufacturer (Bio-rad) and run at 100 V for 60 min.

After transfer the membrane was incubated for 2 h in 5% non-fat dry milk in 1 x TBS-T (0.05% Tween20 in 1 x PBS). For immuno-detection the membranes were incubated overnight at 4 °C with the primary antibody. After washing three times for 10 min in PBS-T the secondary antibody was incubated for 2 h and the membrane was again washed three times in PBS-T prior to detection. The antibodies were diluted in 5% blocking solution with different dilutions depending on the manufacturer's protocol for the specific antibody. The Odyssey® Infrared Imaging System from LI-COR Biosciences was used for detection and analysis.

Table 10: Working dilutions of Primary and Secondary Antibodies

Name	Dilution	Host species	Type	Provider
Rad51	1/500	Mouse	Monoclonal	Genetex
CtIP	1/200	Mouse	Monoclonal	Santa Cruz Bio
Ku80	1/1000	Rabbit	Polyclonal	Cell Signaling
Rad52	1/500	Rabbit	Polyclonal	Santa Cruz Bio
Gapdh	1/10000	Mouse	Monoclonal	Millipore
Gapdh	1/10000	Rabbit	Polyclonal	Santa Cruz Bio
IRDye 680	1/10000	Mouse	Polyclonal	Li-COR Bio.
IRDye 680	1/10000	Rabbit	Polyclonal	Li-COR Bio.

14. Transformation and amplification of plasmid DNA in E.coli

To obtain a sufficient amount of the I-SceI plasmids for the transfection based experiments, plasmids were transformed into the E. coli strain (DH5α) strain by heat shock. For the transformation 50 µl competent XL-1 blue bacteria were mixed together with about 10 - 15 ng of the vector material and incubated for 10 minutes on ice. After a heat shock of 42°C for 50 seconds in the Eppendorf thermo-mixer, the sample was cooled for 10 minutes on ice again. Then 950 µl LB-Medium was added and incubated on a 220 rpm shaker for 1.5 hour at 37°C. 25 and 50 µl of the bacteria suspension was taken and plated on a LB-agar dish with ampicillin resistance for I-SceI plasmids and incubated overnight at 37°C. Single colonies were transferred in a 2 - 5 ml LB medium and incubated for 12 hours on the shaker at 37°C. The bacteria culture was then used to inoculate 200 ml of LB medium. The 200 ml bacteria suspension was grown

overnight at 37°C. Agar dishes and LB medium were supplemented with antibiotics according to the resistance of the plasmids (100ng/ml).

15. Isolation and purification of plasmid DNA

To isolate larger amounts of plasmid DNA, the NucleoBond® Xtra Midi EF endotoxin-free plasmid DNA purification kit from Machery-Nagel (Düren, Germany) was used. In this kit the plasmid is purified by a modified alkaline lysis. The bacterial suspension was transferred into the 50 ml falcon tubes and centrifuged at 4,000 x g for 30 minutes at 4°C. The bacterial pellet was treated further according to the manufacture's protocol with the following differences: At step 14 the centrifugation was performed at 4,000 x g for 1 h at 4°C and at step 15 for 30 minutes.

16. Determination of nucleic acid concentration using Nano Drop

The NanoDrop was used to monitor the purity and concentration of the isolated plasmid DNA. Before the DNA concentration was determined, 1µl TE-EF was pipetted onto the Nano-drop detector and defined as blank. In the next step 1µl of the isolated plasmid DNA that was dissolved in TE-EF and was transferred on the NanoDrop and the optical density of 260 and 280 nm was measured. Based on their respective ring structure and double bonds the bases of the nucleic acids absorb, in the UV-range of 260 nm, while amino acids like tryptophan and phenylalanine show their maximum at 280 nm. The sample was classified as sufficiently pure when the measured ratio was in the range of 1.7 – 2.0. The so purified gRNA and Cas9 plasmids were used for transfection experiments.

17. Restriction digestion of genomic DNA

The digestion of genomic DNA, 15µg of genomic DNA was used for each reaction. Per µg DNA, 0.3 Fast Digest Unit (FDU) of the enzyme were used. The following components were added to the reaction:

DNA X µL (15µg)
FD Restriction Enzyme 4.5µL (4.5 x 1FDU)
FD Restriction Enzyme Buffer (10x) 20µL
Water 200µL

For complete digestion, the reaction mixture was incubated without the enzyme for 30 min at 4°C shaking in a Thermo-mixer. After adding the enzyme the reaction was incubated for 5 hours at 37°C and shaken every 15 min for 15 min.

18. Agarose DNA Gel-electrophoresis

Agarose DNA Gel-electrophoresis was used to separate DNA Sequences according to their size. For running Gels with genomic DNA an 0.8% Agarose gel was prepared by adding 0.8 g Agarose to 100mL 1 x TAE buffer and heating in the microwave. After complete melting of the Agarose, it was poured into a gel chamber of 10 x 7 cm and was left for polymerization. After completely covering the gel with TAE buffer the samples were loaded on the gel with 1/10 Vol. of Fermentas Loading Buffer (6x). The gel was run at 0.5 Volts/cm for 6 hours. The DNA was stained in 50 ml 1 x TAE with 1% Ethidium bromide (EtBr) for 30 min while shaking.

Results

Overview of the CHO model system utilized to investigate the repair of single DSBs and DSB clusters

This section describes in brief the I-SceI based model system that has been previously developed in the Institute of Medical Radiation Biology. We provide an overview of the design and the characterization of this model system that is designed to evaluate the effect of DSB clustering on DSB repair pathway efficiency, cell survival and formation of chromosomal translocations.

DSB clusters of increasing complexity

It is well documented that exposure to high-LET IR results in the generation of complex DSBs and particularly DSB clusters that are speculated to be involved in the increased cell lethality observed after exposure to high-LET IR. However, formation of DSBs by high-LET is associated with additional chemical modifications of DNA bases, as well as with the generation of single strand breaks, which out-number the amount of DSBs generated. To emulate the formation of high-LET generated DSB clusters, an artificial I-SceI based model system was designed. This system allows controlled formation of DSB clusters of increasing complexity in the genome of the corresponding cell lines. In order to achieve this, multiple copies of different size clusters of I-SceI recognition sequences in different orientations were integrated into the genome of CHO cells.

A single I-SceI site represents the simplest directly ligatable form ('D') and serves as control 'single-DSB' in our model system (CHO1xS.D8). The next construct comprises a pair of I-SceI recognition sequences, engineered 200 bp apart, which are either directly oriented to generate ligatable DSB ends (CHO 2xS.D12), or placed in reverse orientation to generate incompatible DSB ends (CHO 2xS.R14). The highest level of clustering complexity investigated comprises of quadruplets of I-SceI-sites engineered at an overall distance of 462 bp in reverse orientation to generate incompatible DSB ends (CHO 4xS.R12) [104]; refer to Figure 18 (taken from [104]. "Therefore, each DSB cluster thus generated is considered as a single chromatin-rupture event of 'complexity' proportional to the number of DSBs present". It is relevant to point out yet again that this model system allows investigation of the effects of "clean DSBs and DSB-clusters" only.

However, it only approximates the complex damage generated by high-LET IR and only with reference to the potential induction of clusters of DSBs [105].

Different complexity levels that were achieved in our CHO based model system and are extensively used in this thesis work are:

i. Simple DSBs (single DSBs) and complex DSB clusters (DSB pairs and DSB quadruplets) (Figure 18 a).

ii. Different degrees of DSB clustering within the same types of I-SceI constructs (DSB pairs), were characterized using southern blotting (Figure 18 c) [104] to estimate the number of integrated I-SceI sites.

iii. DSB clusters with compatible DSB ends ("D") and incompatible DSB ends ("R"). Compatible apical ends in DSBs signify that the DSBs do not require end processing before ligation; and for DSBs having incompatible ends that DNA end-processing will be necessary (Figure 18 a).

iv. DSB clusters have also been integrated in cell lines mutated in c-NHEJ (DNA-PKcs and Ku80) and HRR (XRCC3).

Transient expression of I-SceI endonuclease enzyme into the genome of corresponding cell lines allows the generation of simple DSBs and DSB clusters. At each individual I-SceI site, I-SceI mediated cutting of DNA may be followed by multiple cycles of ligation and re-cutting, which in the presence of DSB-clusters may increase the probability for occasional intervening-fragment-loss, although our model system is not specifically selecting for such events. The distance between adjacent I-SceI sites was chosen as 200 bp as this distance is approximately equal to the average nucleosomal DNA length in chromatin. We reason that this may increase the probability of fragment loss in the DSB-cluster [104, 105].

Each chromatin-rupture event corresponds to DSB lesions of complexity that is proportional to the number of DSBs involved. Attempts to restore the ruptured chromatin may occur by directly ligating the proximal and more stable (in the chromatin context) apical DNA ends; and also by a number of other non-canonical processes (investigated in this thesis) that underpin the negative biological consequences studied [104].

A list of CHO cell clones (normal and mutants) used in this thesis work, their properties in terms of DSB cluster complexity and number of integrations, as well as their designation are discussed in the section below and summarized in Table 11. The details about the methods of generation of

such clones, as well as the precise design of the DSB clusters, are described in the following section (Figure 18 b) and is taken from the previously published work [104], [105] [47].

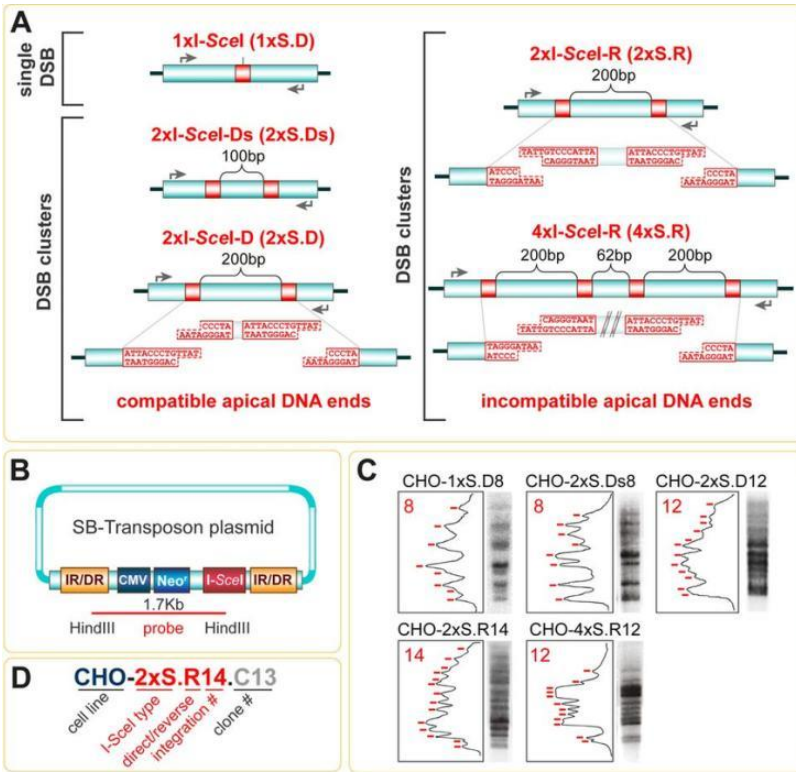

Figure 18: *Approach to generate cell lines with multiple genomic integrations of I-SceI constructs allowing induction of single-DSBs, or DSB-clusters.*

(A)Constructs carrying different combinations of I-*Sce*I sites engineered at specific distances and orientations. The schematics illustrate constructs allowing the generation of single-DSBs, of DSB-pairs at a distance of 200 bp, as well as of DSB quadruplets. In constructs harboring two of more I-*Sce*I sites, the orientation between the sites (Direct: D or Reversed: R) is also indicated, as it results in the generation of compatible or incompatible apical DNA ends after loss of the intervening sequence. The grey arrows represent the locations of forward and reverse primers utilized to amplify the corresponding DNA segment for junction analysis by sequencing. (B) Map of the SB-transposon plasmid carrying the I-*Sce*I construct. The transposase binding sites comprising the IR/DR regions are shown. The region of the plasmid used as a probe in Southern blot analysis is indicated by the red line. CMV–cytomegalovirus promoter, Neo–neomycin resistance. (C) Southern blots analysis of CHO clones obtained after transfection with SB-transposon constructs harboring 1xS.D, 2xS.Ds, 2xS.D, 2xS.R and 4xS.R sites. The number of bands reflects the number of integrations. The densitometry plots on the left show the quantification basis regarding number of integrations in each clone. (D) Outline of the conventions used to name the clones employed in the present work. After the name of the parental cell line (CHO, or XRC1-3), the type of the integrated construct (1xS, 2xS and 4xS) is given, followed by information regarding the relative orientation of the apical I-*Sce*I sites (D-direct or R-reverse). The Ds abbreviation indicates the direct orientation of two I-*Sce*I sites separated by a shorter distance of 100 bp—instead of

Results

the typical distance of 200 bp used in other pairs. The number immediately after orientation represents the number of I-*Sce*I integrations detected in the clone (shown in C for CHO cells). The last component of the name refers to the specific clone (Cx) and is omitted for simplicity in the description of the results. Taken from [104]

Clonal cell lines with multiple genomic integrations of I-SceI recognition site constructs

CHO10B4 cells were selected for the integration of I-SceI constructs and used in the first place in these experiments because they have excellent growth characteristics. The availability of multiple mutants defective in specific DNA repair pathways allows in the Chinese hamster genomic background more comprehensive genetic analysis of the elicited responses. Here, in addition to wt CHO cells, clones with stably integrated I-SceI constructs were generated in the XRC1-3 mutant, lacking DNA-PKcs activity; in the xrs6 cells that are deficient in Ku80. XRCC3 mutants deficient in HRR (irs1 SF) were also stably integrated with I-SceI constructs.

A key step in the development of the model system was the generation and characterization of clonal cell lines with multiple integrations of each I-SceI construct (single, duplets or quadruplets) to allow induction of multiple DSBs or DSB-clusters in each cell line, thus, mimicking the DSBs induced after exposure to IR. This allows the analysis of the consequences of multiple DSBs and DSB clusters on cell survival, genome stability and DDR [104, 105].

To achieve multiple I-SceI-construct integrations in the genome of the selected cell lines, the Sleeping-Beauty (SB) transposon system was utilized (Figure 18 b). The SB transposon mediates efficient chromosomal integration of DNA sequences by a cut-and-paste mechanism. Specifically, SB-transposition is based on two non-autonomous transposon elements: the transposon-donor plasmid, pT2/SVNeo, and the hyperactive SB-transposase-expressing, helper-plasmid pCMV(CAT)SB100x, which catalyzes the transposition event [104]. For efficient genomic integration at multiple copies by transposition, I-SceI constructs are cloned into pT2/SVNeo plasmid between the inverted/direct-repeats (IR/DRs) at the EcoRI restriction site and co-transfected with pCMV(CAT)SB100x. Expanded, neo-resistant clones are analyzed by Southern blotting to determine the number of integrations [104]. The number of integrations detected visually, as well as by densitometry, denotes the number of single-DSBs or DSB-clusters that may be generated in each clone upon expression of I-SceI via transfection of pCMV3xnls-I-*Sce*I plasmid [104].

From the entire selection of available integration-characterized clones, the CHO cells (normal and mutants) that were selected for this thesis are described below in the Table 11. For cell line nomenclature-conventions (Figure 18 c): CHO 1xS.D8.C12 (CHO clone 12, with eight integrations of a single I-*Sce*I site), CHO 2xS.D12.C8 (CHO clone 8, with twelve integrations of I-SceI site pair separated by 200 bp in direct orientation generating DSBs with compatible apical ends), CHO 2xS.R2.C6 (CHO clone 6 , with two integrations of I-SceI site duplets separated by 200 bp in reverse orientation generating incompatible apical ends), CHO 2xS.R6.C5 (CHO clone 5, with six integrations of I-SceI site duplets separated by 200 bp in reverse orientation generating incompatible apical ends), CHO 2xS.R14.C13 (CHO clone 13, with fourteen integrations of I-SceI site duplets separated by 200 bp in reverse orientation generating incompatible apical ends), CHO 4xS.R12.C3 (CHO clone 3, with 12 integrations of I-SceI site quadruplets comprising two pairs separated by 62 bp in an orientation generating incompatible apical ends), XRC1-3 2xS.D10.C7 (XRC1-3 clone 7, a DNA-PKcs mutant, with 10 integrations of I-SceI site duplets separated by 200 bp in direct orientation generating compatible apical ends), XRC1-3 2xS.R10.C1 (XRC1-3 clone 1, with ten integrations of I-SceI site duplets separated by 200 bp in reverse orientation generating incompatible apical ends); xrs6 2xS.R11.C4 (xrs6 clone 4, a Ku80 mutant with 11 integrations of -SceI site duplets separated by 200 bp in reverse orientation generating incompatible apical ends); irs1 SF 2xS.R4.C7 (irs1 SF clone 7, XRCC3 mutant with 4 double I-SceI sites separated by 200 bp in reverse orientation generating incompatible apical ends). To simplify cell line designation in the remainder of the thesis the designation of the clone has been omitted from last position.

Table 11: CHO clones (normal and mutants) their nomenclature and properties.

Cell Line Name	Number of Integrations	Mutation	ISceI orientation
CHO 2xS.R2.C6 CHO 2xS.R6.C5 CHO 2xS.R14.C13 CHO 4xS.R12.C3 CHO1xS.D8.C12 CHO2xS.D12.C8	(2) (6) (14) (11) (7) (12)	Wild Type	Reverse Direct
XRC1-3 2xS.R4.C3 XRC1-3 2xS.R7.C3 XRC1-3 2xS.R10.C1 XRC1-3 2xS.D4.C4 XRC1-3 2xS.D10.C7	(4) (7) (10) (4) (10)	DNA-pkcs	Reverse Direct
xrs6 2xS.R11.C4	(11)	Ku80	Reverse
irs1 SF 2xS.R4.C7 irs1 SF 2xS.D5.C4	(4) (5)	XRCC3	Reverse Direct

1. Optimization of the conditions to properly deliver I-SceI enzyme, into the CHO genome for induction of DSBs and DSB clusters

To elicit the biological response after transfection of cells with the I-SceI expressing plasmid, it was essential to ensure the optimal delivery of the I-SceI enzyme expressing plasmid into CHO cells. I-SceI expressing plasmid was transfected using Amaxa Nucleofector Program U-23. Since the first part of the results in this thesis compares the survival after induction of simple DSBs and DSB clusters in different CHO clones it was essential to have transfection efficiencies that didn't fluctuate much within the same experiment. GFP tagged plasmids were used to measure transfection efficiency 24 hours after the transfection using flow cytometry. It is extremely

important to maintain the plasmid properly and also to avoid constant thawing and freezing of the plasmid, as it might result in lower transfection efficiency.

Transfection efficiency measured using the GFP expressing plasmid is not the same as that of the I-SceI expressing plasmid, but it gives an approximate idea about the state of the cells used with reference to transfectability in that experiment. If the cells to be transfected are not in a proper growth condition, then the transfection by Nucleofection is not efficient and this might result in artifacts (due to presence of non-transfected cells), especially in survival experiments. By measuring the transfection efficiency using GFP tagged plasmid one might thus, have an assessment about the condition of the cells that were transfected. Transfection with I-SceI expressing plasmid didn't affect the cell cycle progression of the transfected cells. Transfected cells were stained with PI stain after 24 h, and the cell cycle analysis was done using flow cytometry.

In the Figure 19 some representative images of transfection efficiency obtained after FACS analysis are shown. Transfection efficiency in CHO clones (CHO 1xS.D8, CHO 2xS.D12, CHO 2xS.R6, CHO 2xS.R14, CHO 4xS.R12), and c-NHEJ mutants (XRC1-3 2xS.R10, and xrs6 2xS. R11) typically ranged between 80-90%.

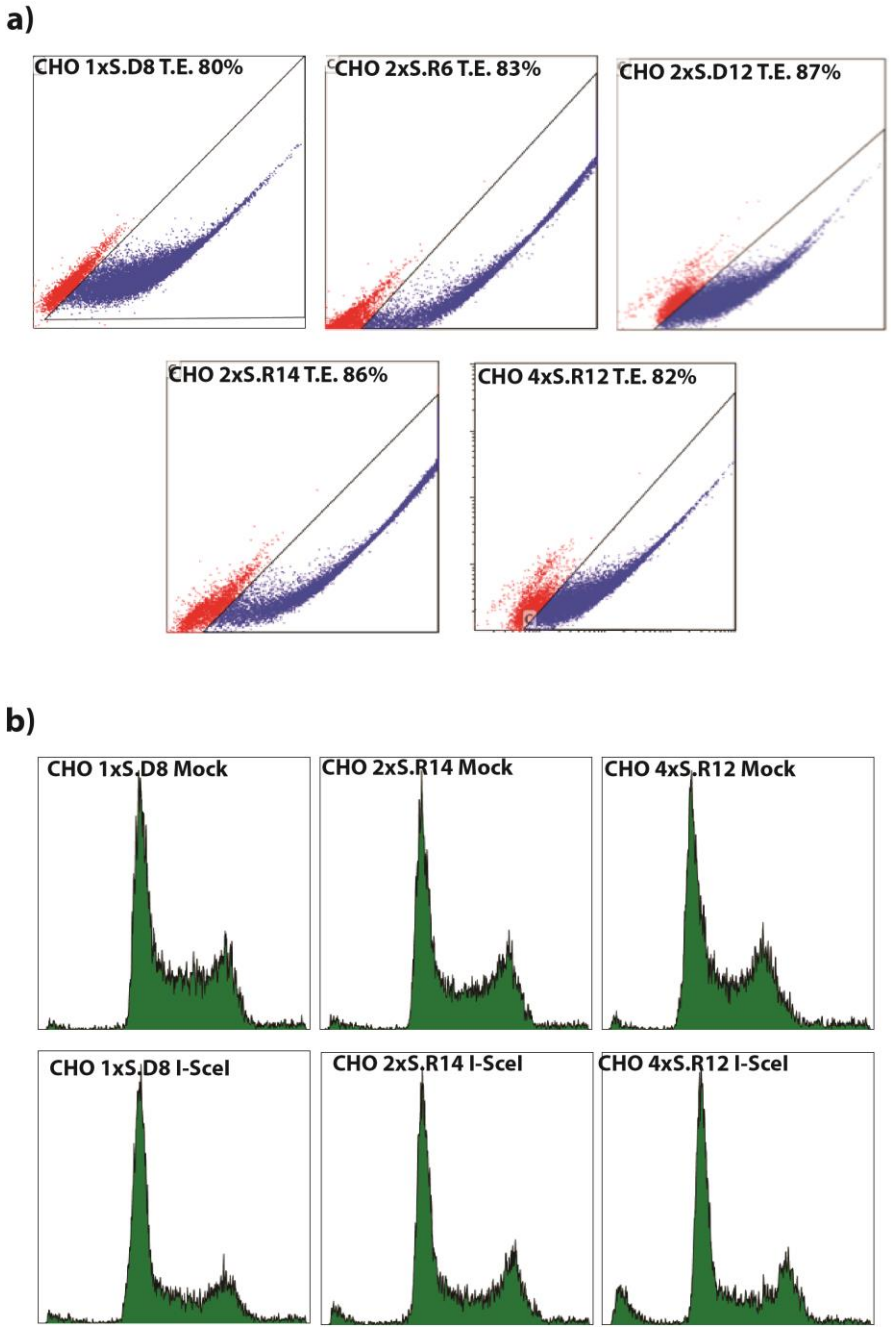

Figure 19: *Transfection efficiency measured in CHO clones.*

a) Representative images of transfection efficiency (T.E.) scored in CHO clones harboring single DSBs and DSB clusters, measured using flow cytometry. The cells were collected 24 h after the transfection with GFP tagged plasmids. Typically T.E. measured was between 80-90%. b) Cell cycle analysis measured using flow cytometry in Mock transfected and I-SceI transfected cells, collected 24 h post nucleofection.

Results

2. DSB clusters and their effect on DDR signaling and DSB repair

The colony formation/clonogenic assay [45] is widely used to evaluate the effect of cytotoxic agents. This assay determines the ability of a single cell to proliferate and form a colony. Clonogenic cell survival assays find wide application and are also used to examine the cytotoxic effects of other agents besides IR, like for example chemotherapeutic drugs. We employ the clonogenic survival assay in our experiments to estimate the effect of DSBs/clusters generated by the I-SceI endonuclease in the above described clones. The cell survival data clearly show that DSB clusters have an increased killing potential as compared to simple DSBs.

To estimate how this strong killing is mediated and in order to validate the survival assay results, we attempted to visualize the (mis)-repair of the enzyme-induced DSBs by analysis chromatid/chromosomal translocations. We have also scored the transformation of DSBs to chromosomal/chromatid breaks. To analyze and score the chromosomal/chromatid type of aberrations, we analyzed approx. 80-100 metaphases in I-SceI plasmid transfected cells after 24 hours by blocking at metaphase with colcemid for 2 hours.

2.1. With increasing complexity of DSB clusters cell survival decreases

To investigate how the complexity of DSB clusters influence the cellular survival, we first tested the survival of CHO clones harboring single I-SceI sites and pairs of I-SceI sites. We have also tested how the I-SceI site's integration numbers affect the cellular survival. For the following experiments clones with, low (2), intermediate (6) and high (14) integration number were used. We expanded our investigations to also include the most complex CHO clones harboring quadruplets of I-SceI sites. The following endpoints were investigated with our experiments: a) effect of DSB clustering on cell survival, b) effect of degree of DSB clustering on cell survival, and c) killing potential of DSB clusters having incompatible ends as compared to DSB clusters having compatible ends.

It has been shown previously that with increasing complexity of DSB clusters cell killing increases [104]**.** Simple DSBs generated after transfection with I-SceI expression plasmids, result in moderate changes in the survival of the corresponding CHO clones, while the generation of complex DSB clusters is associated with increased sensitivity to killing. Strikingly, maximum killing was observed in CHO clones, where efficient cutting at the integrated I-SceI sites, results

in the formation of clusters of four DSBs (4xS.R12). In the CHO clones where I-SceI mediated cutting results in formation of DSB pairs at each integrated site results in better survival than CHO 4xS.R12. But, when all the CHO clones having two I-SceI sites with different number of integration sites were compared, cells having lowest I-SceI integration sites (2xS.R2) survived best, the intermediate clone having six I-SceI sites (2xS. R6) survived less than CHO 2xS.R2, and the cells having fourteen (high) I-SceI integration sites had the worst survival (2xS.R14). This response suggests that with increasing degree of clustering there is increased cell killing (refer to Figure 20).

Another level of DSB cluster complexity was achieved by generating clusters of two I-SceI sites with either directly ligatable "D" DSB ends or incompatible DSB ends. Directly ligatable ends do not require end processing before ligation, while DSB clusters having incompatible ends require DSB end processing before ligation. When processing is required for repair, in "R" type CHO clones, we assume that the corresponding DSB clusters are more complex. Indeed, the results after transfection with I-SceI plasmid show that with increasing need for DSB end processing, there is decreased cell survival.

All the compiled results are presented in the graph below along with the representative scanned images of the colonies of surviving cells (Figure 20).

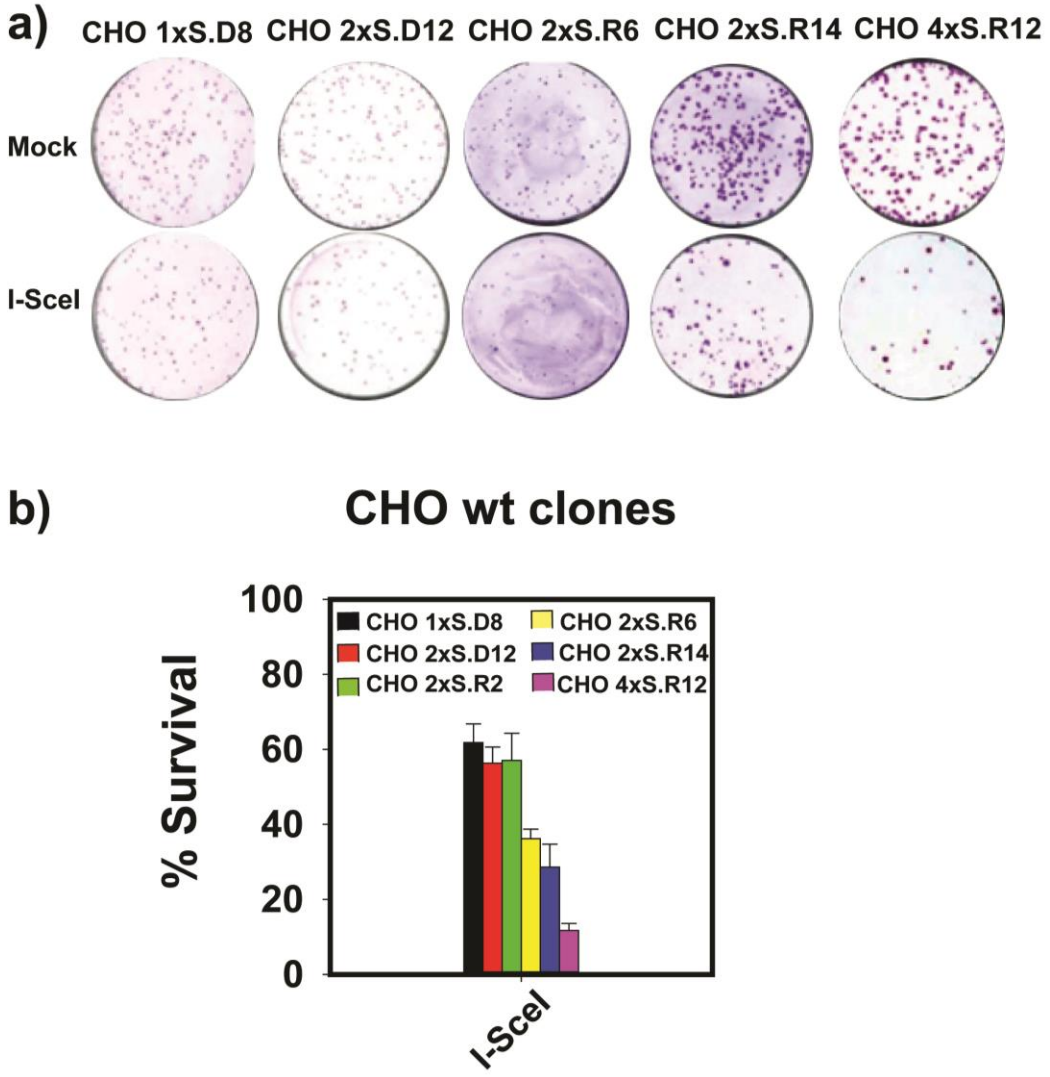

Figure 20: *Increase in degree of complexity of DSB clusters results in decreased cellular survival.*

a) Representative images of scanned petri dishes stained with 0.1% crystal violet, showing the colonies formed by indicated clones 7-8 days after transfection with I-SceI expression plasmid. b**)** Clonogenic survival experiments with CHO 1xS.D8, CHO 2xS.D12 clones, harboring I-SceI sites with ligatable DNA end and CHO 2xS.R2, CHO 2xS. R6, CHO 2xS.R14 and CHO 4xS.R12 cells with I-SceI sites with incompatible DNA ends. The percentage of cell survival was calculated using the plating efficiency of the corresponding mock transfected control clones. Data is compiled from two out of three experiments showing averages ± SD (n=2 for CHO 2xS.R2).

2.2. DDR signaling after generation of simple and clustered DSBs

After generation of DSBs a series of signaling events are triggered that are described in the Introduction. The results discussed in this section are obtained from the indirect

immunofluorescence analysis using confocal microscopy. Immediately after the induction of DNA damage several posttranslational modifications (PTM) arise in the vicinity. These PTM can be visualized as foci under the microscope and the proteins that are essential in DDR signaling get accumulated in these foci. The formation of ɣ-H2AX via phosphorylation of histone H2AX at serine 139 (S139) is a characteristic step among these PTM. These phosphorylated histone domains can be visualized in fluorescence microscopy as visible regions, where a wide range of downstream responses initiate. Another key protein that accumulates in these foci is 53BP1 that is recruited relatively downstream in DDR signaling cascade.

To assess if there is any difference between simple DSBs and DSB clusters in triggering and initiation of DDR response, ɣ-H2AX and 53BP1 foci were scored. One of the earliest events to take place in DDR signaling after DNA damage is phosphorylation of H2AX resulting in formation of ɣ-H2AX foci (a marker for DSB formation) at chromatin. The ɣ-H2AX formation is followed by MDC1 recruitment, followed by Rap80 and RNF8/RNF168 and then 53BP1 is recruited at the breaks. It is quick yet complex process and as the cell progresses through cell cycle Rad51 foci accumulate if the subsequent break is repaired using HRR. In the current set of experiments the presence of ɣ-H2AX foci and/or 53BP1 foci after transfection with I-SceI endonuclease enzyme also confirms the induction of DSBs after transfection.

2.2.1. In CHO wild type clones, numbers of ɣ-H2AX foci formed after induction of simple DSBs or DSB clusters closely match the number of I-SceI integration sites

It has already been reported from our laboratory [104] that complexity of DSB clusters has no impact on triggering of DDR and the accumulation of ɣ-H2AX foci formation. The cells were transfected with I-SceI expressing plasmid and were collected after 8 h and 24 h. Post collection, samples were stained with a specific primary antibody to detect the formation of ɣ-H2AX foci, a surrogate marker for the initiation of DDR signaling after induction of DSBs.

Activation of DDR signaling after transfection with I-SceI, thus confirms that the trends that are observed in survival and repair of cells after I-SceI transfection are indeed due to the formation of DSB clusters. An interesting observation that has been consistent with the previous findings [104] is that the CHO clones harboring either simple DSBs or clustered DSBs form ɣ-H2AX. The numbers of ɣ-H2AX foci that are formed closely match the number of I-SceI recognition sites

integrated into the genome of respective clones. The complexity of the DSB i.e. simple DSBs formed in CHO 1xS.D8 clone, or DSB pairs in CHO 2xS. “D12” and “R 2, 6 and 14” clones; or the DSB clusters in CHO 4xS.R12 clones, they all form the ɣ-H2AX foci that match the number of I-SceI integrations.

The number of I-SceI integration sites into the CHO genome was characterized earlier using Southern Blot technique and has been discussed elaborately in the previously published paper and above [47, 104]. The following results suggest that I-SceI induced DSBs trigger an efficient DDR response and almost all the DSBs and DSB clusters formed are recognized by the DDR apparatus.

While most of DSBs are repaired within 24 hours, some DSBs still remain. The presence of ɣ-H2AX foci remaining even 24 h after damage induction is an indicator of unrepaired breaks or of recurrent breaks. Only when the I-SceI site is mutated then the nuclease stops cutting. Thus, one may speculate that some of the I-SceI sites become accessible at different stages of growth forming ɣ-H2AX foci at later times.

The graph presented (Figure 21) below shows the numbers of ɣ-H2AX foci scored in CHO 1xS.D8, CHO 2xS.D12, CHO 2xS.R6, CHO 2xS.R14, CHO 4xS.R12 after 8 and 24 hours. It can clearly be seen that despite the varying complexity of the DSB lesions (clusters and compatible/incompatible DSB ends) the numbers of foci match their corresponding I-SceI integration sites.

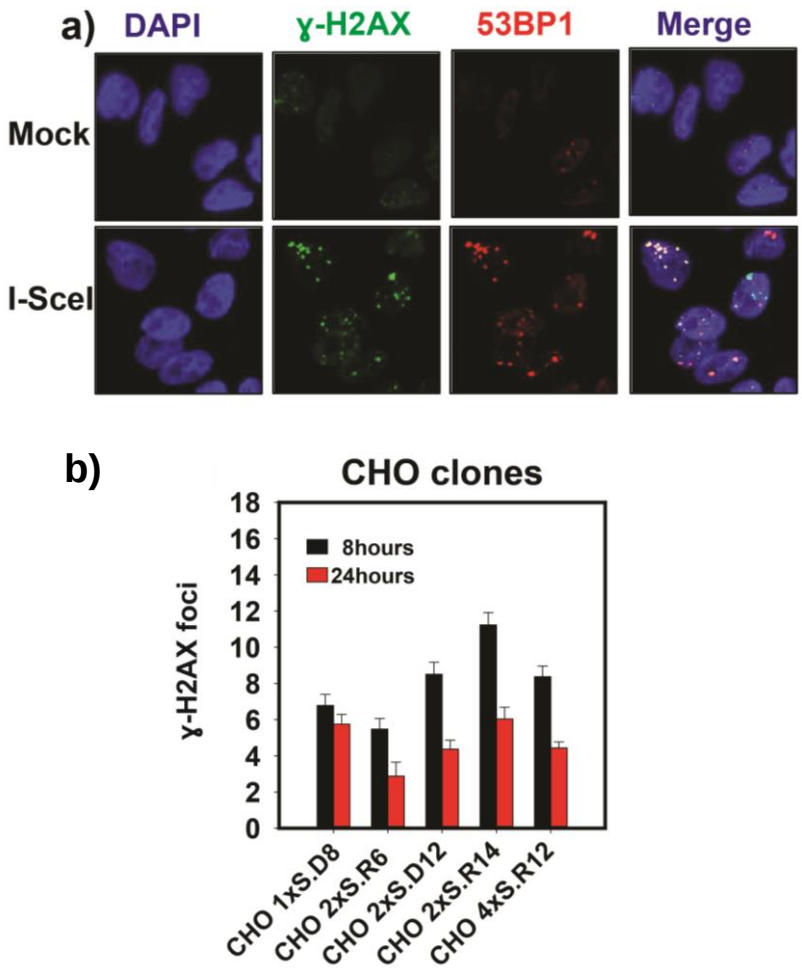

Figure 21: *Accumulation of ɣ-H2AX after I-SceI induced damage.*

Formation of ɣ-H2AX foci at I-SceI mediated single DSBs and DSB-clusters. a) Representative immunofluorescence images of ɣ -H2AX foci in CHO 4xS.R12 clone generated 8 h after transfection. b) Quantitative analysis showing averages ± SE from 2 independent experiments of ɣ-H2AX foci formation in mock transfected and I-SceI transfected cells. The number of foci scored in I-SceI transfected cells is background subtracted.

2.2.2. In comparison to simple DSBs, complex DSB clusters requiring end processing before ligation, show increased accumulation of 53BP1 foci

In our previous experiments prominent increase of ɣ-H2AX foci was observed in CHO clones transfected with I-SceI expressing plasmids in comparison to mock transfected clones. Interestingly, the number of ɣ-H2AX foci scored after transfection strongly correlated with the number of I-SceI integration sites for the indicated clones. This suggested that all I-SceI mediated DSBs have been successfully recognized and processed by the DDR apparatus independently of

their complexity. In order to evaluate how the later steps of DDR are executed and whether there is a DSB cluster complexity dependent response, we have designed experiments in which 53BP1 accretion into damage induced foci was examined. 53BP1 foci formation is strongly dependent on the availability of RNF8 and RBNF168 ubiquitin ligases and is considered as a DDR event, which fully activate DDR and initiate DSB repair by promoting c-NHEJ. In order to establish a connection between DSB cluster complexity and 53BP1 activation, we have scored 53BP1 foci in CHO clones with increasing DSB cluster complexity after mock transfection or transfection with the I-SceI expression plasmid. In the course of the experiments, cells were transfected with I-SceI plasmid and were collected for foci analysis 8 and 24h later.

The results shown in Figure 22 show the numbers of 53BP1 foci and it can be observed that in the CHO clones with increasing complexity of DSB clusters there is increased accumulation of 53BP1 foci. In the CHO clones having DSB clusters with compatible apical ends (CHO 2xS.D12), after I-SceI transfection lower numbers of 53BP1 foci are scored as compared to the CHO clone having DSB clusters with incompatible ends (CHO 2xS.R14). Interestingly, the CHO 2xS.R6 clone having six I-SceI sites in reverse orientation has similar numbers of 53BP1 foci as CHO 2xS.D12 clone. Even though the CHO 2xS.R6 clone yields only six DSB pairs and CHO 2xS.D12 twelve, still the necessity for end processing in the former clone results in greater accretion of 53BP1 foci.

The graph presented below in (Figure 22) shows the numbers of 53BP1 foci scored at 8 and 24 hours after transfection. Notably, in Figure 22 it can be observed that in every CHO clone that requires end processing for repair, the accretion of 53BP1 is increased. *This suggests that in contrast to ɣ-H2AX, 53BP1 shows increased response towards complex DSB clusters, or clusters requiring end processing.* Results are compiled in Figure 22.

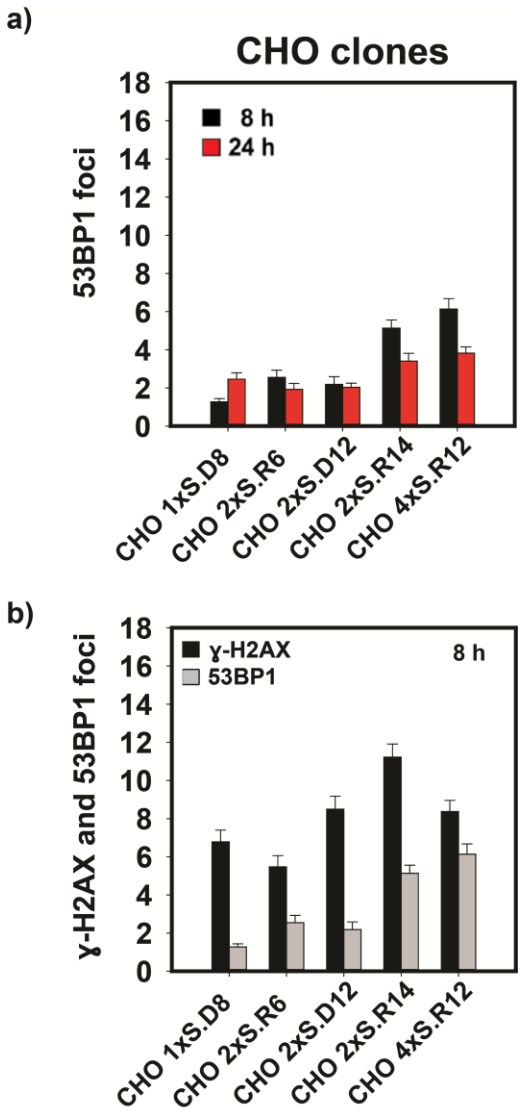

Figure 22: *Accumulation of 53BP1 foci after I-SceI induced damage.*

Formation of 53BP1 foci at I-SceI mediated single DSBs and DSB-clusters. a) Quantitative analysis showing averages ± SE from 2 independent experiments of 53BP1 foci formation in mock transfected and I-SceI transfected cells. The number of foci scored in I-SceI transfected cells is background subtracted. b) Quantitative analysis showing averages ± SE from the same experiments shown above for γ-H2AX and 53BP1 foci at 8h. The number of foci scored in I-SceI transfected cells is background subtracted.

2.3. Chromosomal aberrations after I-SceI induced DNA DSBs

It is known that a certain fraction of unrepaired or mis-repaired DSBs generate different types of chromosomal aberrations (breaks, translocations, dicentrics, deletions etc.) [106]. It is also known that exposure to IR leads to the formation of chromosomal translocations [107]. To examine the

effect of DSB clusters on DSB processing and their propensity towards causing mis-repair events in the form of chromosomal aberrations, we analyzed formation of breaks and chromosomal & chromatid translocations in the above described cell lines. Metaphase spreads were prepared from cells forming simple DSBs (CHO 1xS.D8) and clustered DSBs 24 h after the transfection with I-SceI expressing plasmid. Cells were treated with colcemid for 2 hrs before collection to arrest cells at metaphase for cytogenetic analysis.

2.3.1. Chromosomal/chromatid type of breaks after induction of DSB clusters

We first investigated repair of single DSBs and DSB clusters in the CHO clones transfected with I-SceI enzyme. Cells were collected 24 h after the induction of DNA damage. Metaphase spreads were prepared and the chromatid and chromosomal breaks were scored. Our analysis shows that after the transfection with I-SceI expressing plasmid chromosomal/chromatid type breaks are present in the cells. The results are shown in the Figure 23, and it can be seen that there is no significant effect of DSB complexity on the incidence of breaks 24 h after I-SceI transfection. We find simple DSBs (CHO 1xS.D8) and DSB clusters (CHO 2xS.R14; CHO 4xS.R12) all result in the formation of breaks. The numbers of chromatid breaks scored do not show any correlation with the complexity of the DSBs generated.

We have already seen in the above section that with increasing complexity of DSB clusters the surviving fraction of cells decreases. The results obtained after scoring chromosomal breaks fails to show a similar effect of DSB clustering. So to investigate further the repair defect in the presence of complex DSB clusters, we analyzed chromosomal/chromatid type of translocations (chromosomal exchanges, dicentrics, tricentrics, rings etc.). Indeed, in the remainder of this thesis, cytogenetic analysis will focus on chromosomal/chromatid type translocations for reasons that will become clear from the results to be presented below.

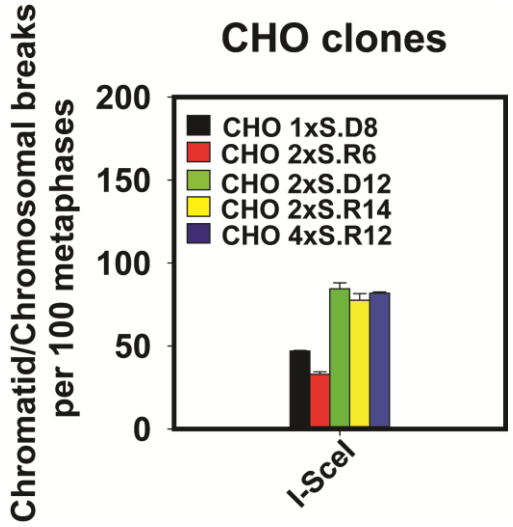

Figure 23: *Chromosomal and chromatid type breaks scored after 24 hours of I-SceI transfection.*

Quantitative analysis of chromatid and chromosome break formation after 24 h. Chromatid breaks scored in mock transfected cells have been subtracted. Quantitative analysis from three independent experiments showing averages ± SD (n=2 for CHO 2xS.R6).

2.3.2. Complex DSB clusters requiring end processing form more translocations

The survival of CHO clones shows a strong dependence on the complexity of DSB clusters. As compared to CHO clones with single I-SceI sites resulting in formation of simple DSBs, the CHO clones harboring pairs and quadruplets of I-SceI sites show increased formation of chromosomal/chromatid type of translocations. Interestingly the CHO clones forming DSB pairs (CHO 2xS.R14) show significantly lower numbers of translocations than cells harboring quadruplets (CHO 4xS.R12).

The effects observed in the different CHO clones are compiled in the graph presented (Figure 24). CHO clones forming the simplest form of DSBs result in lower numbers of translocations as compared to clones harboring DSB clusters. We observe that with increasing number of I-SceI recognition sites (increasing complexity of DSB clusters) more translocations form. We also investigated the response after transfection with I-SceI expressing plasmid in CHO 2xS.R6 (intermediate) and CHO 2xS.R14 (high) clones and obtained results are compatible with those at the survival level. The results shown below in Figure 24 show that DSB clusters of increasing complexity cause increasing numbers of chromosomal translocations.

In CHO clones resulting in the formation of DSB clusters with directly ligatable apical ends, cell survival is higher than in the clones having DSB clusters with incompatible ends. When we investigated the effect of orientation of I-SceI sites (direct and reverse) on the formation of translocations, we observed that in comparison to CHO 2xS.D12 cells, CHO 2xS.R14 cells show a higher incidence of translocations.

In Figure 24 the quantified analysis of translocations scored in the CHO clones having simple DSBs (CHO 1xS.D8), DSB pairs (CHO 2xS.R14) and DSB quadruplets (CHO 4xS.R12) is shown. Also CHO clones having lower numbers of I-SceI integration sites CHO 2xS.R6 and CHO 2xS.D12 (having compatible DSB ends) is shown. *These results in aggregate suggest the involvement of DSB complexity in translocation formation and show a role for end processing in their formation*.

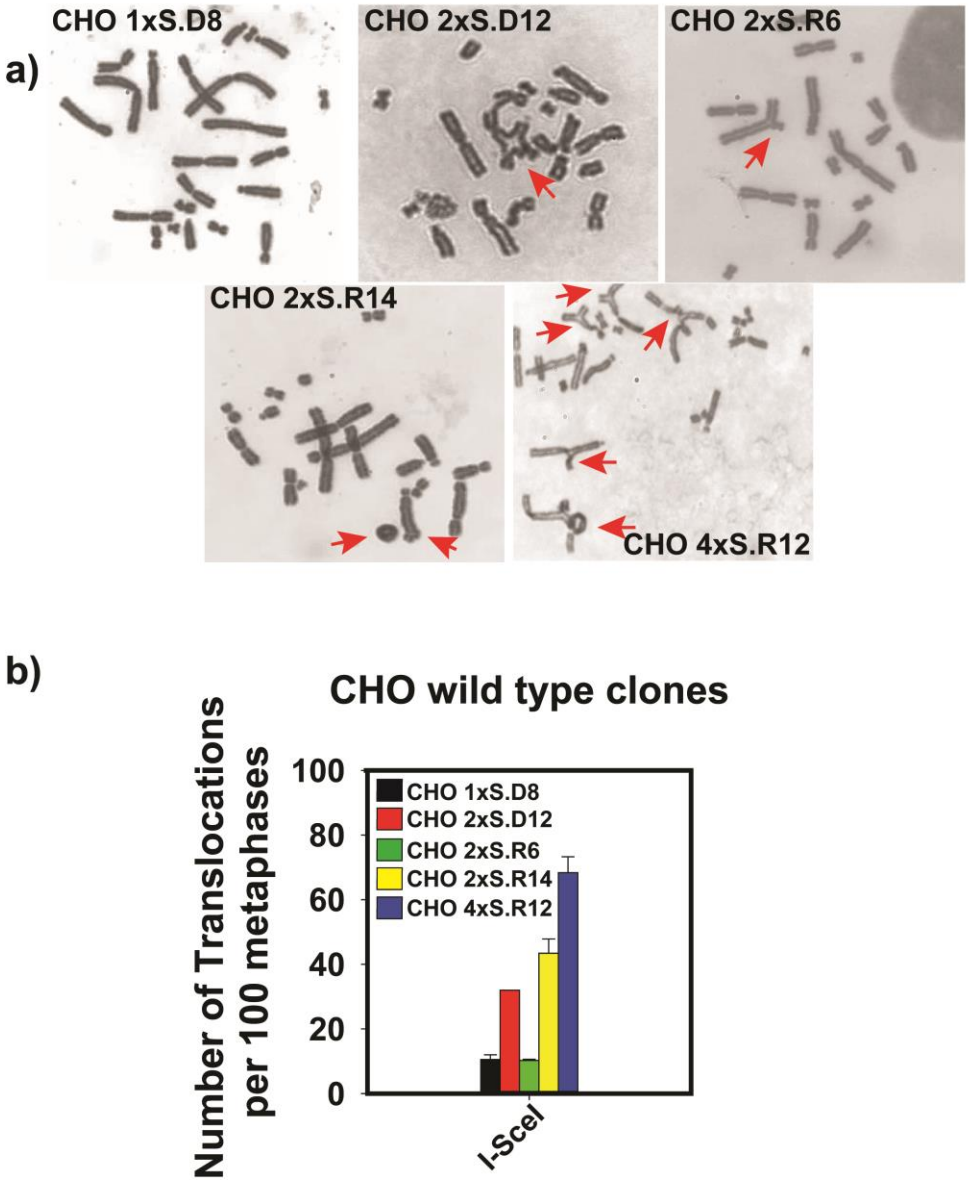

Figure 24: *DSB-clusters requiring end-processing generate more chromosomal aberrations than single-DSBs.*

a) Images of selected metaphases of the indicated CHO clones captured 24 h after transfection with the I-SceI expression plasmid. Red arrows point to chromosomal translocations. b) Chromosomal translocations scored in the different clones as indicated. Results from two out of three independent experiments are shown as average ± SD (n=2 CHO 2xS.R6). Chromosomal translocations scored in mock-transfected cells have been subtracted (0-4).

2.4. Suppression of DNA end processing suppresses translocation-formation

To further investigate the effect of DNA end processing on the formation of translocations in the presence of DSB clusters two approaches were taken. In the first approach CHO clones 2xS.D12

and 2xS.R14 were transfected with ISceI-TREX [108] chimera to not only restrict the DNA but to also digest the ssDNA overhangs and generate DSB with blunt ends. In the second approach, CtIP was depleted using a specific siRNA against it. The results obtained are discussed below.

2.4.1. Blunt DSB ends decrease the number of translocations forming from DSB clusters with incompatible ends

Two different endpoints were measured in this set of experiments: 1). cell survival and 2). translocation formation. Both endpoints suggest an involvement of end processing in the overall response. CHO clones having pairs of I-SceI sites integrated, CHO 2xS.D12 and CHO 2xS.R14, were transfected with ISceI- TREX plasmid. In this constellation the chimeric protein digests the DNA to generate the DSBs but, starts immediately thereafter with the digestion of the generated single strand DNA ends. It is thought that as a result of this activity DSBs with blunt ends are generated.

The results in the Figure 25 show that when the ISceI-TREX plasmid is used for generating DSBs, both CHO 2xS.D12 and CHO 2xS.R14 cells show similar incidence of translocations. Please recall that when these cells were transfected with the standard I-SceI expressing plasmid without TREX activity, CHO 2xS.R14 cells showed a higher incidence of translocations as compared to CHO 2xS.D12 cells and overall the levels of translocations measured were much higher. This observation suggests that the creation of blunt ends at the DSBs diminishes translocation formation significantly.

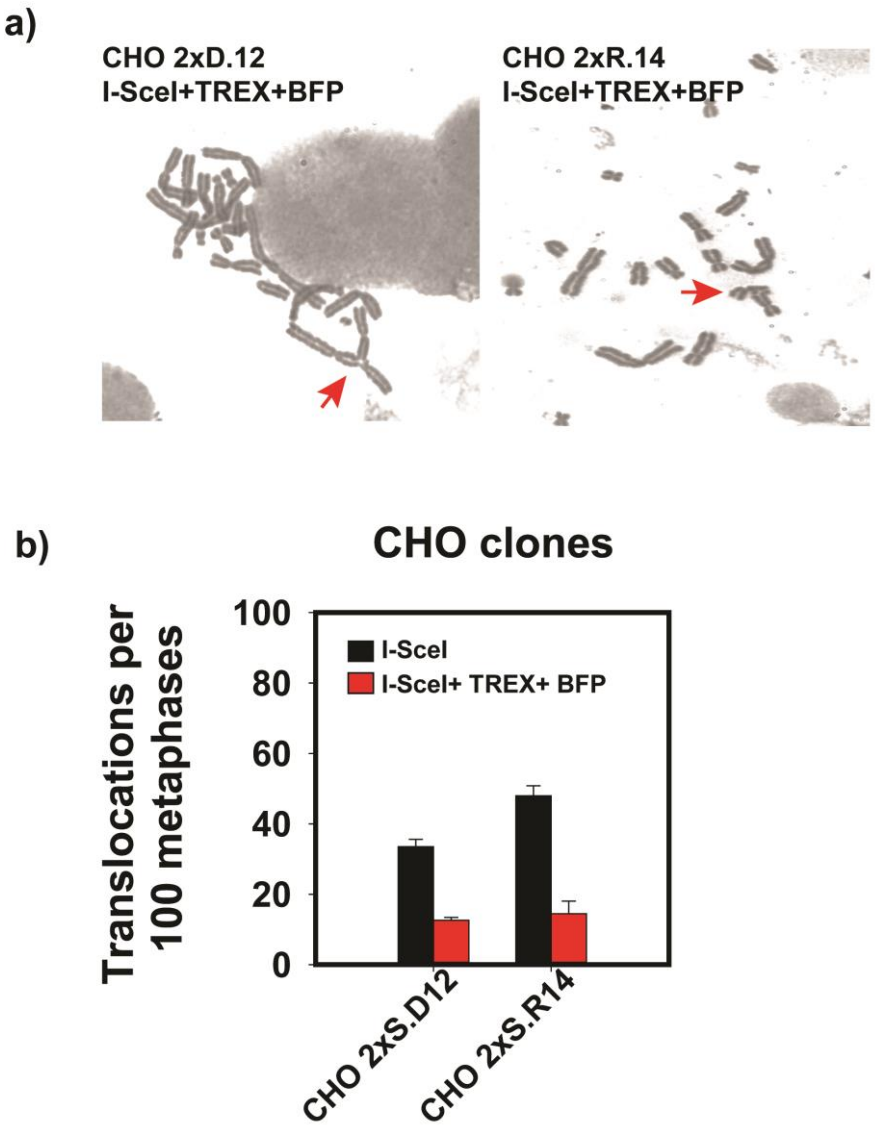

Figure 25: *Translocation formation in CHO 2xD.12 and CHO 2xR.14 cells after transfection with I-SceI-TREX plasmid versus I-SceI plasmid.*

a) Images of selected metaphases of the indicated CHO clones captured 24 h after transfection with the I-SceI-TREX plasmid. Red arrows point to chromosomal translocations**.** b) Translocation formation after transfection with I-SceI-TREX plasmid. Data compiled from two out of three separate experiments showing averages ± SD.

2.4.2. CtIP knockdown reduces translocations, particularly for DSB clusters with incompatible ends

CtIP protein and its orthologs promote resection of DSBs [109] (see Introduction). The results presented in the previous section suggest an involvement of single stranded overhangs in the

formation of chromosomal translocations. We examined whether single stranded overhangs generated by resection have similar effects. Therefore, we depleted the key protein involved in the initiation of resection, CtIP, in the corresponding CHO clones using siRNAs against CtIP.

Figure 26 shows the results obtained with clones harboring DSB clusters of increasing complexity. It is evident that CtIP knockdown suppresses translocation formation and that effect is larger with DSB clusters of high complexity that show higher initial incidence of translocations. In CHO 1xS.D8 clone having simple DSBs there is no change in the translocations, while the clones with DSB pairs and clusters show a greater decrease in the numbers of translocations. *These results confirm that single stand DNA overhangs favor the formation of translocations.*

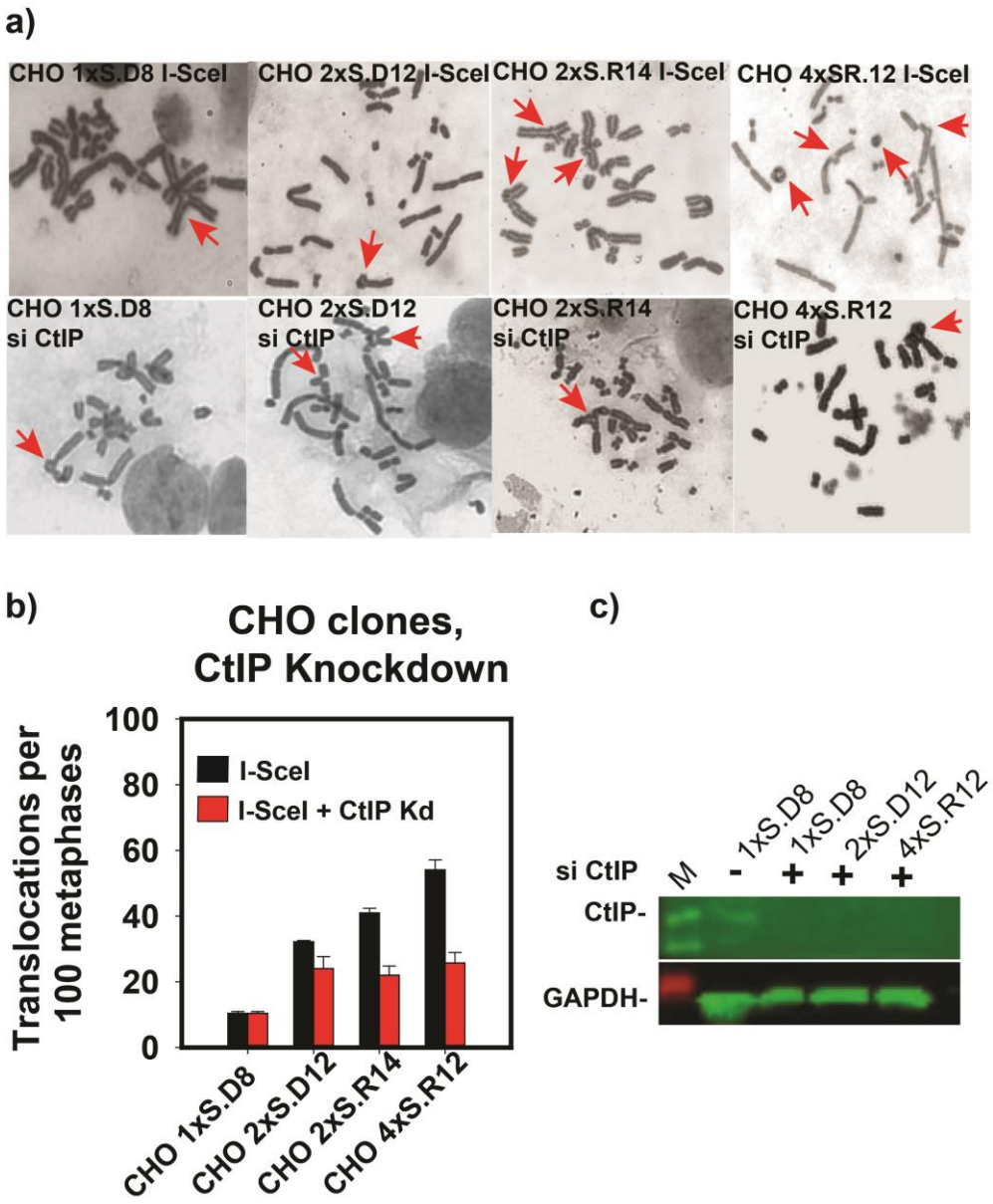

Figure 26: *Chromosomal translocations in CHO clones as indicated after knocking down CtIP.*

a) Images of selected metaphases of the indicated CHO clones captured 24 h after transfection with the I-SceI plasmid following CtIP knockdown. Red arrows point to chromosomal translocations**.** b) Translocations after transfection with I-SceI- plasmid following CtIP knockdown. Data compiled from two out of three experiments showing averages ± SD (n=2 for CHO 2xS.D12). C). Western blot confirming the CtIP knockdown.

Until now we focused on effects generated by DSB clusters of different complexity on cell survival and chromosome aberration formation. In the following sections we will focus our attention on the role of the four DSB repair pathways in the repair of simple DSBs and DSB clusters and how engagement of these pathways contributes to the above effects.

Results

3. Repair pathways involved in the repair of DSB clusters

One likely major hallmarks of high LET IR is the generation of DSB clusters. With increasing LET there is more effective killing of the cells and the dose required is less as compared to the dose of lower LET that is required to produce a similar effect. DSB clusters are thought to suppress c-NHEJ because cells deficient in this pathway show similar radio-sensitivity to high and low LET IR [79, 104, 110].

Recently it has been suggested that in mammalian cells ~70% of DSBs induced by low LET are repaired by c-NHEJ, whereas DSBs induced by high-LET IR are preferentially repaired by HRR [111]. However, higher utilization of HRR after exposure to high-LET IR is not compatible with large increase in translocations observed. HRR is an error-free repair pathway. *Indeed, the chromosomal translocation data suggest that some DSBs are repaired by error-prone repair pathways.* We first study the role of c-NHEJ in the repair of DSB clusters.

3.1. The role of c-NHEJ in the repair of DSB clusters assayed by measuring cell survival

Role of c-NHEJ in the repair of DSB clusters was studied in CHO clones where simple DSBs and DSB clusters are generated after expression of I-SceI. To study the effect of c-NHEJ deficiency on the repair of DSB clusters, CHO wild type clones were treated with 5μM of the specific DNA-PKcs inhibitor NU7441. To verify the results obtained in CHO wild type clones, CHO clones deficient in Ku80 (xrs6 2xS.R11) and DNA-PKcs (XRC1-3 “2xS.R4, 2xS.R10”; and “2xS.D4, 2xS.D10”) were also used.

3.1.1. Simple DSBs depend more on c-NHEJ than DSB clusters

CHO clones harboring simple DSBs (1xS.D8) and DSB clusters (2xS.R14) were treated with 5μM NU7441 for 24 hours, starting 2 hours after transfection with the I-SceI expressing plasmid, to allow the cells to attach to the surface of the dish. The results are presented in Figure 27. It can be seen that there is greater decrease in survival in CHO 1xS.D8 than in CHO 2xS.R14 after inhibition of DNA-PKcs. *These results suggest that simple DSBs utilize DNA-PKcs dependent c-NHEJ to a greater extent than DSB clusters.*

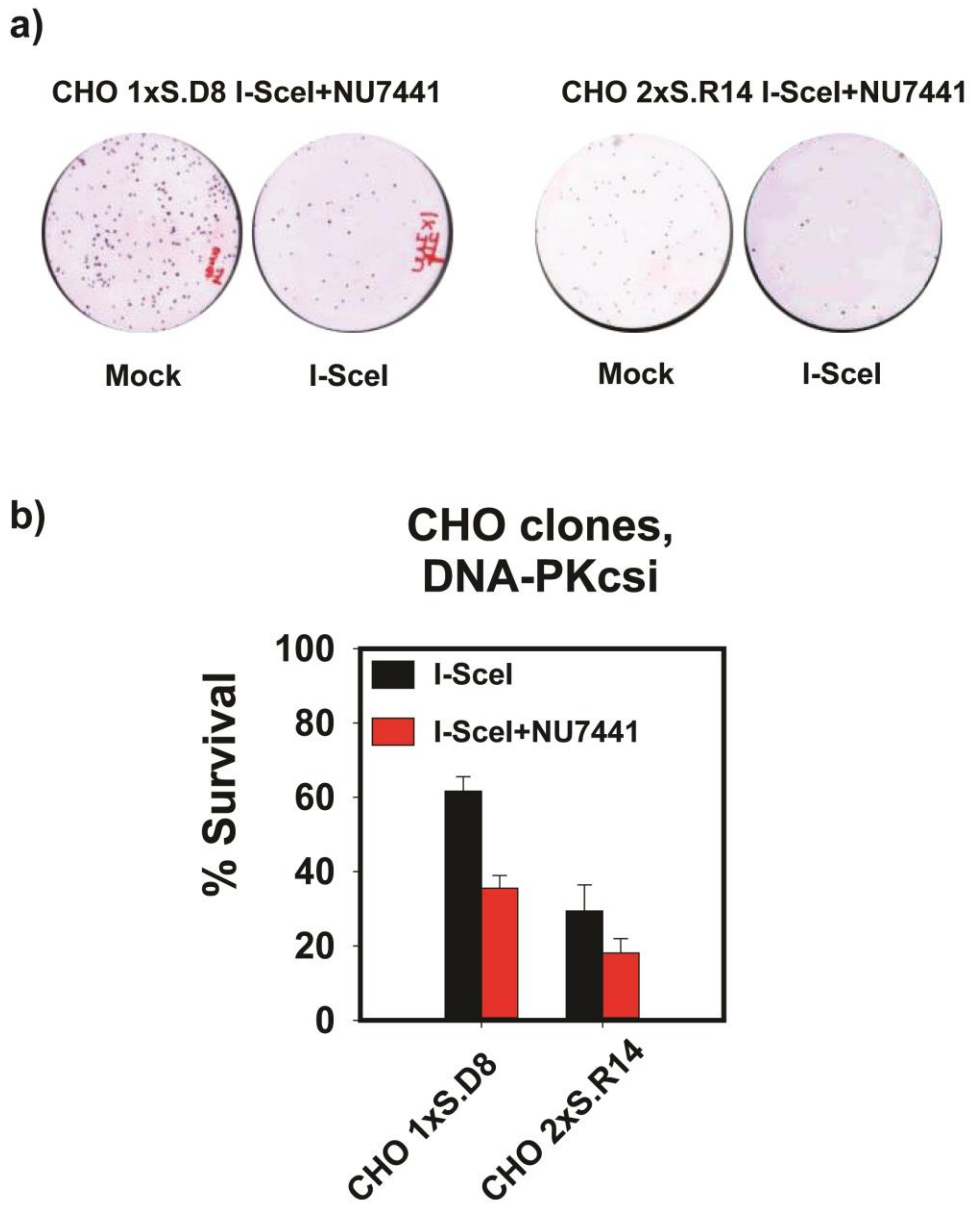

Figure 27: *Effect of DNA-PKcs inhibition in cells harboring simple DSBs and DSB clusters.*

a) Representative cell culture dishes showing colonies forming after transient expression of I-*Sce*I in different CHO clones as indicated. In each dish cells were plated immediately after transfection and incubated for 7–8 days to allow colony formation. 5µM NU7441 was added 2 h after the transfection and was washed off 24 h later. b) Survival of transfected cells treated with 5 µM NU7441 calculated using the plating efficiency measured in mock-transfected cells treated with 5µM NU7441. Data compiled from three experiments showing averages ± SD.

3.1.2. DSB clusters in DNA-PKcs deficient cells cause extensive cell killing independently of clustering but dependently of end processing

We showed above that chemical inhibition DNA-PKcs in wild-type CHO cells harboring DSB pairs (CHO 2xS.R14) increases cell killing. To confirm this response we investigated the response in XRC1-3 clones (DNA-PKcs deficient) harboring pairs of I-SceI sites. Cell survival in different XRC1-3 clones is similar to that seen in CHO wild type clones treated with DNA-PKcs inhibitor NU7441. The XRC1-3 clones used in this set of experiments have four and ten integration sites of DSB pairs in direct or reverse orientation. Cell survival after the formation of DSB clusters is similar in clones with DSB pairs in reverse orientation and similar to the results obtained with wt CHO clones treated with NU7441. This suggests that in the absence of DNA-PKcs simpler DSB pairs produce similar response as the more complex quadruplets in CHO 4xS.R12 clones. Here cell killing is so high that surviving cells might represent the population of un-transfected cells.

We investigated the effect of DNA end processing on cell survival of cells where DNA-PKcs was inhibited or mutated. Here the degree of clustering affects cell survival only in the XRC1-3 clones harboring DSB pairs with compatible ends. In the XRC1-3 clones with incompatible DSB ends, no additional effect from higher numbers of DSB clusters is seen, i.e. XRC1-3 2xS.R4 and XRC1-3 2xS.R10 clones show similar cell survival after transfection with I-SceI.

Figure 28 shows that after transfection with I-SceI, CHO cells with DSB quadruplets survive similarly to CHO cells with DSB pairs (incompatible ends) after treatment with NU7441. *These results suggest that DNA-PKcs deficiency renders cells sensitive to simple DSBs or to DSB clusters with incompatible ends*.

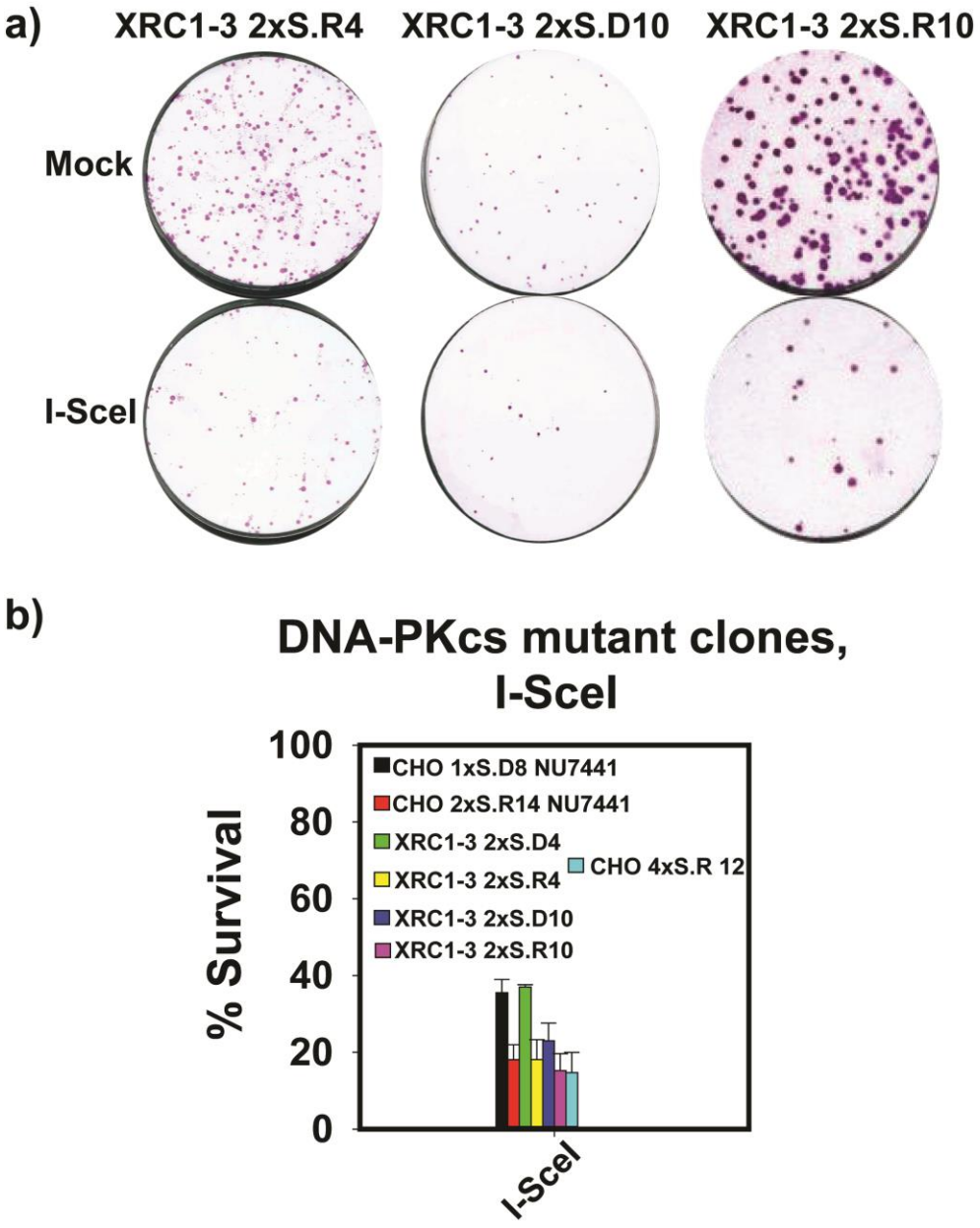

Figure 28: *Cell Survival measured in DNA-PKcs deficient XR-C13 cells forming DSB clusters with compatible and incompatible ends.*

a) Representative cell culture dishes showing colonies forming after transient expression of I-*Sce*I in different XRC1-3 clones as indicated. In each dish cells were plated immediately after transfection and incubated for 7–8 days to allow for colony formation. b) Survival of transfected cells was calculated using the plating efficiency measured in mock-transfected cells of the same clone. Data compiled from three experiments showing averages ± SD (n=2 for XRC1-3 2xS.D4).

Results

3.1.3. Ku80 mutation has similar effects as DNA-PKcs mutation

An essential component of DNA-PK complex, besides DNA-PKcs, is the Ku70/80 heterodimer. We utilized xrs6 2xS.R11 (Ku80 mutant) clones for the experiments described in this section. The Ku80 mutant clone harboring low number (xrs6 2xS.R4) of I-SceI pairs in reverse orientation shows low survival even after mock treatment and was therefore excluded from further experiments. In the clone with eleven I-SceI sites, mock treatment results in a plating efficiency of around 25%, while the clone with four integrations has a plating efficiency of 2%. The results in Figure 29 show cell survival normalized to the plating efficiency of mock-treated cultures. These results suggest that Ku80 is important for normal cell survival and that its mutation sensitizes cells to DSBs in ways similar to that observed in DNA-PKcs deficient cells.

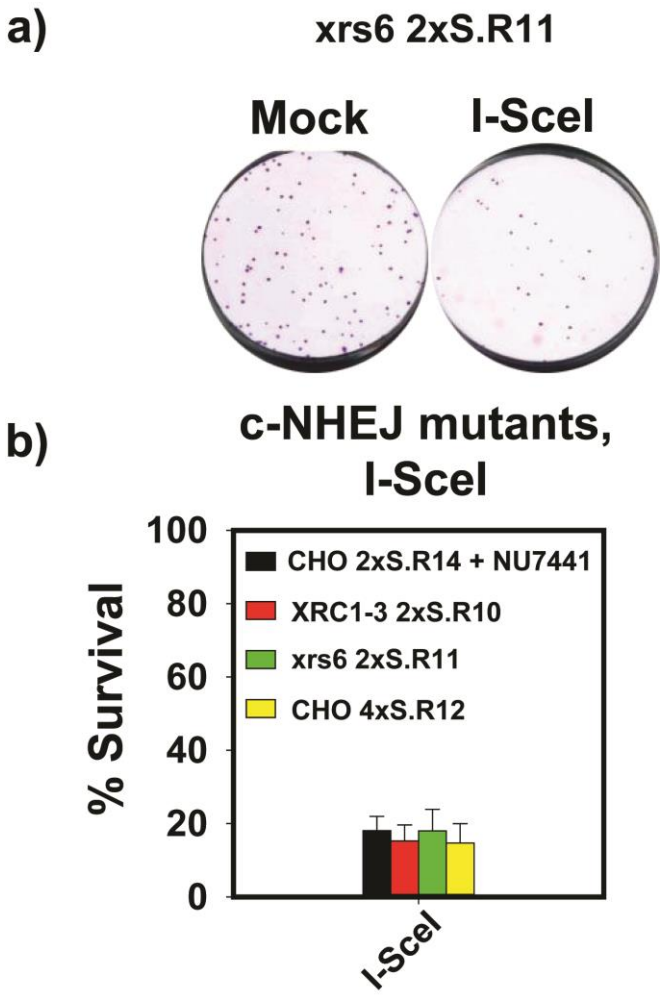

Figure 29: *Cell survival in Ku80 deficient xrs6 cells harboring DSB clusters with incompatible ends.*

a) Representative cell culture dishes showing colonies forming after transient expression of I-*Sce*I in xrs6 2xS.R11 clone as indicated. In each dish cells were plated immediately after transfection and incubated for 7–8 days to allow for colony formation. b) Survival of transfected cells calculated using the plating efficiency measured in mock-transfected cells of the same clone. Data compiled from three experiments showing averages ± SD.

3.2. DDR signaling in response to DSB clusters in DNA-PK deficient condition

We investigated DDR inception by scoring ɣ-H2AX foci in DNA-PKcs mutant clones (XRC1-3 2xS.R4, XRC1-3 2xS.R10; XRC1-3 2xS.D10; and xrs6 2xS.R11) 8h after the transfection with I-SceI. Figure 30 shows the results and it can be seen that cells elicit a DDR response similar to that of wild type cells. Interestingly, even in c-NHEJ mutant clones the number of ɣ-H2AX foci scored closely matches the number of I-SceI integration sites.

We further investigated the recruitment of 53BP1 under the same conditions and found that at 8 h, there is a greater accumulation of 53BP1 foci in the DNA-PKcs mutant XRC1-3 as compared to the Ku80 mutant xrs6 2xS.R11. These results suggest that in response to DSB clusters, there is normal initiation of DDR in the mutants, but that DDR progression in terms of 53BP1 foci formation is more pronounced in the DNA-PKcs mutant (XRC1-3 clones) than in Ku80 mutant (xrs6) clones. The results of these experiments are shown in Figure 30.

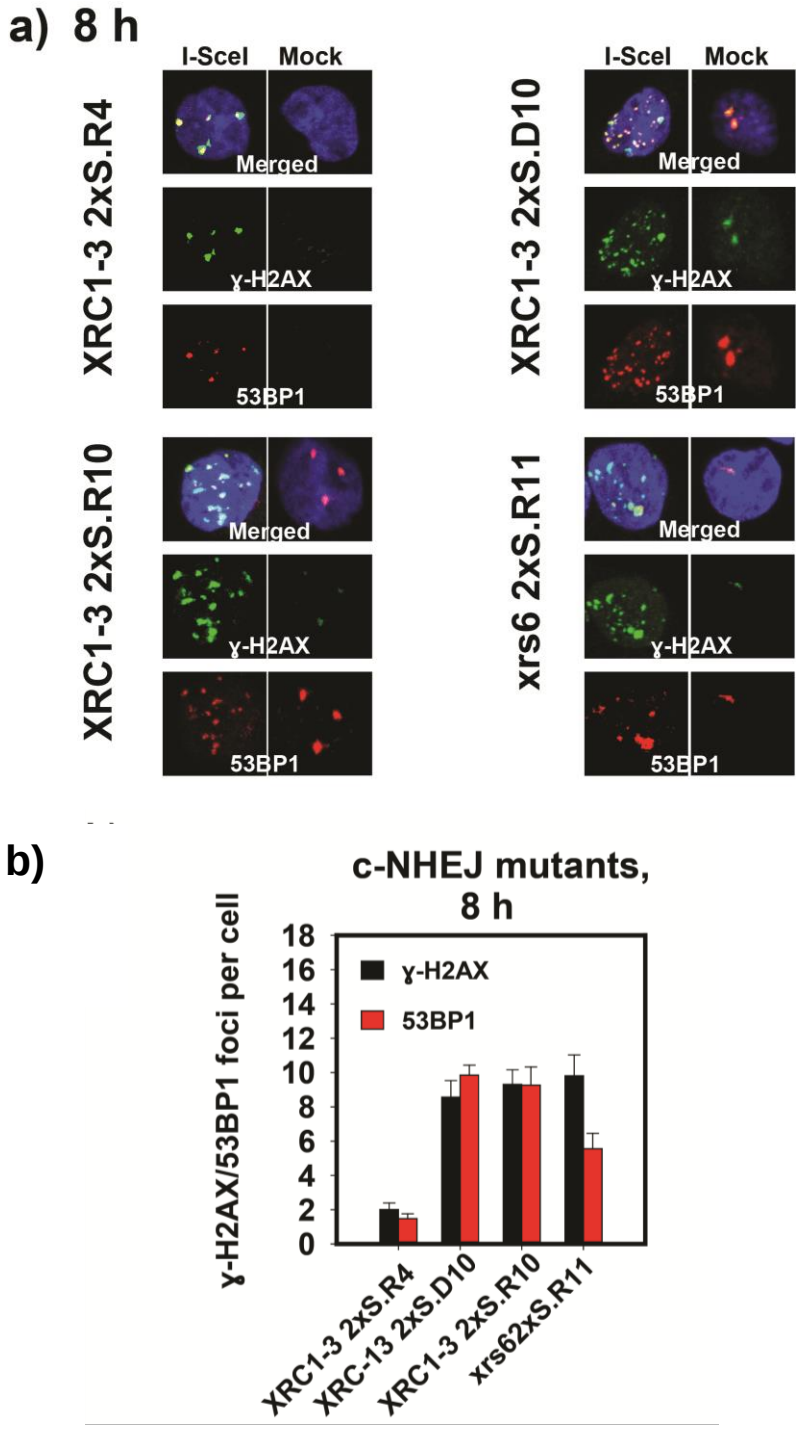

Figure 30: Formation of γ-H2AX foci and 53BP1 foci in c-NHEJ mutant clones.

Formation of γ-H2AX and 53BP1 foci at I-SceI mediated DSB-clusters in XRC1-3 and xrs6 2xS.R11 clones. a) Representative immunofluorescent images of γ -H2AX and 53BP1 foci in the indicated clones 8 h after transfection. b) Quantitative analysis showing averages ± SE from 2 independent experiments of γ-H2AX and 53BP1 foci formation in mock transfected and I-SceI transfected cells. The number of foci scored in I-SceI transfected cells is background subtracted. Data compiled from two experiments (n=1 for XRC1-3 2xS.D10).

Results

3.3.1. Inhibition of DNA-PKcs generates a larger increase of translocation formation for simple DSBs than DSB clusters

DNA-PKcs inhibition with NU7441 suppresses c-NHEJ. To investigate the effect of this inhibition on translocation formation, we treated the CHO clones, CHO 1xS.D8 and CHO 2xS.R14, with 10 µM NU7441. This treatment increases the number of translocations in both clones. Notably, the increase is greater in the clone sustaining simple DSBs (CHO 1xS.D8) than in the clone sustaining DSB pairs generating incompatible apical ends.

The DNA-PKcs mutant cell line, XRC1-3 2xS.R10 shows also under these conditions high numbers of translocations and the response is similar to that seen in the CHO wild type clone 2xS.R14 after treatment with NU7441. The XRC1-3 2xS.D10 clone having ten I-SceI integration sites in direct orientation also shows high number of translocations but, the numbers are lower than in XRC1-3 2xS.R10 cells. The CHO 1xS.D8 clone shows after treatment with NU7441 a large increase in translocation formation. As expected, XRC1-3 cells show no differences in translocation formation after treatment with NU7441. These results suggest that c-NHEJ is extensively used in cells sustaining simple DSBs and that therefore its inhibition causes large increases in translocation formation. On the other hand, DSB clusters seem to use c-NHEJ to a lesser degree and therefore its inhibition has only a moderate effect on translocation formation. The results of these experiments are summarized in Figure 31.

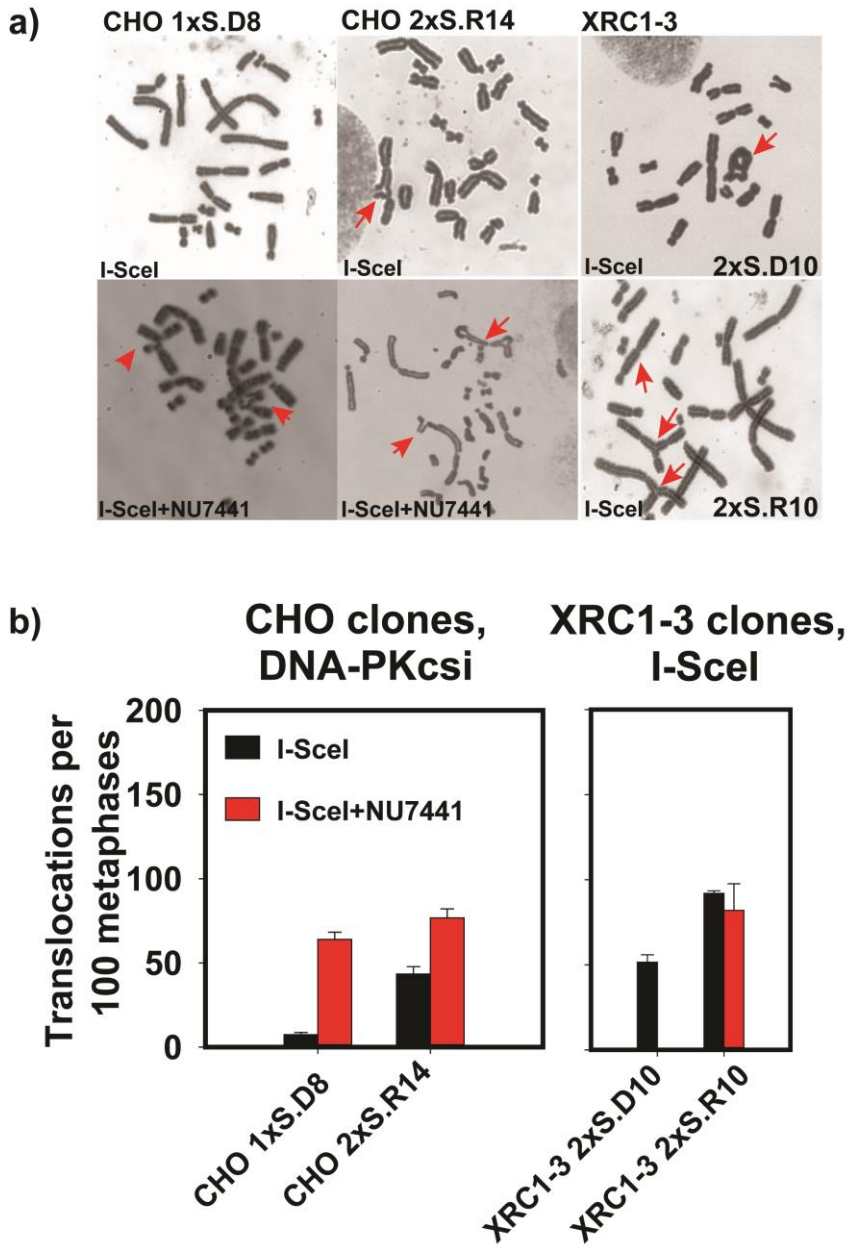

Figure 31: *Translocation formation after DNA-PKcs inhibition.*

a) Images of selected metaphases of the indicated CHO and XRC1-3 clones captured 24 h after transfection with the I-*Sce*I expression plasmid. 10 µM NU7441 was added 2 h after transfection with I-SceI. Red arrows point to chromosomal translocations. b) Quantitative analysis of chromosomal translocations scored in the different clones as indicated. Chromosomal translocations scored in mock-transfected cells have been subtracted (0-5). Data compiled from two out of three experiments showing averages ± SD (n=2 CHO 1xS.D8 I-SceI+ NU7441; and XRC-13 2xS.R10 I-SceI+ NU7441).

Results

3.3.2. The number of DSB clusters has little effect on translocation formation in DNA-PKcs mutants

To investigate the effect of the number of DSB clusters generated in a cell on translocation formation in DNA-PKcs deficient cells, we tested the XRC1-3 2xS.R4 and 2xS.R10 clones as described above. It is evident that both clones show similar formation of translocation formation despite the widely different numbers of DSB clusters generated, suggesting an early saturation of the system (Figure 32). This result is reminiscent to the response seen at the survival level. It is also notable that the results obtained with these XRC1-3 clones are similar to those of CHO clones with integrated quadruplets of I-SceI sites. Figure 32 summarizes the results of this experiment.

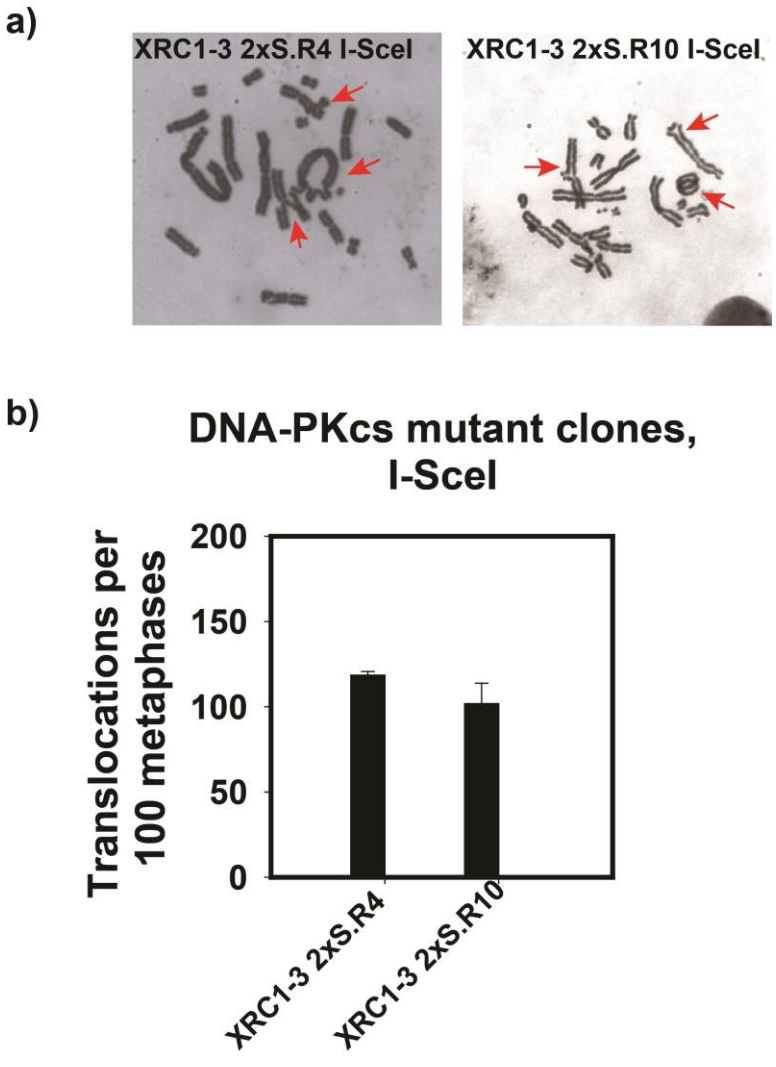

Figure 32: *Translocations in DNA-PKcs mutant XR-C13 clones forming DSB clusters with incompatible ends.*

a) Images of selected metaphases of the indicated XRC1-3 clones captured 24 h after transfection with the I-*Sce*I expression plasmid. Red arrows point to chromosomal translocations. b) Quantitative analysis of chromosomal translocations scored in the different clones as indicated. Chromosomal translocations scored in mock-transfected cells have been subtracted (0-4). Data compiled from two out of three independent experiments showing averages ± SD.

3.3.3. DSB clusters with compatible apical ends result in lower number of translocations in DNA-PKcs deficient cells

We investigated the effect of DNA-PKcs deficiency in the XR-C13 2xS.D4, 2xS.D10 clones in which pairs of DSBs are generated in direct orientation that require therefore no processing before ligation. The presence of directly ligatable DSB clusters results in lower numbers of translocations than DSB clusters with incompatible ends. Figure 33b shows the results obtained. To further test the role of end processing in translocation formation under conditions of DNA-PKcs deficiency, we transfected cells with the I-SceI-TREX plasmid [108] that will generate blunt ends not only in the clones with compatible but also in those with incompatible ends. The results in Figure 33C show similar numbers of translocations XRC1-3 2xS.D10 and XRC1-3 2xS.R10 clones confirming that the form of end processing affects the formation of translocations.

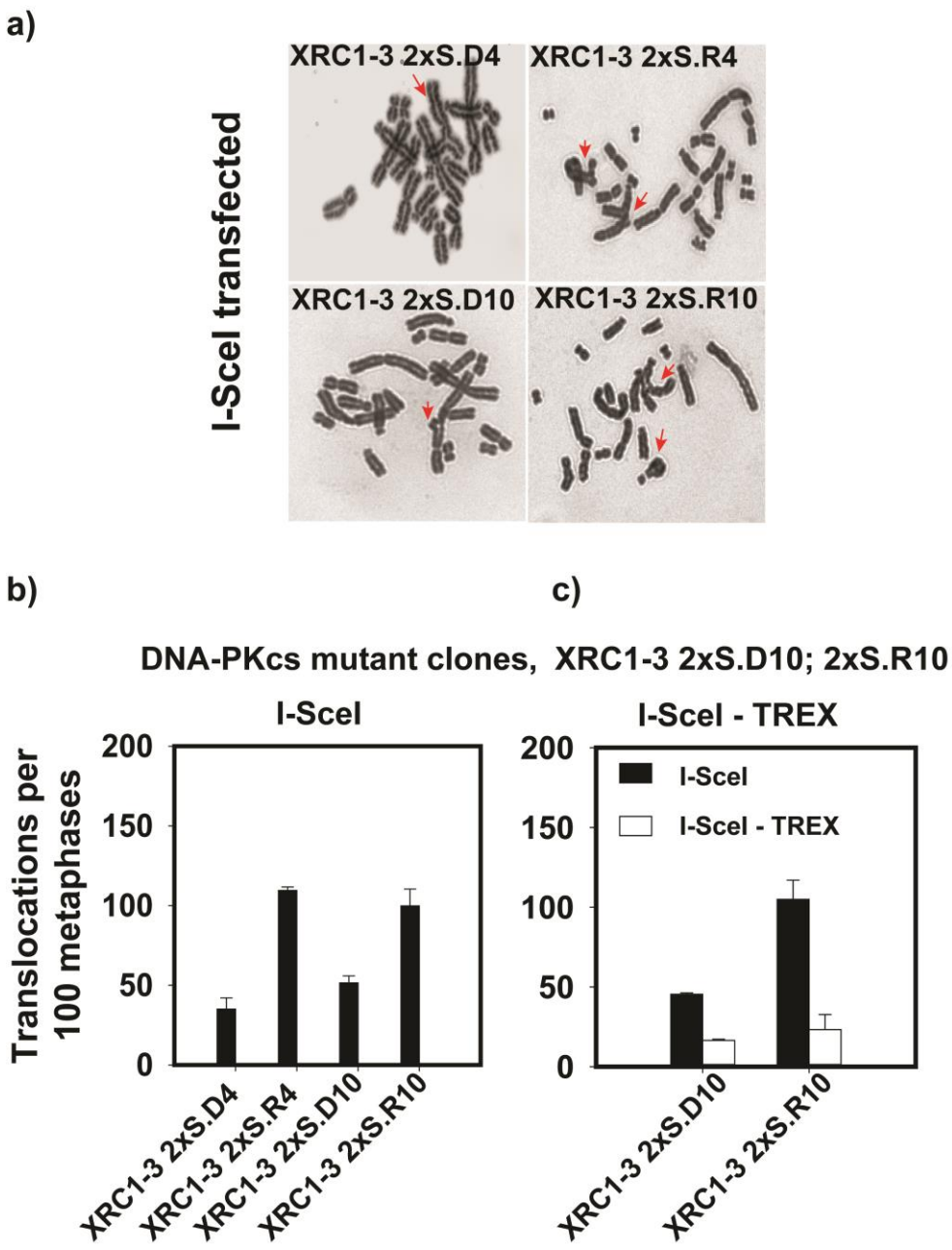

Figure 33: *DSB clusters with compatible apical ends result in lower number of translocations in DNA-PKcs deficient cells*

a) Images of selected metaphases of the indicated XRC1-3 clones captured 24 h after transfection with the I-*Sce*I expression plasmid. Red arrows point to chromosomal translocations. b) Quantitative analysis of chromosomal translocations scored in the different clones as indicated. Chromosomal translocations scored in mock-transfected cells have been subtracted (0-5). Data compiled from two out of three independent experiments showing averages ± SD (n=2 XRC1-3 2xS.D4).

Results

3.4. a) The Ku80 mutant xrs6 2xS.R11 shows lower levels of chromosome translocations following formation of DSB clusters than DNA-PKcs mutants

We scored the number of chromosomal translocations in the xrs6 2xS.R11 clone. At the cell survival level, we observed a similar sensitivity between xrs6 2xS.R11 clones and the DNA-PKcs mutant clone, XRC1-3 2xS.R10, after transfection with the I-SceI plasmid. Strikingly this response cannot be replicated at the level of translocation formation. Indeed significantly less translocations are scored in xrs6 2xS.R11 than in XRC1-3 2xS.R10 cells and even in CHO 2xS.R14 cells The results obtained are shown in Figure 34. The results suggest that different deficiencies in components of c-NHEJ generate different effects on translocation.

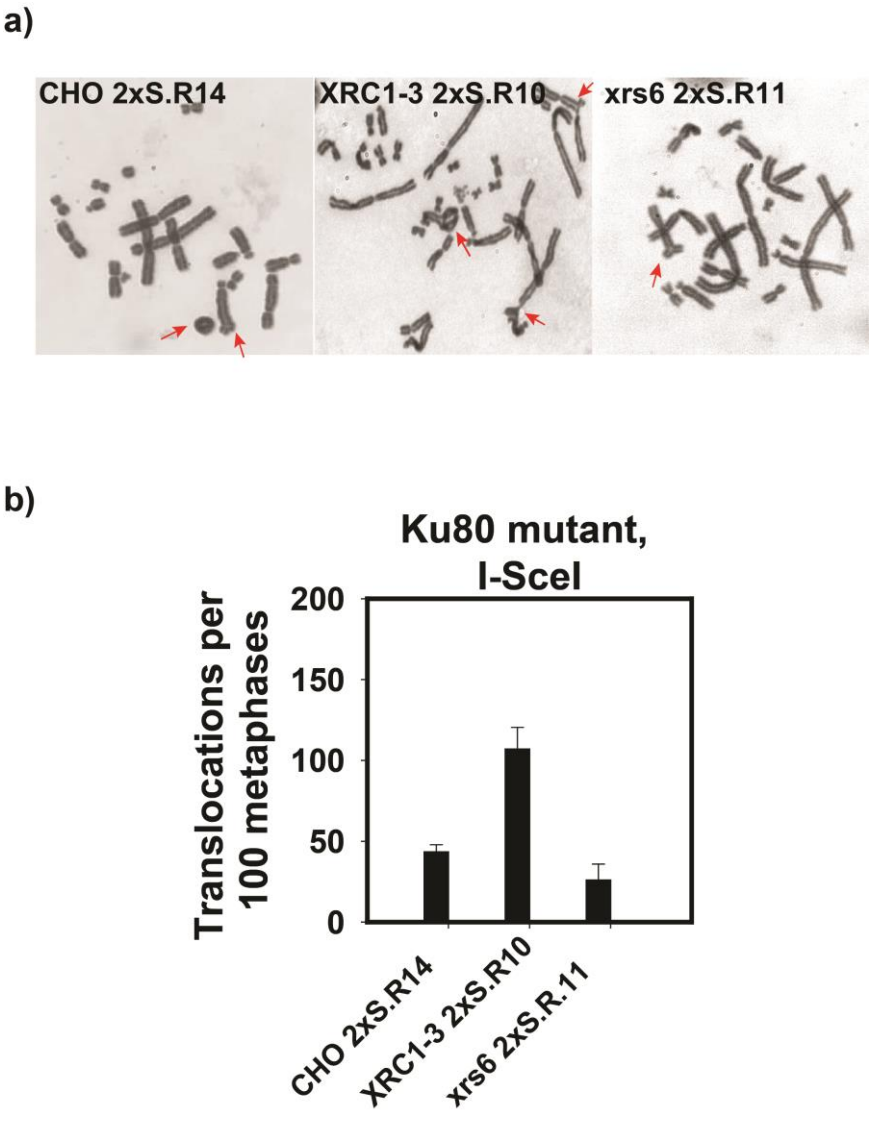

Figure 34: *Translocations from DSB clusters are lower in Ku80 mutants than in DNA-PKcs mutants.*

a) Images of selected metaphases of the indicated clones captured 24 h after transfection with the I-*Sce*I expression plasmid. Red arrows point to chromosomal translocations. b) Quantitative analysis of chromosomal translocations scored in the different clones as indicated. Chromosomal translocations scored in mock-transfected cells have been subtracted (0-4). Data compiled from three separate experiments showing averages ± SD.

3.4. b) Ku80 knockdown reduces translocation formation from DSB clusters

To confirm the above observations of Ku effects on chromosome translocation formation, we knocked down Ku80 in CHO 2xS.R14 and CHO 1xS.D8; and XRC1-3 2xS.R10 cells. The results are summarized in Figure 35. As expected, the number of translocations scored increases in the CHO 1xS.D8 clones where simple DSBs are formed [112], but decreases in the CHO 2xS.R14 clone that forms DSB clusters. In the DNA-PKcs mutant, knockdown of Ku80 has no effect on translocation formation. *These results confirm the above stated distinct effects between Ku80 and DNA-PKcs deficiencies in translocation formation from DSB clusters.*

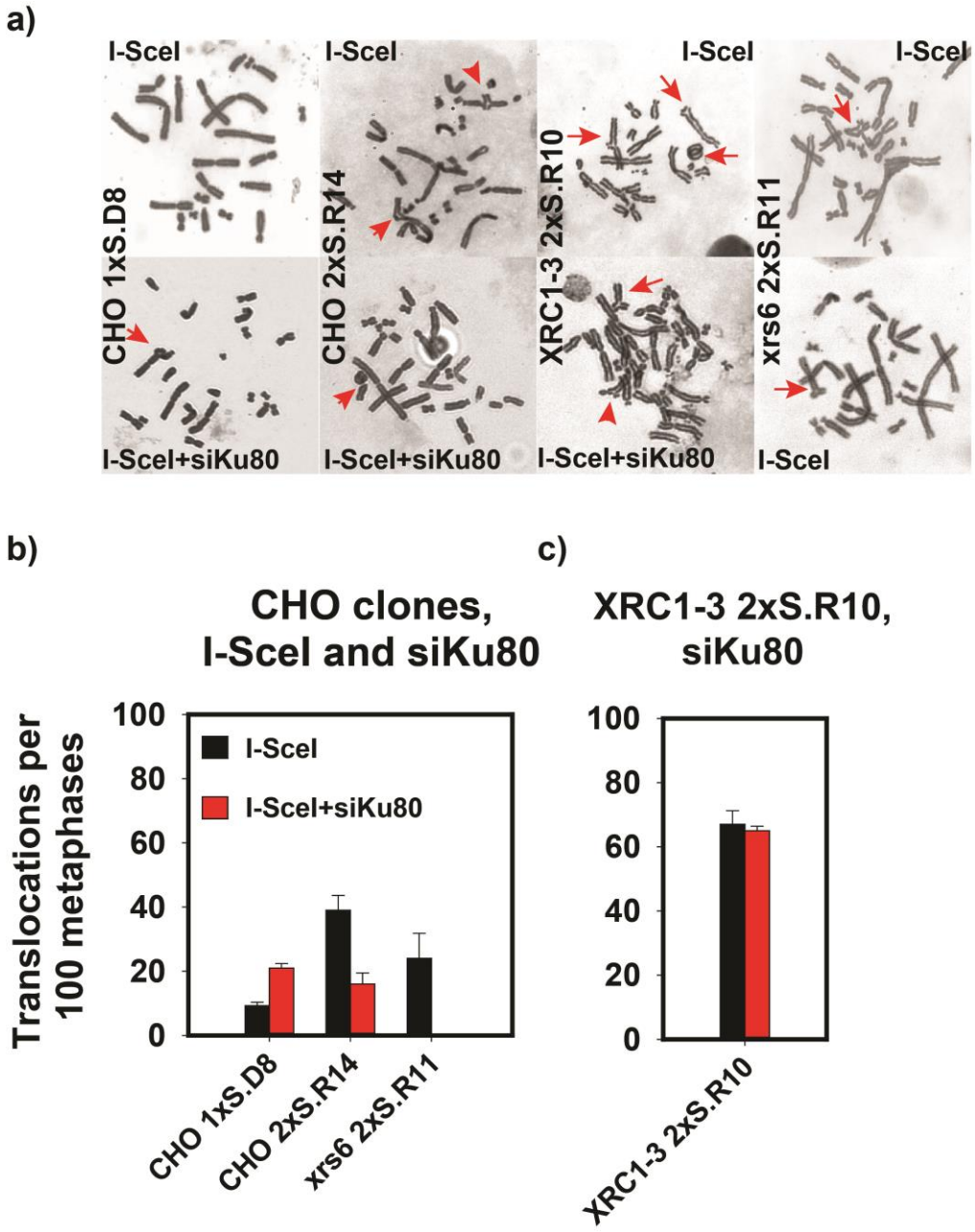

Figure 35: *Ku80 knockdown results in decrease in translocations from DSB clusters.*

a) Images of selected metaphases of the indicated clones captured 24 h after transfection with the I-*Sce*I expression plasmid. Red arrows point to chromosomal translocations. b) Quantitative analysis of chromosomal translocations scored in the different clones as indicated. CHO clones were transfected with I-SceI plasmid and siRNA against Ku80. Chromosomal translocations scored in mock-transfected cells have been subtracted. Data compiled from three experiments c) Quantitative analysis of chromosomal translocations scored in the XRC1-3 clone as indicated. Chromosomal translocations scored in mock-transfected cells have been subtracted. Data compiled from two experiments showing averages ± SD.

Results

4. Role of HRR in repair of DSB clusters

As mentioned above the possible involvement of HRR in the processing of high LET induced DNA DSBs remains uncharacterized. However, there is some discrepancy regarding the increased usage of HRR following high-LET irradiation. In this section we will investigate the role of HRR in the repair of DSB clusters.

To study the role of HRR in the repair of DSB clusters, CHO wild type clones were treated with 25 μM of Rad51 inhibitor, BO2, or an ATR inhibitor (5 μM VE-821) [45, 113, 114] and cell survival or chromosome translocation formation were measured. Also CHO mutants deficient in XRCC3 (irs1 SF) were used. Rad51 foci formation was also analyzed using indirect immunofluorescence. To score Rad51 foci in S/G_2- phase, we pulse-labeled cells with EdU for 30 min before the collection of the samples at 15 h and 24 h.

4.1. HRR deficiency sensitizes cells to simple DSBs more than to DSB clusters

To investigate the response of inhibition of HRR on the processing of DSB clusters we employed two different methods. In one method we inhibited Rad51 and in the other method we inhibited ATR. Inhibition of Rad51 and inhibition of ATR results in inhibition of HRR [113]. First we will discuss the response observed after inhibition of Rad51 using the specific inhibitor BO2.

4.1.a. Survival of CHO clones after chemically inhibiting Rad51 using BO2

To chemically inhibit HRR, 25 μM BO2 was added 2 hours after the transfection with I-SceI expressing plasmid. The inhibitor was removed by washing it off with pre-warmed PBS 24 h later. The results presented in Figure 36 show that there is a significant reduction in the fraction of cells surviving when sustaining either simple DSBs or DSB clusters in CHO 1xS.D8 and CHO 2xS.R14, respectively. *We conclude that like c-NHEJ, HRR also plays a crucial role in the repair of the I-SceI induced breaks – both simple DSBs and DSB clusters, but, simple DSBs show a greater dependence.*

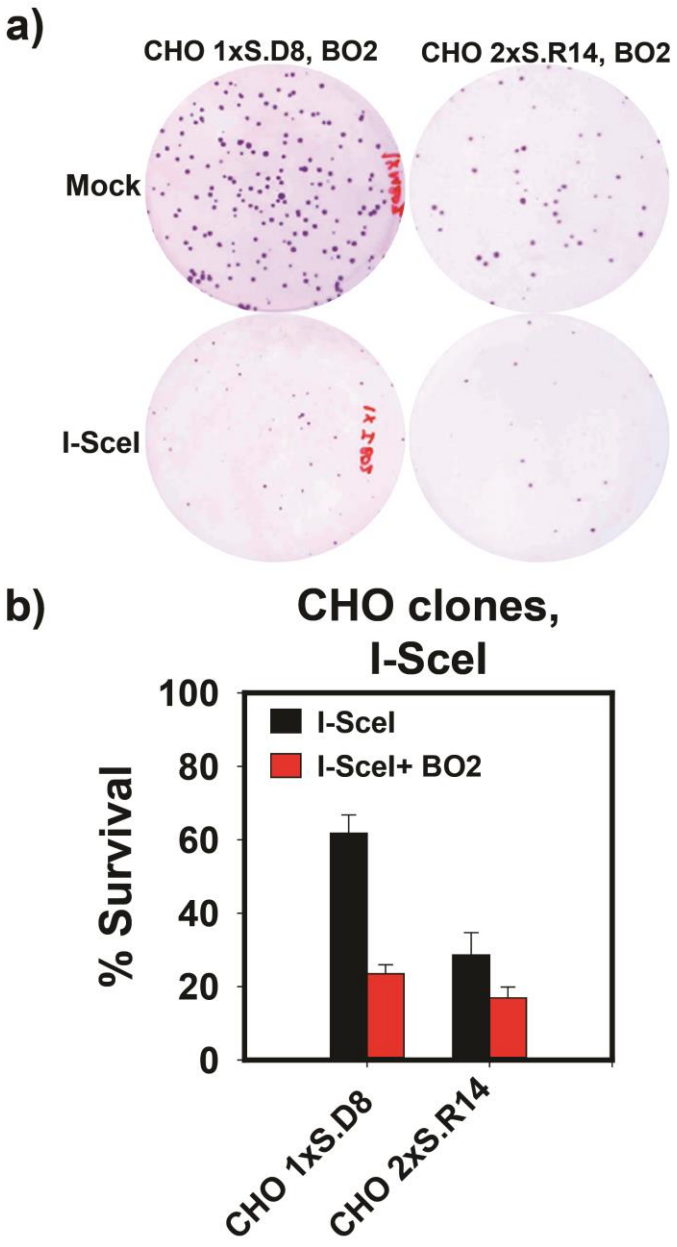

Figure 36: *Survival in CHO clones having simple DSBs and DSB clusters after inhibition of Rad51 using BO2.*

a) Representative cell culture dishes showing colonies forming after transient expression of I-*Sce*I in different CHO clones as indicated. In each dish cells were plated immediately after transfection and incubated for 7–8 days to allow colony formation. 25µM BO2 was added 2 h after the transfection. b) Survival of transfected cells treated with 25µM BO2 calculated using the plating efficiency measured in mock-transfected cells treated with 25µM BO2 of the same clone. Data compiled from three separate experiments showing averages ± SD.

Results

4.1.b. Survival of CHO clones after chemical inhibition of ATR

It is known that ATR inhibition inhibits HRR [45, 114, 115]. We therefore used in our experiments VE-821, a specific ATR inhibitor, at a concentration of 5 μM. The results in Figure 37 show that after inhibition of ATR, cells are sensitized to the induction of simple DSBs and DSB clusters. Here again, cells sustaining simple DSBs show greater sensitization. We conclude that *inhibition of HRR sensitizes cells to simple DSBs and DSB clusters and that the effect is stronger for simple DSBs.*

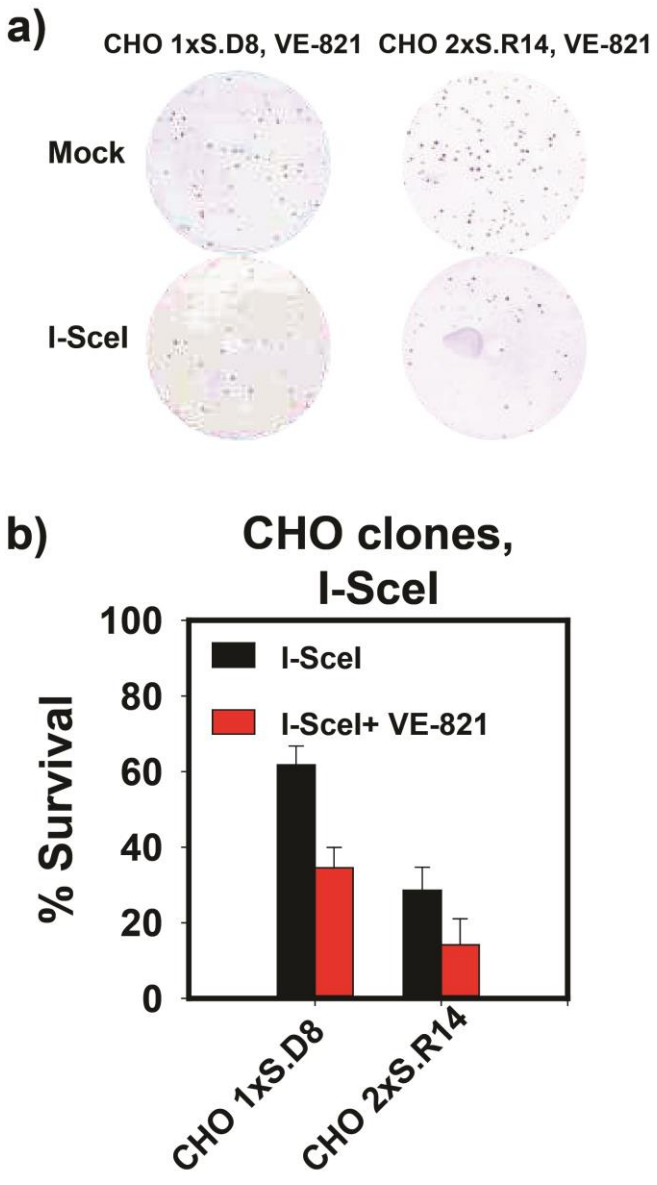

Figure 37: *Survival in CHO clones harboring simple DSBs and DSB clusters after inhibition of ATR using VE-821.*

a) Representative cell culture dishes showing colonies forming after transient expression of I-*Sce*I in different CHO clones as indicated. In each dish, cells were plated immediately after transfection and incubated for 7–8 days to allow colony formation. 5µM VE-821 was added 2 h after the transfection. b) Survival of transfected cells treated with 5µM VE-821 calculated using the plating efficiency measured in mock-transfected cells treated with 5µM VE-821 of the same clone. Data compiled from two independent experiments showing averages ± SD.

4.2. Detection of HRR function at DSB clusters by Rad51 foci formation

Rad51 foci are widely accepted as the surrogate marker for functional HRR. We investigated recruitment of Rad51 simple DSBs and DSB clusters. The results obtained are presented in Figure 38. The results presented are specific for G2 phase cells. To enable cell cycle specific analysis DAPI and EdU intensity were analyzed to define G2 cells. G2 cells sustaining simple DSBs efficiently develop RAD51 foci suggesting that they utilize HRR. Similar observations are made in the CHO clone harboring fourteen DSB pairs. 53BP1 is used here as the marker for DSBs to avoid the high background seen when scoring ɣ-H2AX foci. Interestingly CHO clones having simple DSBs (CHO 1xS.D8) show greater incidence of Rad51 foci as compared to the CHO clone harboring DSB pairs (CHO 2xS.R14).

For simple DSBs, Rad51 foci peak at 15 h and by 24 h most of them have resolved. For DSB clusters in CHO 2xS.R14 we see high number of Rad51 and 53BP1 foci but little evidence for resolution by 24 h. *We conclude that HRR engages to the processing of simple DSBs and DSB clusters but may only operate productively on simple DSBs.* The quantified results are presented in Figure 38.

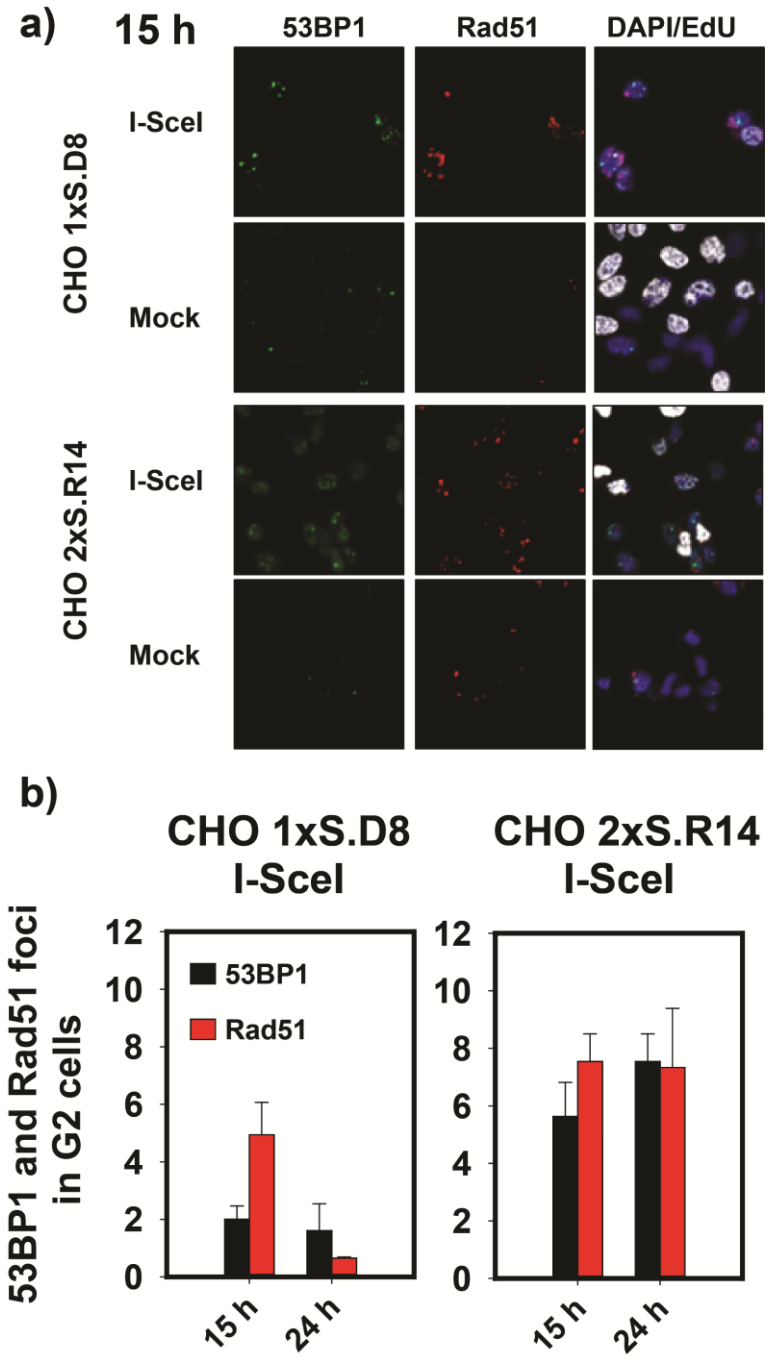

Figure 38: *Accumulation of Rad51 foci in G2 phase in CHO clones.*

Formation of 53BP1 and Rad51 foci at I-SceI mediated DSB-clusters in CHO clones forming simple DSBs and DSB clusters (DSB pairs). a) Representative immunofluorescent images of 53BP1 and Rad51 foci (also EdU and DAPI stained) in the indicated CHO clones generated 15 h after I-SceI transfection. b) Quantitative analysis showing averages ± SE from 2 independent experiments of 53BP1 and Rad51 foci formation in mock transfected and I-SceI transfected cells. The number of foci scored in I-SceI transfected cells is background subtracted. EdU positive cells were used to exclude the S phase cells and the DAPI:EdU intensity was used to gate the G2 cells accordingly. To gate specifically the G2 cells the values of DAPI and EdU intensities obtained from IMARIS software were used to

Results

sort the cells using MS word Excel spreadsheets. Cells were sorted according to plot generated keeping the values of DAPI and EdU intensities on X and Y axis respectively. Data compiled from two separate experiments.

4.3.1. HRR mutants harboring I-SceI pairs show higher incidence of translocations than corresponding CHO clones

We investigated formation of translocations from DSB clusters in an HRR deficient background. We used the HRR mutant clone irs1 SF 2xS.R4 and compared the results to those of CHO 1xS.D8, CHO 2xS.R6 and CHO 2xS.R.14 clones. In an HRR deficient background higher incidence of chromosomal translocations is observed 24 h after transfection as compared to CHO 2xS.R6 cells. Notably, the incidence of translocations in irs1 SF 2xS.R4 cells is similar to that of CHO 2xS.R14 clone. We conclude that *abrogation of HRR enhances formation of chromosomal translocations.* The results obtained are compiled in Figure 39.

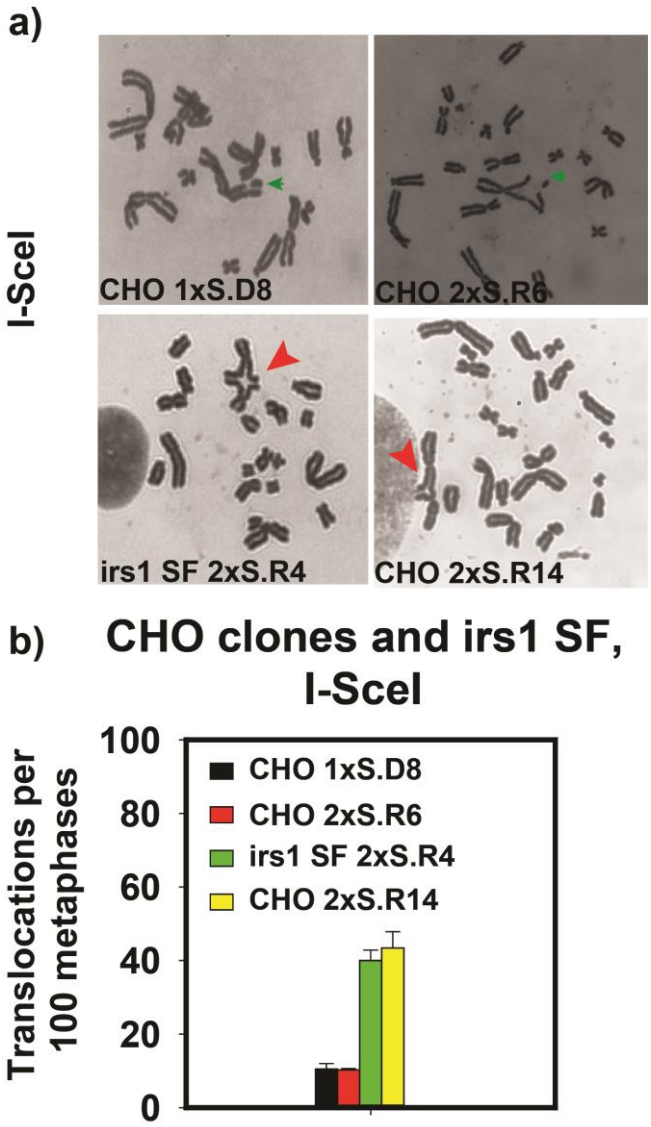

Figure 39: *Translocations in CHO wild type and HRR deficient cells with DSB clusters.*

a) Images of selected metaphases of the indicated CHO and Irs1 SF clones captured 24 h after transfection with the I-*Sce*I expression plasmid. Red arrows point to chromosomal translocations. Green arrows point to chromatid breaks. b) Quantitative analysis of chromosomal translocations scored in the different clones as indicated. Chromosomal translocations scored in mock-transfected cells have been subtracted (0-3 in CHO clones; and 2-6 in irs1 SF 2xS.R4). Data compiled from two experiments showing averages ± SD.

4.3.2. Simple DSBs show more pronounced increase in the number of translocations after inhibition of HRR than DSB clusters

CHO wild type clones forming simple DSBs and CHO 2xS.R14 generating DSB clusters were treated with 25 µM BO2 for 24 h after transfection with I-SceI. CHO 1xS.D8 cells that form

simple DSBs after transfection with I-SceI show an increase in the numbers of chromosomal/chromatid translocations. But, the number of translocations decreases significantly in the presence of DSB clusters with incompatible ends (CHO 2xS.R14). A point to be considered here is that this response was observed after chemical inhibition of HRR using BO2. The results shown in Figure 40 show the numbers obtained after damage induction post I-SceI transfection and treatment with BO2 2 hours later. Similar experiments with CHO 4xS.R12 forming DSB quadruplets show no effect after treatment with BO2.

To further confirm the role of HRR in the repair of DSB clusters, Rad51 was depleted in CHO wild type clones (1xS.D8; 2xS.R14; and 4xS.R12). Cells were grown for 48 hours and then were transfected with siRNA against Rad51. Around 3.5 mio cells per 5 µl of siRNA were transfected and then allowed to grow in 150mm. Approximately, 24-26 h later the cells were again transfected with same volume of siRNA together with I-SceI plasmid. 24 h after the second transfection, cells were treated with colcemid for 2 h as described above and samples were collected and analyzed for chromosomal aberrations using the same method as described above.

The results in Figure 40 show greater increase in translocation formation in CHO 1xS.D8 cells forming simple DSBs, as compared to the CHO 2xS.R14 cells forming DSB pairs. Surprisingly, no additional effect is observed in the most complex CHO 4xS.R12 clone forming DSB quadruplets. *All above observations suggest an increased involvement of HRR in repairing simple DSBs in comparison to the DSB clusters and that the efficiency of HRR decreases with the increasing DSB complexity*.

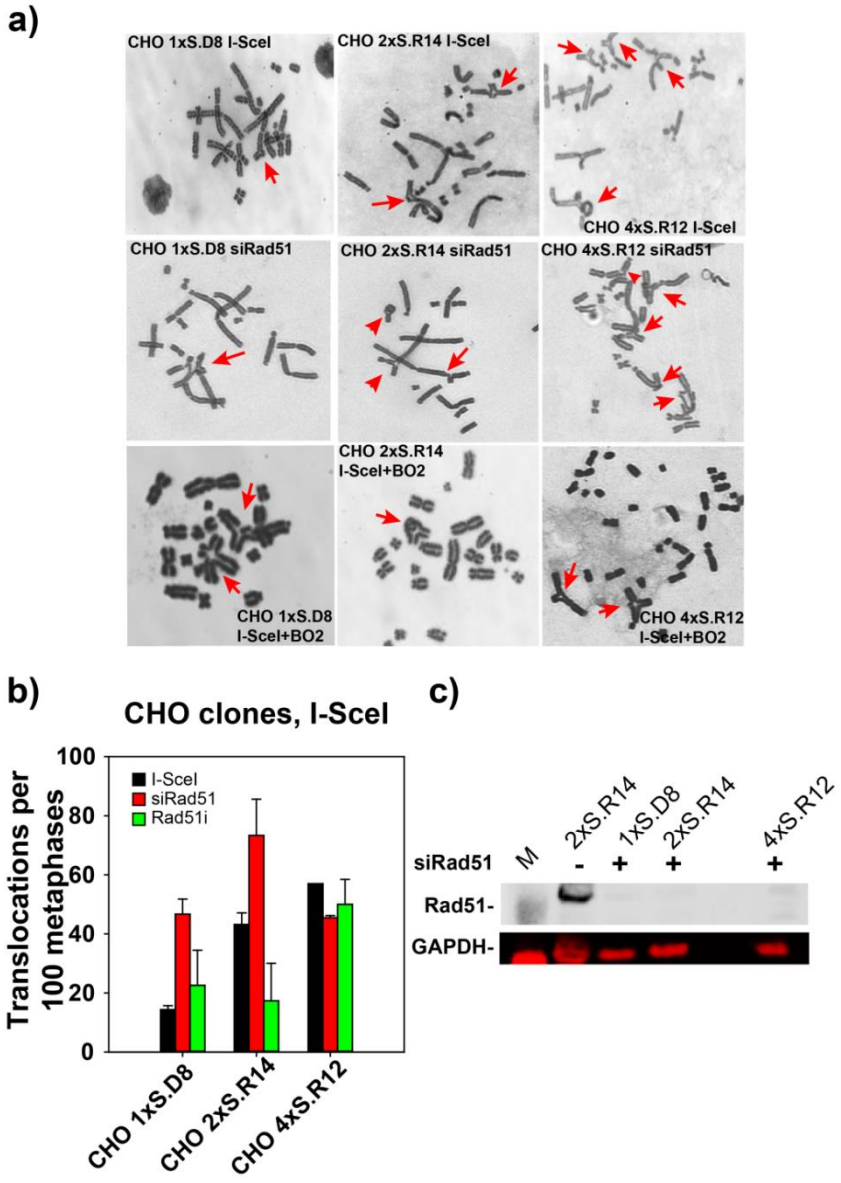

Figure 40: *Translocations after abrogation of HRR in CHO wild type cells harboring simple DSBs and DSB clusters.*

a) Images of selected metaphases of the indicated CHO clones captured 24 h after transfection with the I-*Sce*I expression plasmid. 25 µM BO2 was added 2 h after transfection with I-SceI. siRad51 was used to knock down Rad51 and siRNA transfection was done twice on two subsequent days 24-26 h apart. Red arrows point to chromosomal translocations. b) Quantitative analysis of chromosomal translocations scored in the different clones and different conditions as indicated. Chromosomal translocations scored in mock-transfected cells have been subtracted (numbers ranged between 0-5 after treatment with BO2 and 4-10 after knockdown with siRad51). Data compiled from two out of three experiments showing averages ± SD (n=2 in CHO 4xS.R12). c) Western blot showing Rad51 knock-down.

Results

4.3.3. DSB clusters requiring DNA end processing show reduction in chromosomal translocation formation after inhibition of ATR.

The results presented in Figure 41 show the number of translocations formed in CHO clones (1xS.D8; and 2xS.R14) after inhibition of ATR post transfection with I-SceI endonuclease. It can be seen that the clone, which requires DNA end processing before ligation (CHO 2xS.R14) shows a significant reduction in the numbers of translocations after ATR inhibition. This response is similar to the response observed after treatment with BO2 in presence of simple DSBs and DSB clusters. Like Rad51 inhibition, ATR inhibition decreases translocation formation in cells with DSB clusters with incompatible apical ends.

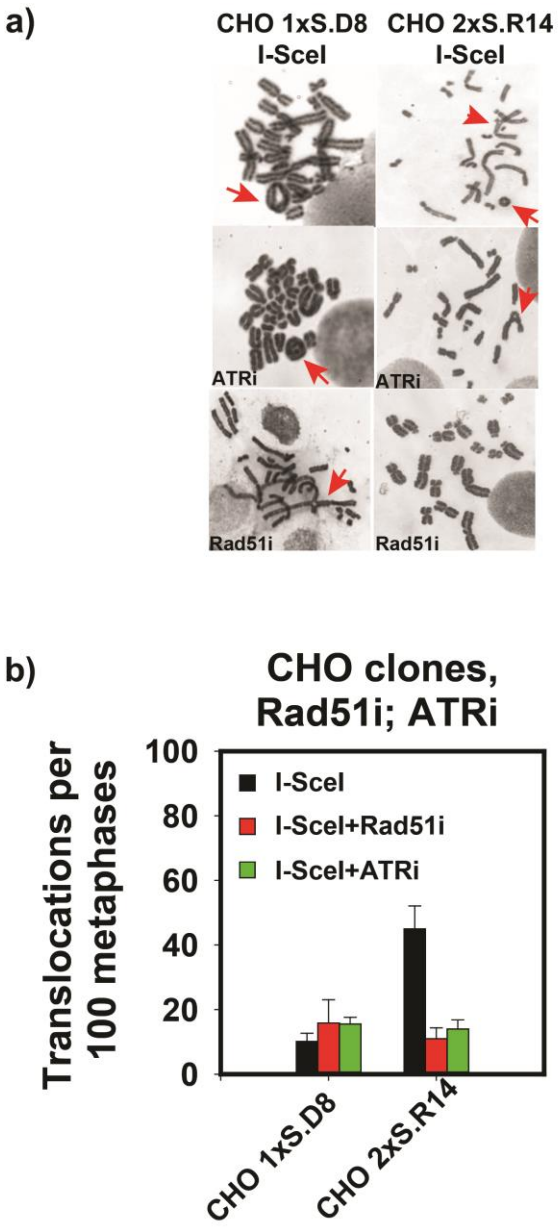

Figure 41: *Number of translocations in CHO wild type and XR-C13 clones harboring simple DSBs and DSB clusters.*

a) Images of selected metaphases of the indicated CHO clones captured 24 h after transfection with the I-*Sce*I expression plasmid. 25µM Rad51i (BO2) and 5µM ATRi (VE-821) were added respectively 2 h after transfection with I-SceI. Red arrows point to chromosomal translocations. b) Quantitative analysis of chromosomal translocations scored in the different clones as indicated. Chromosomal translocations scored in mock-transfected cells have been subtracted. Data compiled from two experiments showing averages ± SD.

4.3.4. Role of HRR in the repair of DSB clusters under DNA-PKcs deficiency

Conceptually if either of the two major DSB repair pathways is abrogated, then the second pathway may compensate for the deficiency. We designed experiments to investigate repair in DNA-PKcs mutant clones in the presence of DSB clusters after Rad51 inhibition using 25 µM of the BO2 inhibitor. The results are compiled in Figure 42 and show that in XRC1-3 2xS.R10 cells Rad51 inhibition sensitizes cells to the presence of DSB clusters. A similar response was observed after inhibition of ATR using 5 µM VE-821. There was further sensitization of DNA-PKcs mutant clones after induction of DSB clusters in the presence of VE-821.

After treatment with 25 µM BO2 and 5 µM VE-821 in XRC1-3 2xS.R10 cells, we observe a significant reduction in the number of translocations. But, depletion of Rad51 in XRC1-3 2xS.R10 cells shows no effect on translocation formation. Figure 42 shows that in comparison to untreated cells, Rad51 depleted XRC1-3 cells harboring DSB clusters show similar levels of translocation formation, although chemical inhibition of Rad51 caused a strong reduction in translocation formation**.** We *suggest that when HRR is defective in a DNA-PKcs mutant background, other error-prone pathways benefit from the excessive end processing and cause an increase in translocation formation.*

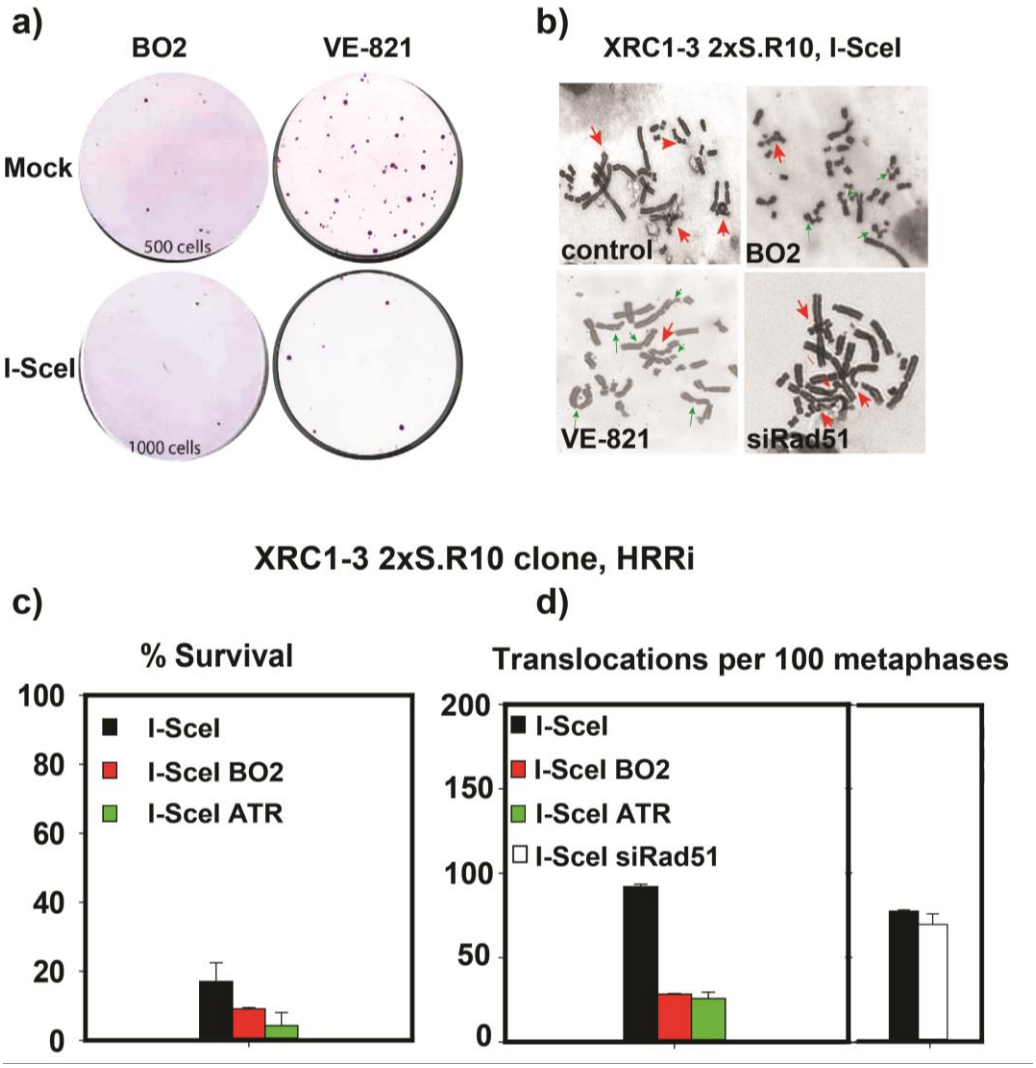

Figure 42: *Survival in DNA-PKcs deficient cells having DSB clusters after abrogation of HRR.*

a) Representative cell culture dishes showing colonies forming after transient expression of I-*Sce*I in XRC1-3 2xS.R10 clone as indicated. In each dish cells were plated immediately after transfection and incubated for 7–8 days to allow colony formation. 25 µM BO2 and 5µM VE-821 were added to the respective dishes 2 h after the transfection. b) Images of selected metaphases of the indicated XRC1-3 2xS.R10 captured 24 h after transfection with the I-*Sce*I expression plasmid. 25µM BO2 and 5µM VE-821 was added to the respective dishes 2 h after transfection. Red arrows point to chromosomal translocations. c) Survival of transfected cells treated with 25 µM BO2 and 5µM VE-821 respectively, calculated using the plating efficiency measured in mock-transfected cells treated with 25 µM BO2 and 10 VE821 of the same clone. Data compiled from two independent experiments. d) Quantitative analysis of chromosomal translocations scored in the XRC1-3 2xS.R10 clone as indicated. Chromosomal translocations scored in mock-transfected cells have been subtracted (0-10 after treatment with BO2 and ATRi; and 0-3 after knockdown with siRad51). Data compiled from two out of three separate experiments showing averages ± SD (n=2 I-SceI + ATRi).

Results

5. Role of alt-EJ in repair of DSB clusters

In the above sections we have seen that the presence of DSB clusters impair DSB repair process resulting in strong killing effect and increased chromosomal translocations. Also we were able to confirm the involvement of CtIP mediated resection processes in the repair of DSB clusters resulting in the higher incidences of translocations. In the previous sections we were also able to show that DSB clustering hampers proper functioning of HRR. So we designed experiments to investigate the involvement of end processing mediated (resection dependent) error-prone pathways in the repair of DSB clusters. As first step we investigated the role of alt-EJ in the repair of simple DSBs and DSB clusters.

Work from our Institute showed that with increasing DSB clustering there is increased processing by alt-EJ [104]. Parp1 is a key player in alt-EJ and is involved in base excision repair (BER) as well. Parp1 inhibitors are used in the clinic to treat of various forms of cancer, especially BRCA1/2 mutated breast and ovarian cancers.

5.1. Inhibition of alt-EJ modestly sensitizes to killing cells harboring simple DSBs or DSB clusters

CHO wild type clones sustaining simple DSBs and DSB clusters (CHO 1xS.D8 and 2xS.R14 respectively) after transfection with I-SceI were treated with 5 μM of PJ34. The results in Figure 43 show a modest or insignificant decrease in the numbers of surviving cells. The inhibitor PJ34 stayed in the medium for the entire duration of incubation of the survival experiments i.e. for 7-8 days until the colonies were fixed and stained for analysis. The modest effect suggests that alt-EJ is not required in the repair of DSBs and DSB clusters.

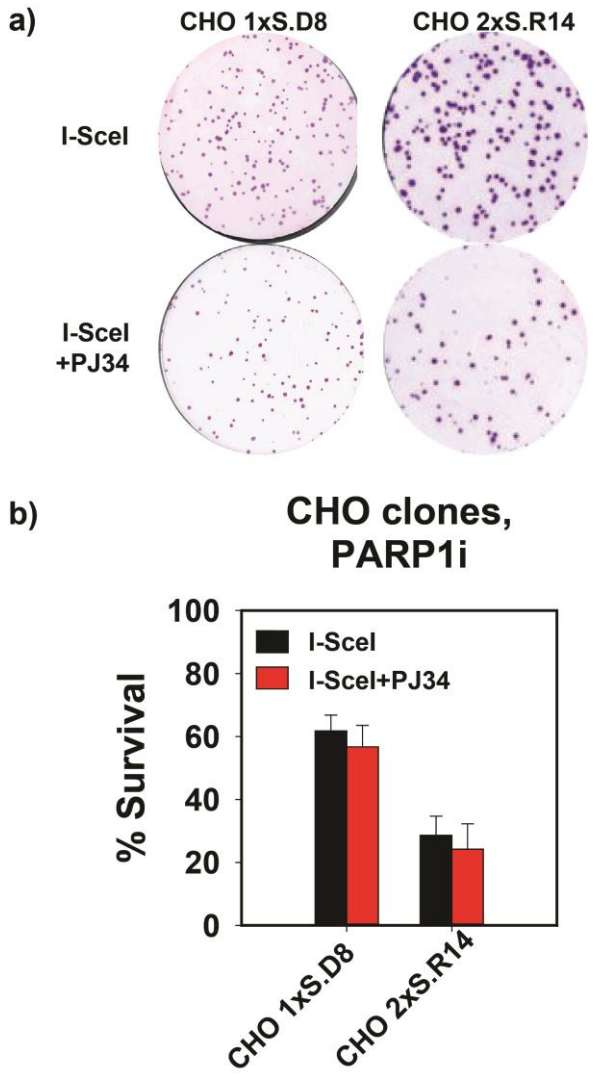

Figure 43: *Chemical inhibition of alt-EJ inflicts modest effect on the survival of cells harboring simple DSBs or DSB clusters.*

a) Representative cell culture dishes showing colonies forming after transient expression of I-*Sce*I in different CHO clones as indicated. In each dish cells were plated immediately after transfection and incubated for 7–8 days to allow colony formation. 5 μM PJ34 was added 2 h after the transfection. b) Survival of transfected cells treated with 5 μM PJ34 calculated using the plating efficiency measured in mock-transfected cells treated with 5 μM PJ34 of the same clone. Data compiled from two out of three experiments showing averages ± SD (n=2 for CHO 1xS.D8 I-SceI+PJ34).

5.2. alt-EJ contributes to the repair of DSB clusters but causes translocations

Since the effect of Parp1 inhibition is modest on the processing of single DSBs and DSB clusters, when measured at the cell survival level, we investigated its effect on translocation formation

using our CHO clones. alt-EJ is widely considered as a mediator of translocations. We investigated therefore its role in the formation of translocations following the induction of simple DSBs and DSB clusters. In previously published work from our lab it has been shown that with increasing complexity of DSB clusters, there is increased involvement of alt-EJ in translocation formation [104]. Here, chromosomal translocations were analyzed, 24 h after the I-SceI transfection. Cells were treated with 5 μM PJ34, 2 h after the transfection and analysis was carried out at metaphase. The results compiled in Figure 44 show a more significant reduction in the numbers of translocations after treatment with PJ34 in the CHO 2xS.R14 clone (that yields DSB pairs upon induction of DNA damage). In contrast, there is no significant change in the incidence of translocations after treatment with PJ34 in the CHO 1xS.D8 clone resulting in the formation of simple DSBs.

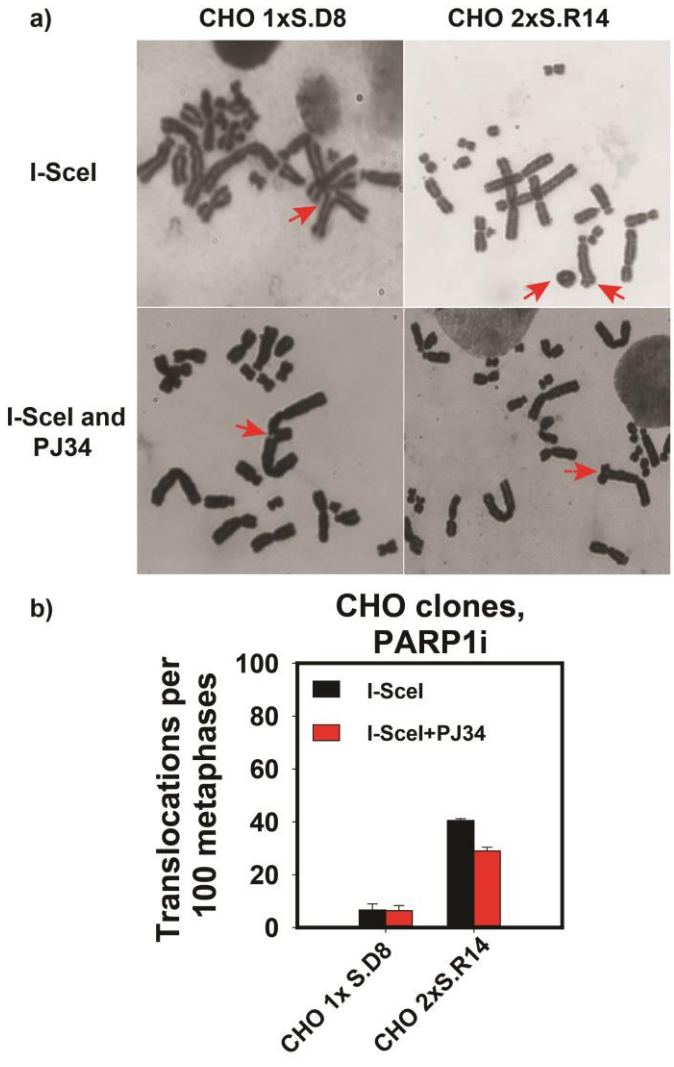

Figure 44: *alt-EJ mediated repair of DSB clusters translocations.*

Results

a) Images of selected metaphases of the indicated CHO clones captured 24 h after transfection with the I-*Sce*I expression plasmid. 5μM PJ34 was added 2 h after transfection with I-SceI to inhibit alt-EJ. Red arrows point to chromosomal translocations. b) Quantitative analysis of chromosomal translocations scored in the different clones as indicated. Chromosomal translocations scored in mock-transfected cells have been subtracted (0–4 per 100 metaphases). Data compiled from two experiments showing averages ± SD.

5.3. In the absence of both c-NHEJ and alt-EJ, DSB clusters cause strong cell killing

We have seen in the previous sections that DSB clusters sensitize cells to a lesser extent than simple DSBs when c-NHEJ is somehow compromised. To investigate the contribution of alt-EJ on the repair of DSB clusters following inhibition of DNA-PKcs, we treated CHO clones 2 h after transfection with I-SceI expressing plasmid, with 5μM NU7441 and 5 μM PJ34. Both inhibitors were kept in the medium for 24 h and were then washed-off, pre-warmed media was added and cells were incubated for 7 days. The results presented in Figure 45 show a significant decrease in the number of surviving cells in the CHO 2xS.R14 clone after combined inhibition of DNA-PKcs and Parp1. The decrease is comparatively lower in CHO 1xS.D8.

These observations suggest that after induction of DSB clusters where c-NHEJ fails, alt-EJ is utilized more frequently. As DSB complexity is increased, there is decreased dependence on DNA-PK-mediated c-NHEJ and increased dependence on alt-EJ. By inhibiting alt-EJ on top of DNA-PKcs inhibition, enhanced cell killing is observed in the clones sustaining DSB clusters as compared to those sustaining simple DSBs.

To confirm the above observations, we treated the DNA-PKcs mutant XRC1-3 2xS.R10 with PJ34 and the results show decreased cell survival after induction of DSB clusters following inhibition of Parp1 (Figure 45). A similar effect is also observed in other c-NHEJ deficient mutants such as the Ku80 mutant, xrs6 2xS.R11. Here again, a low survival is measured after inhibition of Parp1 following the induction of DSB clusters (Figure 45).

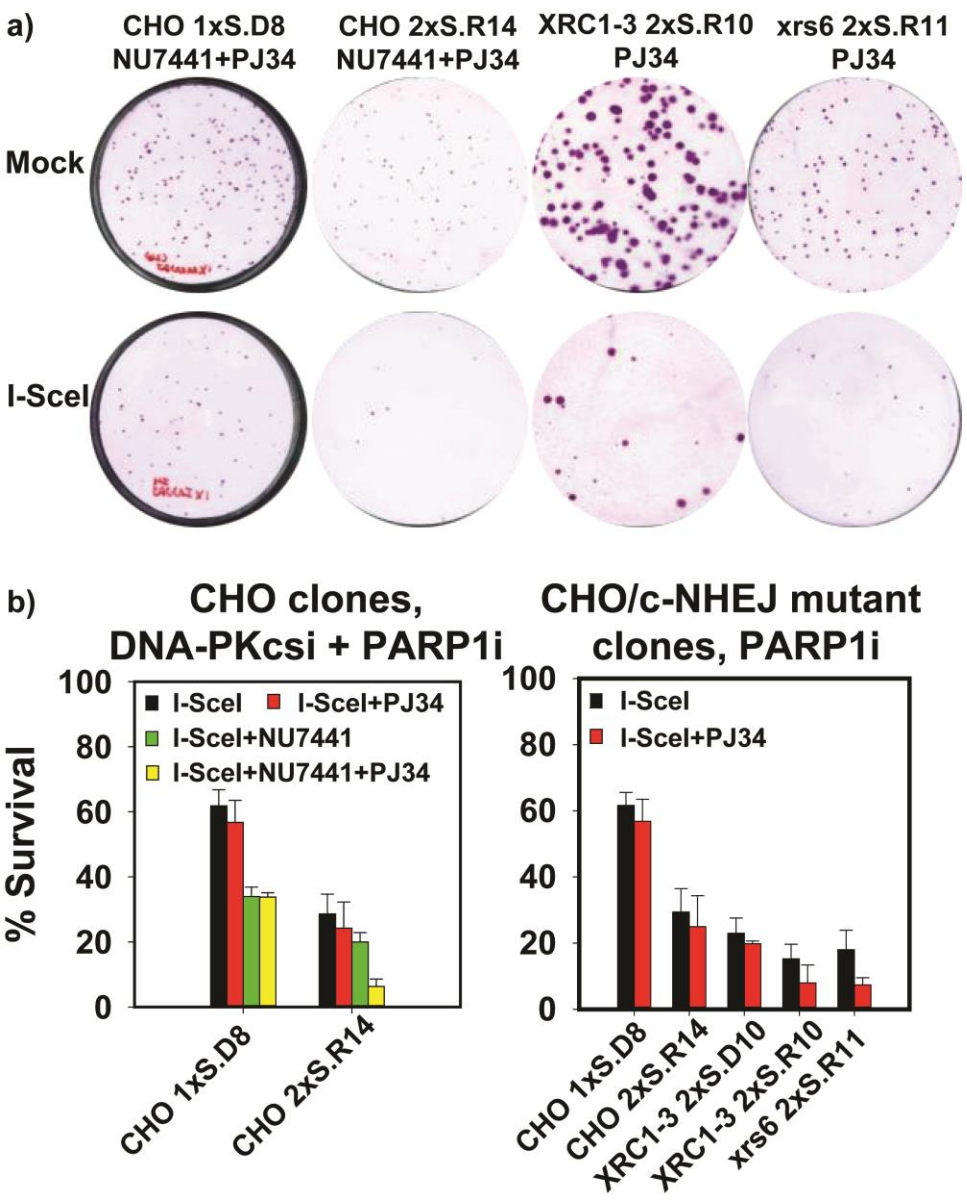

Figure 45: *Survival measured after the combined inhibition of DNA-PKcs and Parp1 (c-NHEJ and alt-EJ).*

a) Representative cell culture dishes showing colonies forming after transient expression of I-*Sce*I in different CHO clones as indicated. In each dish cells were plated immediately after transfection and incubated for 7–8 days to allow colony formation. The indicated inhibitors were added 2 h after transfection and were washed off 24 h later. b) Survival of transfected cells was calculated using the plating efficiency measured in mock-transfected cells of the same clone. Data compiled from two out of three experiments showing averages ± SD (n=2 for I-SceI+PJ34 treated CHO 1xS.D8, XRC1-3 2xS.D10 and xrs6 2xS.R11).

5.4.1. DSB clusters with incompatible apical ends cause high numbers of translocations after combined inhibition of DNA-PKcs and Parp1, but not after combined inhibition of Ku80 and Parp1

Inhibition of alt-EJ in the wild type CHO clones discussed above suppresses translocation formation. But, interestingly when DNA-PKcs was inhibited/deficient, suppression of alt-EJ increased translocation formation in the CHO 2xS.R14 clone where pairs of DSB with incompatible apical ends form. In CHO 1xS.D8 clone on the other hand, no increase in translocations was seen after combined inhibition of c-NHEJ and alt-EJ.

To confirm the above observations the DNA-PKcs mutants XRC1-3 clones (2xS.R4, 2xS.R10; and 2xS.D4, 2xS.D10) were treated with 5 µm PJ34. A similar trend was observed here again and both the XRC1-3 clones with DSB clusters generating incompatible apical ends show an increase in translocation formation. Interestingly, in the same constellation of experiments, the number of translocations forming in XRC1-3 2xS.D4 and XRC1-3 2xS.D10 decrease. *These results again direct our attention towards the crucial role of the nature of DNA ends in translocation formation*. The results of these experiments are shown in Figure 46.

To further investigate the effect of combined inhibition of c-NHEJ and alt-EJ on translocation formation we tested the xrs6 2xS.R11 clone (deficient in Ku80). Cells were treated with 5 µM PJ34 after transfection with I-SceI and were collected 24 h later for analysis. The results in Figure 46 show a reduction in the number of translocations after treatment with PJ34. This is not unexpected, as inhibition of alt-EJ results suppresses translocation formation. But, what is mostly striking is that *the two key components of DNA-PK complex have different effects on the processing of DSB clusters*. The results of this experiment are summarized in Figure 46.

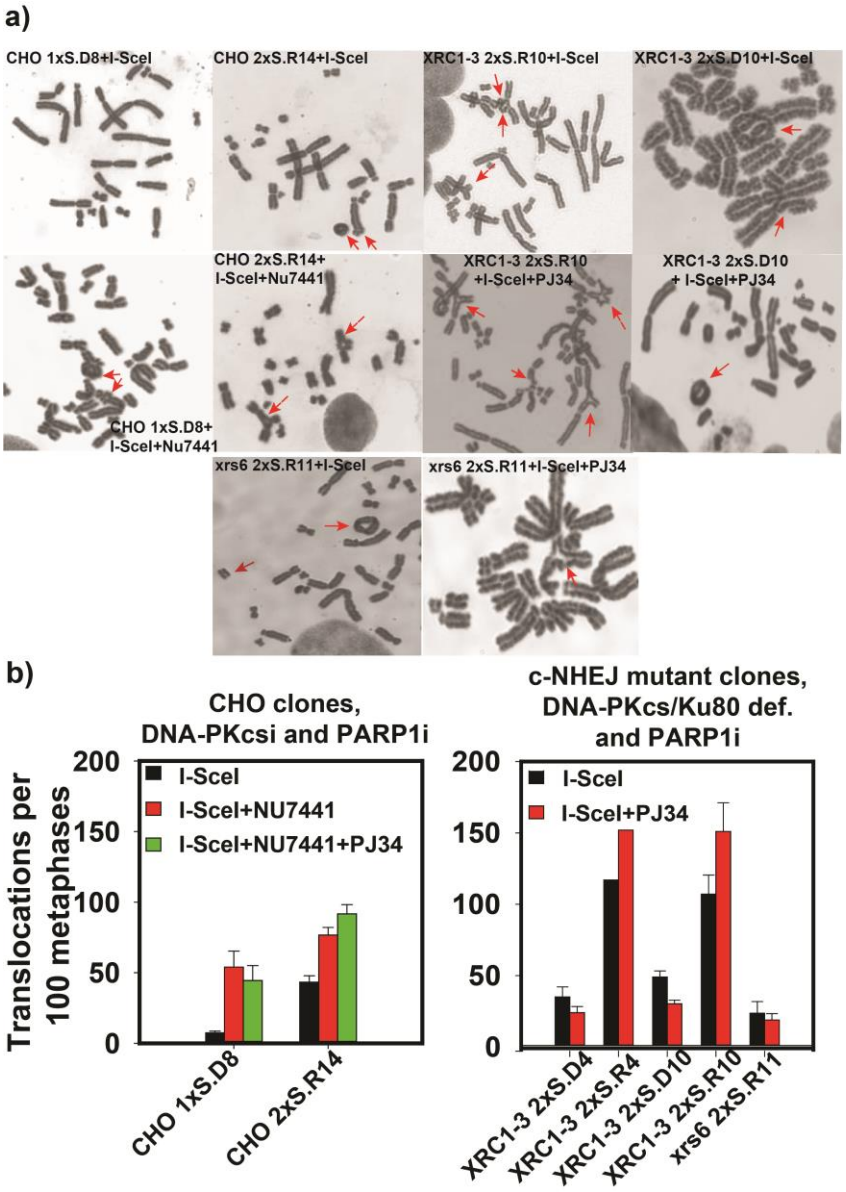

Figure 46: *Translocations in CHO clones treated with NU7441 (10 µM) and c-NHEJ mutant clones, transfected with I-SceI plasmid and treated with 5µM PJ34.*

a) Representative metaphase spreads collected 24 h after transfection with I-SceI plasmid and after treatment with 10 µM NU7441 (CHO clones only) and 5 µM PJ34, in the indicated clones. b) Qualitative analysis of data in the cells transfected with I-SceI plasmid treated with and without 10 µM NU7441 (CHO clones only) and 5 µM PJ34 in the indicated clones. Data compiled from two experiments showing averages ± SD (n=3 in CHO 2xS.R14 and XRC1-3 2xS.R10 transfected with I-SceI and treated with NU7441+PJ34 and PJ34 respectively; and data shown from one experiment out of two showing similar trends in XRC1-3 2xS.R4 I-SceI+PJ34).

5.4.2. End processing increases translocation formation after inhibition of alt-EJ in DNA-PKcs deficient clones sustaining DSB clusters with incompatible ends

To confirm the role of DSB end-processing in translocation formation, we transfected XRC1-3 2xS.D10 and XRC1-3 2xS.R10 clones with I-SceI–TREX chimera [108] to generate blunt ends at the DSBs formed. Figure 47 show the results. Indeed we see that in the presence of DSB blunt ends, there is no increase in translocation formation in the XRC1-3 2xS.R10 clone after inhibition of Parp1; and the number translocations is similar in both XRC1-3 clones. After transfection with I-SceI-TREX chimera the number of translocations is also suppressed in the XRC1-3 2xS.R10 clone after inhibition of Parp1. Overall, similar numbers of translocations are measured under these conditions in XRC1-3 2xS.D10 and XRC1-3 2xS.R10 clones.

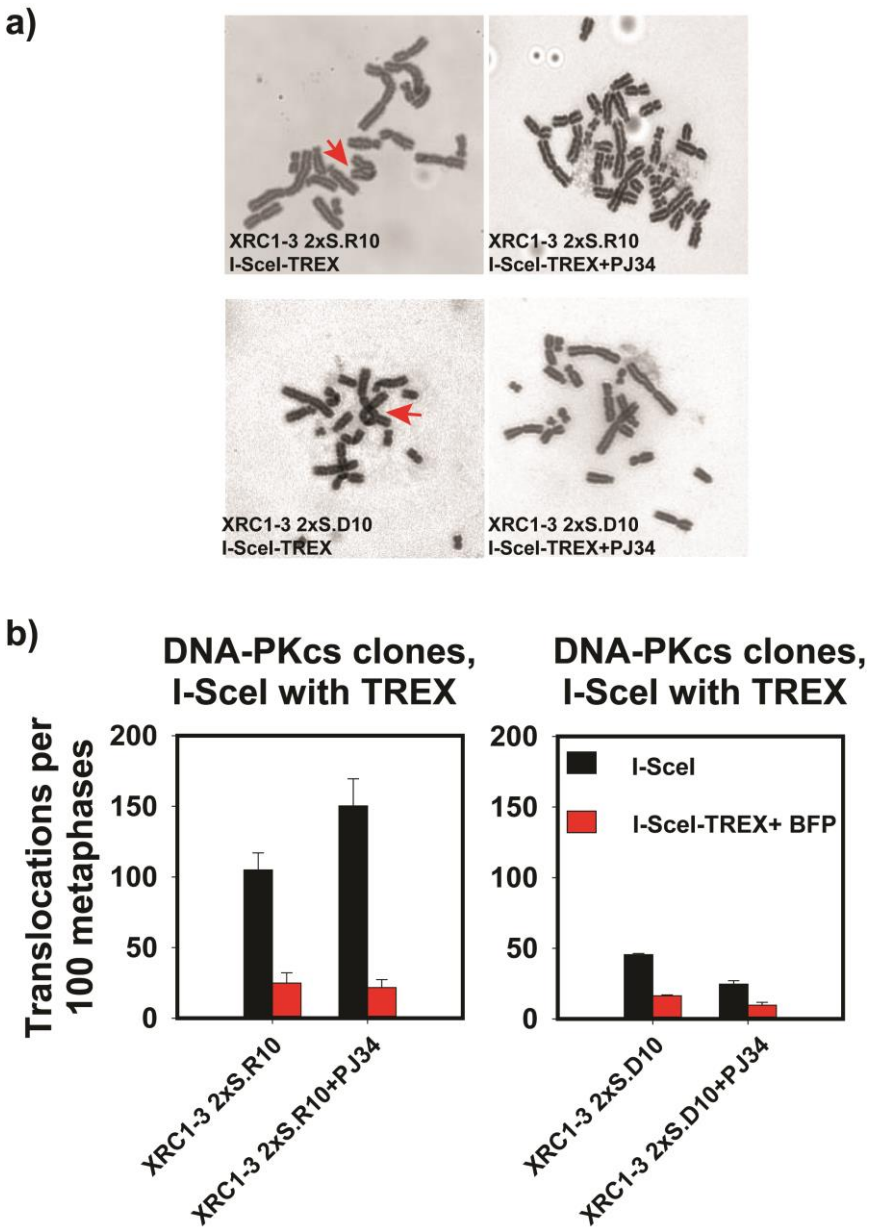

Figure 47: *Translocations in DNA-PKcs deficient cells having DSB clusters with incompatible and compatible ends transfected with I-SceI and I-SceI-TREX plasmid.*

a) Representative metaphase spreads collected 24 h after transfection with I-SceI-TREX plasmid treated with and without 5 µM PJ34, in XRC1-3 2xS.R10 (upper) and XRC1-3 2xS.D10 (lower). I-SceI alone is the control where the cells were transfected with I-SceI expressing plasmid in XRC1-3 2xS.R10 (left) and XRC1-3 2xS.D10 (right). Red arrows mark the translocations. b) Qualitative analysis of data in cells transfected with I-SceI-TREX plasmid treated with and without 5 µM PJ34. Data compiled from three experiments showing averages ± SD.

Results

5.4.3. Parp1 inhibition after CtIP depletion leaves translocation formation from DSB clusters unchanged

CtIP is the key mediator of end-resection mediated repair processes. alt-EJ depends therefore on CtIP function. To confirm the involvement of CtIP mediated responses in our model system and to investigate the causes of residual translocations after CtIP depletion, we inhibited Parp1 with 5 µM PJ34 in CHO clones following transfection with the I-SceI expressing plasmid.

Confirming the dependency of alt-EJ on CtIP mediated resection, no further suppression in translocation formation was observed after combined CtIP depletion and Parp1 inhibition in CHO 2xS.R14 and CHO 4xS.R12 cells sustaining DSB clusters with incompatible ends (Figure 48).

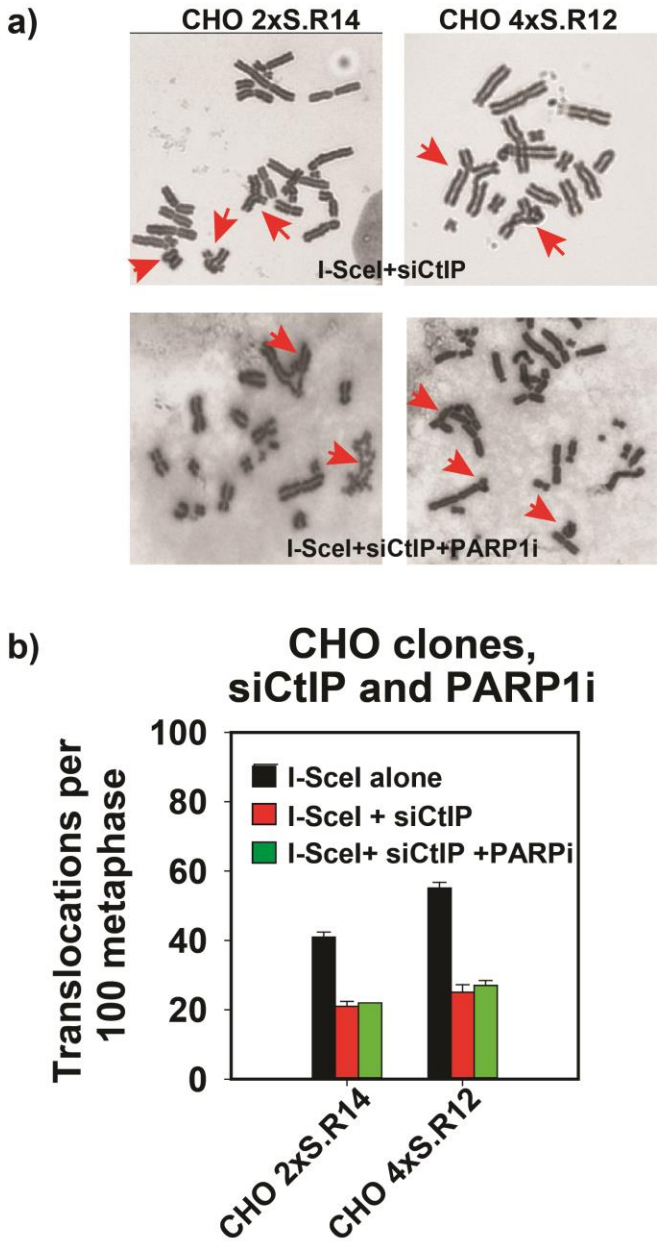

Figure 48: *Translocations in CHO clones sustaining DSB clusters after CtIP depletion and Parp1 inhibition.*

a) Representative metaphases collected at 24 h after transfection with I-SceI plasmid in CtIP depleted cells. 5 µM Parpi, PJ34 was added 2 h after I-SceI transfection. Red arrows mark the translocations. b) Translocations were measured 24 h after transfection with I-SceI and depletion of CtIP. Parpi was added 2 h after I-SceI transfection. Data compiled from two different experiments showing averages ± SD.

6. Role of Rad52 dependent pathways in the repair of DSB clusters

To examine the role of SSA in cell killing and chromosome aberration formation after exposure to high LET IR we further tested our model system in appropriately designed experiments. Astonishingly our results show a diminished role for HRR in the processing of DSB clusters with increasing complexity, but suggest a strong contribution from resection dependent pathways. Another striking observation was translocation formed from DSB clusters when they generated incompatible ends in DNA-PKcs deficient and Parp1 inhibited condition. To examine what pathway is causing translocations in the absence of both c-NHEJ and alt-EJ we therefore, investigated the role of Rad52 mediated repair in the processing of simple DSBs and DSB clusters. Rad52 is a key protein of SSA, a highly mutagenic and error prone pathway that could also cause translocations.

6.1. Translocations measured in CHO clones after Rad52 knockdown

To investigate a contribution of SSA in translocation formation we transfected CHO wild type clones (CHO 1xS.D8, CHO 2xS.R14 and CHO 4xS.R12) with a siRNA targeting Rad52. Rad52 depleted cells were transfected with I-SceI and siRad52, 24 h later, and translocation formation was measured 24 h later. The results obtained are shown in Figure 49. It is evident that Rad52 depletion decreases translocation formation, especially when DSB clusters are generated. Since SSA involves annealing of homologous repeat sequences that flank a DSB, sequencing experiments are required to confirm that what we see is indeed Rad52 mediated SSA.

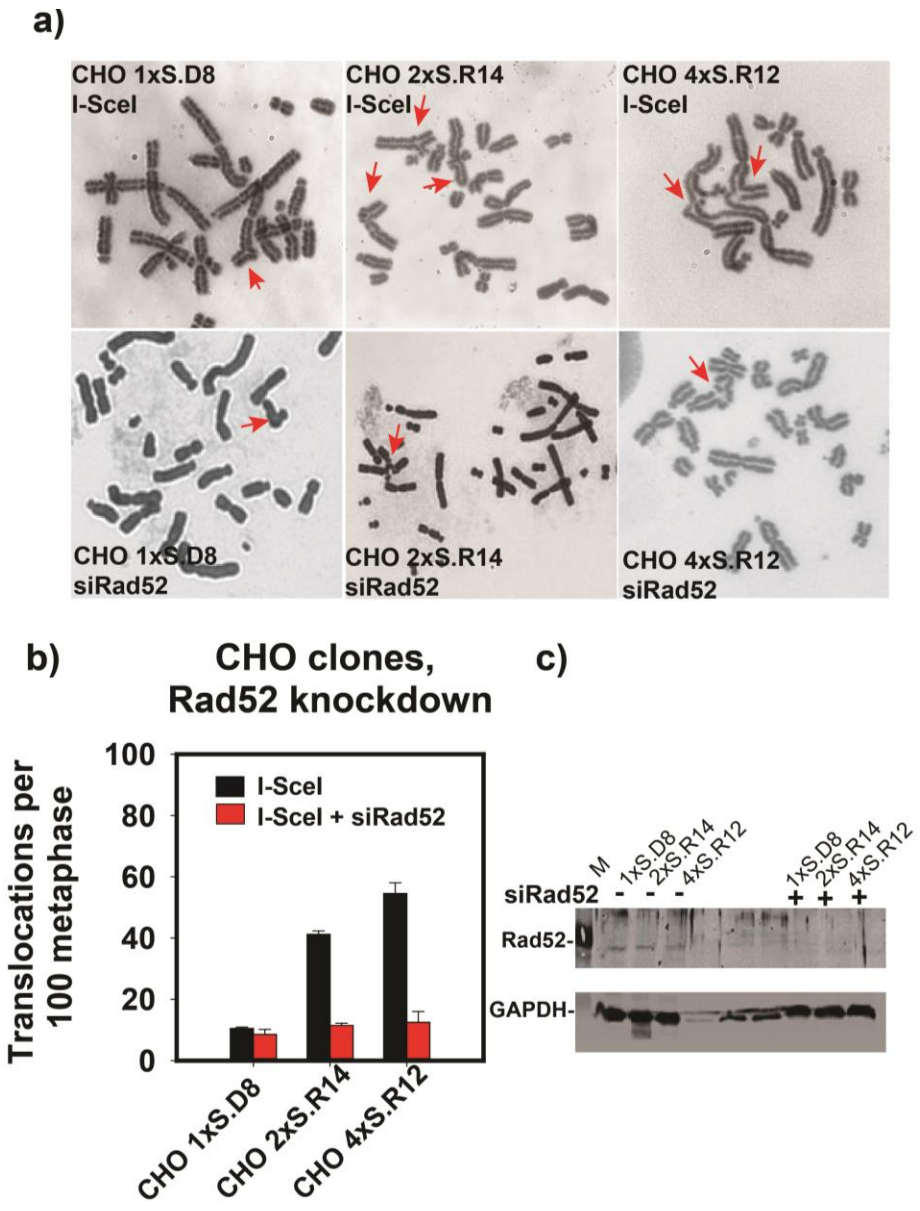

Figure 49: *Translocations in CHO clones after Rad52 depletion.*

(a) Representative metaphase spreads collected 24 hours after I-SceI transfection in Rad52 depleted cells. Red arrows mark translocations; (b) Quantitative analysis of translocations formed in CHO clones 24 h after I-SceI transfection in Rad52 depleted condition. Data compiled from two out of three independent experiments showing averages ± SD. (c) Western blots confirming Rad52 knock down.

6.2. Translocations measured in CHO clones after depletion of CtIP and inhibition of Rad52

After depletion of CtIP we observed that there was a significant reduction in number of translocations forming from DSB clusters. Yet the decrease in translocations seen after depletion of Rad52 is greater. It is widely accepted that error prone Rad52 mediated pathways are resection mediated and that for Rad52 mediated SSA, CtIP mediated end resection is necessary [95].

We designed therefore experiments such that in the CHO clones forming DSB clusters (pairs and quadruplets) we first depleted CtIP and 2 h after the transfection with I-SceI enzyme we added (10 µM) of a Rad52 inhibitor. The results show that in comparison to the control condition, a strong decrease in number of translocations is seen. A further decrease is seen after inhibition of Rad52 in CtIP depleted condition (Figure 50). These results suggest that in presence of DSB clusters Rad52 mediated repair does not essentially depend on CtIP mediated resection. However, it may also indicate that residual resection as a result of incomplete CtIP depletion allows SSA to operate.

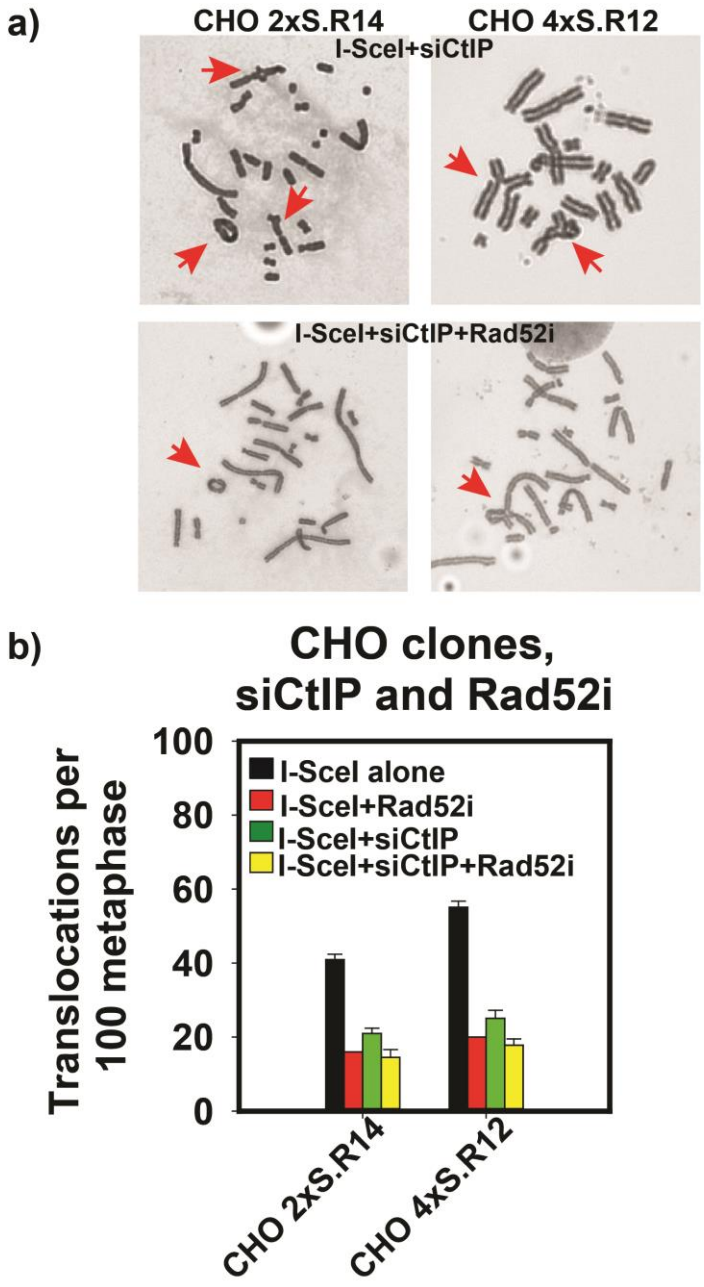

Figure 50: *Translocations in CHO clones having DSB clusters after CtIP depletion and Rad52 inhibition.*

a) Representative metaphases collected at 24 h after transfection with I-SceI plasmid in CtIP depleted cells. 10 µM Rad52i 6-OH DOPA was added 2 h after the I-SceI transfection. Red arrows mark the translocations. b) Translocations were measured 24 h after transfection with I-SceI and depletion of CtIP. Rad52i was added 2 h after I-SceI transfection. Data compiled from two different experiments showing averages ± SD (data shown from one experiment after Rad52 inhibition [Red bar in the graph]).

Results

6.3. Translocations measured in XRC1-3 clones after depletion /inhibition of Rad52

Following our experiments in XRC1-3 2xS.R10 clone sustaining DSB clusters with incompatible ends that show increased incidence of translocations after inhibition of Parp1 we inquired whether SSA is involved in the translocation formation. Therefore, we inhibited/depleted Rad52 in the XRC1-3 2xS.R10 clone.

Strikingly, a decrease in the number of translocations is observed after inhibition of Rad52 in this DNA-PKcs mutant clone. This is effect is opposite to that seen after inhibition of Parp1. An interesting experiment would be to inhibit both Rad52 and Parp1 in the XRC1-3 clone to investigate whether in absence of Parp1 in a DNA-PKcs deficient condition, Rad52 contributes more to translocation formation (our preliminary results show that after combined inhibition of Parp1 and Rad52, the number of translocations observed are same as after inhibition of Rad52 alone). *The results in Figure 51 confirm the involvement of Rad52 mediated error-prone DSB processing along with alt-EJ in the formation of translocations*.

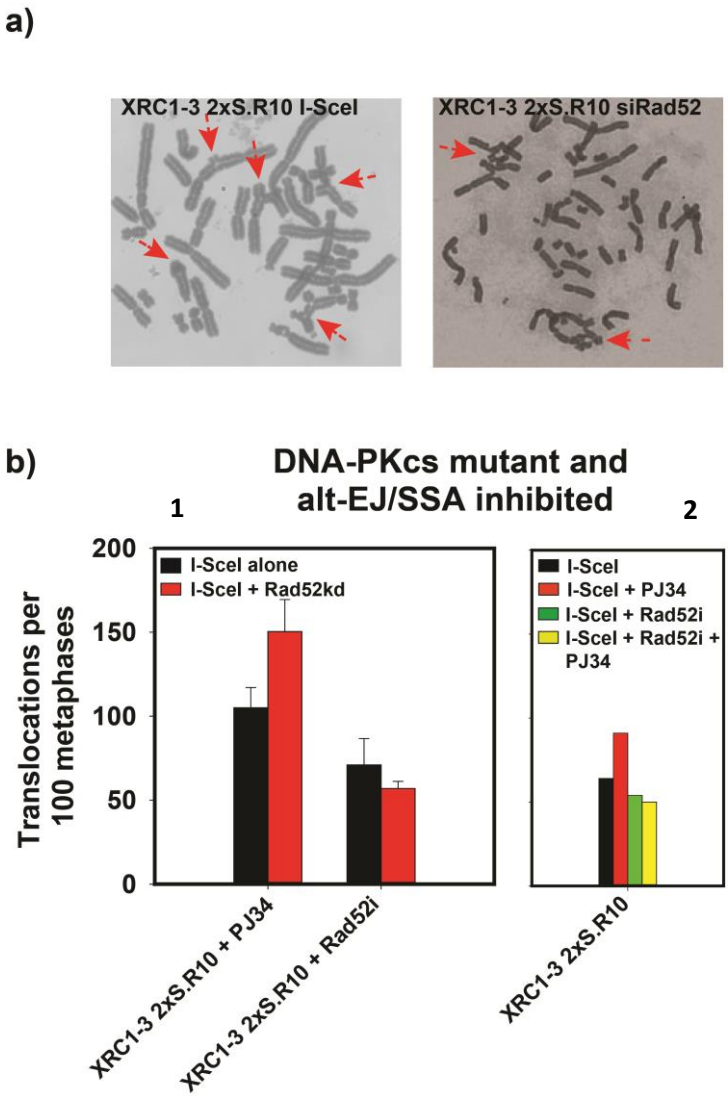

Figure 51: *Translocations in XRC1-3 clone having DSB clusters after Rad52 inhibition/depletion.*

a) Representative metaphases 24 h after I-SceI transfection in Rad52 depleted/inhibited condition. Red arrows mark the translocations. b) Translocations were measured 24 h after transfection with I-SceI and depletion or inhibition of Rad52. The condition depicting treatment after inhibiting Parp1 using 5μM PJ34 is shown to compare the opposite effects seen after inhibiting alt-EJ and Rad52 mediated pathways respectively. b1) Data compiled from two different experiments showing averages ± SD (n=1 after siRNA knock down; and n=2 after Rad52i in 10μM concentration 6-OH-DOPA; both conditions gave similar response). b2) n=1 for the condition with combined Parp1 and Rad52 inhibition in XRC1-3 2xS.R10.

Results

Discussion

Here we test the hypothesis that DSB clusters represent a highly dangerous form of DNA damage with a particularly high risk for mis-repair as a consequence of the destabilization of chromatin. It is hypothesized that erroneous processing of DSB clusters leads to formation of chromosomal aberrations and ultimately to the cell death. DSB clustering as a cause of irreversible radiation effects has been suggested in the past but mainly tested after IR using mathematical modeling and fitting to cell survival and DSB-repair results [33].

To overcome the limitations of the stochastic nature of IR-mediated induction of DSBs, a restriction endonuclease (RE)-based system was developed promising to generate more conclusive answers in this important question. The approach taken involves the generation of DSBs by I-SceI endonuclease. Since the recognition sequence of I-SceI is not present in the genome of higher eukaryotic cells, it offers the possibility of generating different constellations of DSBs in a controlled manner by integrating appropriately constructed vectors in the genomes of test cells and generating DSBs by transient transfection with a vector expressing the I-SceI enzyme. To mimic IR in its ability to generate multiple DSBs, the model developed uses the Sleeping Beauty DNA transposition technology to also achieve multiple integrations in the genome of the I-SceI containing constructs [33].

I-SceI based model systems were developed in wt, c-NHEJ and HRR deficient CHO cells. Besides generating clean DSBs with this system the distances between consecutive DSBs can also be varied. The distances were engineered to resemble the winding of DNA around either one or two nucleosomes plus the linker regions. This allows analysis of the probability for repair accidents caused by the simultaneous cleavages at two or more sites that may generate nucleosome loss and thus chromatin destabilization.

As a control, a model system for simple DSB as typically induced by RE was also generated [33, 47]. DNA damage resulting in DSB clustering due to exposure to high LET radiation is more extensive and complex in comparison to DNA damage due to low LET [30]. In terms of genomic stability, high LET exhibits a variety of signatures of chromosomal aberrations [116]. Radiation-induced chromosomal aberrations represent an early marker of late effects, including cell killing and transformation [117].

Translocations result in the formation of new combinations in the genome as they are generated when ends of two or more DSBs are rejoined. They are mis-repair events arising mostly from processing errors at DSBs. Since HRR is an error-free pathway and not known to contribute to the formation of translocations and c-NHEJ infrequently results in the formation of translocations, other error-prone pathways like alt-EJ and SSA (Rad52 mediated) may opportunistically result in the formation of translocations. "Requirement for translocations to form is that the ends of the participating DSBs, which for each DSB at induction are directly adjacent and therefore privileged for rejoining, drift apart and join with ends from neighboring DSBs also experiencing processing complications" [104]. The number DSBs that are left unrepaired and still haven't been rejoined also critically affect translocation formation. The design of HRR or c-NHEJ repair is such that they oppose drifting of the DNA ends, so when this drifting of DNA ends happens, it might well be the result of an accident caused by a failure of these repair pathways as a consequence of other intervening biological processes [104].

Drifting of DSB ends might happen due to several processes such as:

- If DSB processing is impaired then DSB ends remain opened for longer time and thus, the chance of them to drift apart by diffusion increases [104].
- Regular ongoing activities on chromatin can result in end-drifting of DNA ends. These ongoing processes include processes such as transcription and replication, as well as general and local chromatin remodeling, and scheduled global condensation/de-condensation (e.g. before or after mitosis).
- In addition, drifting of DNA ends may also be facilitated by the generation of DSB-clusters resulting in chromatin destabilization. In this work we have focused mostly on the generation of DSB clusters as form of IR induced DNA damage.

With increasing LET a proportional increase in occurrence of chromosomal aberrations is observed [118] and it correlates very nicely with the strong killing effect observed after increasing the LET [104]. But, what proportion of DSBs are processed by each pathway/s, and what causes the greater incidence of chromosomal aberrations is not known yet. To investigate the specific repair processes that are involved in the repair and processing of DSB clusters, our CHO based model is an extremely beneficial biological tool that assists in providing insights into the mechanisms of repair/mis-repair of DSB clusters.

1. To introduce damage in the cells we first transfected our test cells with the I-SceI expressing plasmid using nucleofection, one of several transfection methods. After induction of DNA damage we observe that **with increasing DSB clustering and complexity an increased cell killing and incidence of translocations is seen.** The reproductive cell death measured by the colony forming assay for simple and clustered DSBs show a strong killing effect when DSB clusters are present. The explanation for decreased survival can be that with increasing number of DSBs in a cluster, nucleosomes may be lost causing local disruption of chromatin **(**Figure 20).

2. Next we try to explain how the cellular repair machinery deals with simple DSBs and clustered DSBs. For this we measured chromosomal aberrations (specifically chromatid and chromosomal translocations) using classical cytogenetics. The model for formation of translocations suggests that "chromosome exchanges result from the interaction of two or more breaks in close spatial and temporal proximity, where the wrong chromosome ends are joined [119], [120], whereas chromatid breaks are caused by the lack of repair". We find from our experiments that the numbers of translocations are significantly increased in the clones with DSB clusters (CHO-2xS.R14 and CHO 4xS.R12) compared to the clone having single DSBs (CHO-1xS.D8). **These observations imply that DSB clusters lead to repair accidents and therefore, that they could be the main cause for lethal events leading to the high killing observed in survival experiments** (Figure 24).

3. It can also be seen that with the decrease in number of I-SceI sites (referred to as degree of DSB clustering) in the constellation of two I-SceI sites per constructs (DSB pairs) in the CHO clone CHO 2xS.R6 a better cell survival is seen. Better survival response also concurs with the lesser number translocations observed in this particular CHO clone. In contrast the CHO clone with higher degree of DSB clustering (CHO 2xS.R14) show significantly high number of translocations, and the higher incidence of chromosomal aberrations reflects on the increased cellular killing that is observed. This shows that not only the complexity of DSB clustering but also **the degree of DSB clustering influences the repair outcome** (Figure 20; Figure 24).

It remains to be investigated whether the distance between the two I-SceI sites leads to the high frequency of mis-repair events. This question can be addressed by generating clones with 500 and 1000 bp space between I-SceI sites and measuring translocations after DSB induction. The analysis of translocation frequencies in our I-SceI model-systems by whole genome sequencing

or fluorescence in situ hybridization (FISH) would reveal further important information about the formation of translocations from simple DSBs as compared to clustered DSBs. With the observations made in our CHO based model system we could establish the effects of presence of DSB clusters in the genome and their detrimental effects on the repair outcome. We observe effects corresponding to those made in cells exposed to high LET radiation. Complex DSB clusters are formed at a higher rate in cells exposed to high LET and have widely been considered as the reason for higher RBE values of high LET IR.

High LET radiation has higher RBE than the low LET radiation and results in increased cellular killing. The effects are till now attributed to the physical properties of IR which result in formation of more complex closely spaced DSB clusters (higher numbers of DSB clusters are seen when the cells are exposed to high LET IR). The DSBs that are generated by high LET IR are thought to be more clustered and are more complex in nature and more often may result in processing errors. In the following sections we have tried to investigate the repair pathways that are employed in the processing of DSB clusters.

4. c-NHEJ is functional throughout the cell cycle and it has fast repair kinetics. Experimentally it has been shown that after exposure to high LET IR c-NHEJ is impaired and is not utilized efficiently to process the subset of DSBs determining cell survival [121, 122]. In c-NHEJ mutant cells lines defective in either **DNA-PKcs (XR-C13) or Ku80 (xrs6), we found that DSB clusters are not processed efficiently. But, DNA-PKcs defects result in significantly higher numbers of chromosomal aberrations than Ku80 defects.** In previously published work from our lab, we found out that compared to the DSB clusters, simple DSBs show greater response to DNA-PKcs inhibition (NU7441 inhibitor). The response was measured using the clonogenic survival assay or translocation formation [104]. We have confirmed this response in the present thesis and determined that with increasing DSB cluster complexity there is decreased utilization of c-NHEJ. We could clearly observe that in cells where simple DSBs are present (CHO 1xS.D8) the decrease in survival is greater than the decrease observed in cells sustaining DSB clusters (CHO 2xS.R14) (Figure 27). Similarly, the increase in the number of translocations is greater in CHO 1xS.D8 (simple DSBs) than in CHO 2xS.R14 (DSB pairs) (Figure 31). This response suggests that with increasing DSB clustering the dependency on c-NHEJ for the repair of DNA breaks is decreased. DNA-PKcs mutant clones and Ku80 mutant clones sustaining DSB pairs

could also confirm these observations. But, interestingly, with these clones (Ku80 mutant xrs6 2xS.R11) we found that a similar degree sensitization to killing (Figure 29) was accompanied by low numbers of translocations as compared to the DNA-PKcs mutant. In fact the numbers of translocations in xrs6 2xR11 cells were lower than in the CHO 2xR14 clone (Figure 34). Similar observations were made after knocking down Ku80 in CHO clones (CHO 1xS.D8 and CHO 2xS.R14). After knocking down Ku80 an overall decrease in the formation of chromosomal translocations is observed in CHO 2xS.R.14 clone (Figure 35). Furthermore, knocking down Ku80 in CHO 1xS.D8 (Simple DSBs) results in an increase in translocations as one would expect; and XRC1-3 cells having DSB clusters resulted in no significant change in the numbers of translocations (Figure 35). More work is required to describe the role of Ku80 in the formation of translocations in cells sustaining DSB clusters. m-FISH analysis can also add information on the exact type and frequency of chromosomal aberrations forming.

It has been long known that exposure to high LET IR renders wild-type cells extremely sensitive and they survive worse than after exposure to low LET radiation. It is also known that the c-NHEJ deficient cells are killed by high and low LET radiation with the same efficiency, though a clear mechanistic explanation for this response is still lacking. According to one model this effect might be due to the generation of small (~40 bp) DNA fragments that inhibit c-NHEJ by preventing the normal function of Ku [123]. Atomic force microscopy imaging shows the presence of small DNA fragments resulting from clustered DSBs and the small (<30 bp) DNA fragments generated from clustered DSBs have also been propose to compromise Ku function. Additional work shows that DNA–PK, a complex between the Ku and DNA–PKcs, is also inhibited by short (14–20 bp) DNA fragments. [33]

Hence it can be said that one of the possible reasons for increased efficiency of high LET radiation is the generation of DSB clusters that compromise c-NHEJ as demonstrated in previous work [104] and also confirmed here in this work, independently of whether Ku can bind to the generated DNA fragments or not. “It is notable that as DNA-PKcs inhibition brings the translocation yields of single-DSBs to the level constitutively seen by DSB-quadruplets, with or without inhibitors, DNA-PKcs inhibition brings cell killing of low LET radiation to levels observed after exposure to high LET radiation, irrespectively of inhibitor treatment” [104].

5. Based on the observations made thus far, which show that in the CHO clones with an increase in DSB clusters c-NHEJ inhibition causes no further increase in translocations, it can be stated that DSB clusters result in the formation of translocations that are not due to processing utilizing c-NHEJ. It was observed that in CHO clones sustaining DSB clusters, both CHO 4xS.R12 (used in [104]) and CHO 2xS.R12 (confirmed also in this work and [104] which upon I-SceI transfection show high incidence of chromosomal translocations; show marked reduction in numbers of translocations after inhibition of Parp1 by using 5μM PJ34 (Figure 44). These results confirm that **DSB clusters utilize alt-EJ more frequently which results in increased incidence of chromosomal translocations.** A possible explanation for the results showing decrease in the numbers of translocations from DSB clusters after inhibition of alt-EJ might be that after their induction, DSB clusters destabilize chromatin thus facilitating the drifting of DNA ends apart. This drifting of DNA ends feeds translocation formation; and "alt-EJ operates on destabilized chromatin more efficiently than c-NHEJ and is predominantly responsible for translocation formation esp. in the experimental system used here in this work" [104].

6. We also observed that the DSB clusters with incompatible ends (CHO 2xS.R14) show higher numbers translocations than the DSB clusters having compatible ends (CHO 2xS.D12) (Figure 24). Even the survival of the cells is significantly better when the DSB clusters have compatible ends (Figure 20). These results suggest that requirement for DNA end processing results in worse survival and increased formation of translocations. This observation was experimentally confirmed using 2 approaches; one is an indirect approach in which plasmid resulting in expression of I-SceI-TREX chimera after transfection, was used (Figure 25); and the other a more direct approach using siRNA against CtIP to inhibit DNA end resection (Figure 26). In the former approach the I-SceI-TREX plasmid upon transfection results in induction of DSBs that immediately are further digested resulting in generation of DSB blunt ends. In the second approach CtIP is knocked down and this results in inhibition of DNA end resection. It can be observed that with inhibition of resection or creation of blunt ends, there is decrease in the number of translocations and the decrease is more pronounced in DSB pairs and quadruplets with incompatible ends, than in simple DSBs and DSB clusters with compatible ends. We can thus, deduce from these results that with increase in DSB clustering and with increase in their complexity (quadruplets are more complex than doublets/pairs) repair pathways requiring DNA end resection are predominantly employed (Figure 26). This observation is in concordance with

the recently published review article [30] where a model hypothesizes that processing of DSB clusters (high LET induced) might require an increased involvement of resection mediated processes. We saw in the presence of DSB clusters particularly when they generate incompatible apical ends, a reduction in the incidence of translocations (CHO 2xS.R14 and CHO 4xS.R12) after knocking down CtIP. These results confirm that **increased requirement of DSB end processing by DSB clusters results in an increase in numbers of translocations.**

The role of resection mediated pathways on the formation of translocations can also be seen in the DNA-PKcs deficient cells (XRC1-3). Here particularly, DSB clusters with incompatible ends result in an increase in the number of translocations after inhibition of Parp1 (Figure 46). In the presence of DSB clusters with compatible ends "XRC1-3 2xS.D10" a similar response was observed where inhibition of Parp1 dependent alt-EJ results in decrease in the occurrence of translocations (Figure 46). To investigate whether the effect observed in XRC1-3 2xS.R10 (having incompatible DSB ends) is due to the presence of incompatible DSB ends (that necessitates the need for resection mediated pathways) I-SceI-TREX plasmid was used to generate DSBs with blunt ends. After generation of DSB blunt ends there is a reduction in the numbers of translocations and the effect on numbers of translocations is similar to that observed in the DSBs with compatible DNA ends (Figure 47). So in summary, in the DNA-PKcs deficient condition, an opposite effect on the formation of translocations is seen i.e. after the inhibition of alt-EJ rather than an increase a decrease in number of translocations. This was quite an interesting observation and we further investigated what repair pathway resulted in increase in the translocations when both DNA-PKcs dependent c-NHEJ and Parp1 were inhibited. We will discuss this interesting observation again later in this section.

It has been widely stated in the literature that instead of c-NHEJ it is HRR that has more profound role in the repair of DSB clusters produced after exposure to high LET IR [102, 124, 125]. But, one might argue that since HRR is an error free pathway, then why after exposure to high LET radiation there are increased occurrence of chromosomal aberrations (esp. in G2 phase cells) [126]? One possible explanation is that instead of the cells using resection dependent error free HRR, they use instead other resection dependent but error prone pathways that cause the increased formation of chromosomal translocations observed.

The results obtained after knocking down CtIP confirm that with increasing LET there is an increased utilization of resection mediated pathways in the processing of DSB clusters. It can be clearly seen that after knocking down CtIP, there is a decrease in translocation formation in the CHO clones that have DSB clusters with incompatible ends "R". This decrease is not observed in the case of induction of simple DSBs, and in the case of DSB clusters with compatible ends, the decrease observed after CtIP knockdown is lower than the decrease observed in the case of DSB clusters having incompatible ends (Figure 26).

7. Furthermore, as Rad51inhibition results in inhibition of HRR we knocked down Rad51 [103] and scored chromosomal translocations in cells harboring simple DSBs (CHO 1xS.D8) and DSB clusters (CHO 2xS.R14 and CHO 4xS.R12). We observed an increase in translocation formation in the testing cells sustaining simple DSBs. A significant increase in the numbers of translocations is also observed in the CHO 2xS.R14 clones forming DSB pairs with incompatible ends. This increase was significant but smaller than the increase seen in the CHO 1xS.D8 clone. Interestingly, no additional change in translocation formation was seen in the CHO 4xS.R12 clone forming DSB quadruplets (Figure 40). Chemical inhibition of Rad51 using the inhibitor BO2 gave also similar trends in the CHO 1xS.D8 clones forming simple DSBs (a slight increase in numbers of translocations is seen) and in the CHO 4xS.R12 clones (DSB quadruplets; no change in the numbers of translocations is seen), but, interestingly there is a significant reduction in numbers of translocations after BO2 treatment in DSB pairs having incompatible ends (CHO 2xS.R14) [Figure 40]. This result suggests that in the 2xR constellation chemical inhibition of Rad51 exerts a dominant negative effect that prevents the operation of translocation forming DSB pathways. This is another fully unexpected and highly relevant observation that requires more in depth analysis.

The above observations suggest decreased involvement of HRR in the repair of DSB clusters a conclusion that is further supported by the results obtained from the colony forming assay (Figure 37) and by scoring Rad51 foci (Figure 38). A reduction in the survival was seen for cells sustaining simple DSBs and DSB clusters, but the decrease is greater in cells sustaining simple DSBs than DSB clusters (Figure 37). Similar observations could also be made after measuring Rad51 foci, 15 hours after transfection (Figure 38). After measuring Rad51 foci in G2 cells, it can be seen that cells having simple DSBs have higher ratio of Rad51 foci formation (8 single DSBs), in comparison to CHO cells having DSB clusters with incompatible ends (14 DSB pairs). **Thus,**

we can conclude that with increasing DSB clustering, there is decreased involvement of HRR. This conclusion differs from reports in the literature, which suggest larger utilization of HRR after exposure to high LET radiation [102, 124, 125], but it also provides an explanation for the increase in chromosome aberration formation in cells exposed to high LET radiation [30].

8. Previous work from our lab shows [104] extensive deletions at the repair junctions of DSB clusters (in CHO 4xR12 more extensive deletion are seen than in the CHO 2xR14 clones) and increased processing of DSB clusters by alternative end joining. We have also seen thus far that with increasing DSB clustering there is increased involvement of CtIP mediated resection pathways and decreased involvement of HRR. Taking all these observations into consideration we finally tested the role of Rad52 mediated pathways (SSA) in the processing of DSB clusters. It is known that Rad52 mediated SSA is highly mutagenic causing extensive deletions and possibly also chromosomal translocations [93]. To test SSA involvement in the endpoints measured here, we knocked down Rad52 [103] in the CHO clones forming simple DSBs, and DSB clusters with incompatible DSB ends (CHO 2xS.R14 and CHO 4xS.R12). The results for total chromosomal translocations show a Rad52 dependent decrease in translocations (Figure 49). **Rad52 depletion decreases translocations, particularly in the cells harboring DSB clusters.** A similar observation was made in the XRC1-3 (DNA-PKcs mutant) clones, where after depletion of Rad52 a reduction in the numbers of translocations was seen (Figure 51). Interestingly, inhibition of Parp1 resulted here in an increase in the numbers of translocations. So the decrease seen after Rad52 depletion suggests error prone processing resulting in the formation of translocations after inhibition of alt-EJ that was in fact mediated by a Rad52 dependent error prone processing pathway. This intriguing observation requires further experimentation to characterize the underpinning mechanisms.

All these observations are in concordance with the suggested nature of Rad52 mediated SSA. Rad52 mediated SSA is extremely error prone, requires extensive resection and result in extensive deletions and chromosomal translocations [127, 128]. But, to confirm that the Rad52 dependent response that we are getting in our CHO based model system is indeed due to the involvement of SSA (or because of some other Rad52 dependent pathway) it will be important to sequence the repaired I-SceI sites to see whether the rejoined junctions have repeats or not. Also it will be interesting to see by using sequencing techniques how alt-EJ and Rad52 mediated (SSA) actually operate and how they contribute to the formation of chromosomal translocations.

9. It will also be interesting to investigate the possible role of CtIP independent resection pathways in the repair of DSB clusters. It is also striking that there was much greater reduction in the number of translocations after depletion of Rad52 (Figure 49) or inhibition of ATR (Figure 41) than after inhibition of CtIP alone (Figure 26). To find a possible explanation we inhibited Rad52 and Parp1 respectively in CtIP depleted CHO clones forming DSB clusters (CHO 2xS.R14 and CHO 4xS.R12) and found that after depletion of CtIP, when alt-EJ is inhibited no additional response is seen in the numbers of translocations in the presence of DSB clusters (Figure 48). In contrast Rad52 inhibition in combination with CtIP depletion results in a further decrease in the numbers of remaining translocations (Figure 50). Further experiments will test the involvement of CtIP independent processing mechanisms in this endpoint.

Summary

The results presented in this thesis reveal that with increasing DSB clustering and thus with increasing complexity of the DSB, there is increased engagement of DNA end processing pathways utilizing CtIP. However, as of yet uncharacterized CtIP-independent DSB processing pathways may also engage. DSB clustering and thus increased complexity of DSBs causes a larger dependence on "error-prone" DSB processing pathways such as alt-EJ and SSA. In this setting, it seems that the resection independent c-NHEJ and the resection dependent and error-free HRR play a less significant role in the repair of more complex DSB clusters.

Increased involvement of HRR in the repair of complex DSBs induced after exposure to high LET IR has been suggested in the literature but has not been confirmed in biological systems in which defined forms of complex DSBs have been generated; as it was carried out here. One apparent discrepancy with this framework of thinking is that since HRR is an error free repair pathway, its increased utilization would contradict the greater incidence of chromosomal aberrations forming after exposure to high LET IR. It is therefore possible that although HRR engages, it cannot complete processing and thus other resection mediated error prone pathways take over causing the translocation observed.

The biological system that has been used in this thesis is a unique tool that allows us to introduce clean DSBs and clusters of DSBs in a controlled manner. The plethora of clones that are available with these integrations give us a diverse range of DSB complexity ranging from simple DSBs to

DSB pairs and even DSB quadruplets in CHO wild type, and in mutants of DNA-PKcs, Ku80 and XRCC3. These clones allow the investigation as to which repair pathways engage as the complexity of the DSB increases, and how this causes the increased occurrence of chromosomal translocations. Key findings of these experiments are summarized below:

Inhibition of Parp1 dependent alt-EJ results in the expected decrease in the formation of translocations, with the decrease being more significant in clones with DSB clusters. This expected decrease is not observed in DNA-PKcs clones harboring incompatible DSB ends and instead a significant increase in translocations is observed. On the other hand, in DNA-PKcs clones harboring DSB clusters with compatible ends, a decrease in translocations is seen after inhibition of Parp1. These results suggest that end processing has an important role in the repair of complex DSB clusters and that this contributes significantly to the formation of translocations. The opposite trend of that seen in DNA-PKcs deficient "R" orientation clones suggests that another pathway besides alt-EJ underpins the formation of translocations – this was indeed confirmed after depletion of Rad52.

Ku80 mutation also abrogates c-NHEJ and shows a similar sensitization to killing as the DNA-PKcs mutant "R" orientation clone. But, strikingly Ku80 mutation resulted in a decrease in chromosomal aberration formation from DSB clusters. The effect that was observed in the xrs6 2xS.R11 clone could also be checked in the CHO 2x S.R14 clone and XRC1-3 2xS.R10 clone and the results suggest that while in the DNA-PKcs mutant no additional effect in translocation formation is observed, a decrease is observed in the CHO 2xS.R14 clone.

Furthermore cell survival, immunofluorescence and cytogenetics experiments in the CHO clones sustaining simple and complex DSBs suggest that with increasing DSB complexity there is decreased involvement of HRR. Surprisingly chemical inhibition of Rad51 decreased the numbers of translocations in the CHO 2xS.R14 clone, although knockdown generated an increase. Survival experiments conducted with the RAD51 inhibitor BO2 also showed a greater reduction with simple DSBs.

Lastly the results presented in this work also show that as compared to simple DSBs, DSB clusters show greater utilization of Rad52 for processing. Rad52 knockdown in clones harboring DSB clusters we see greater decrease than in clones harboring simple DSBs.

Outlook

For future work it would be interesting to utilize Next Generation Sequencing techniques to analyze the repair junctions in the cells having simple DSBs or DSB clusters; depleted for Rad52 (SSA) and Parp1 (alt-EJ), and comparing the two results. The comparison will give a clearer picture about the role of these two error prone pathways in the formation of translocations. Increased accretion of 53BP1 in the more complex DSB clusters with incompatible ends in comparison to the DSBs and DSB clusters having compatible ends should be explored also further. It would also be interesting to measure apoptosis from simple DSBs and DSB clusters after knocking down 53BP1. It would also be interesting to see the effect of other resection mediators like EXO1 and BLM2 in the formation of translocations. Ongoing works in our lab using Nano pore sequencing technology tries to establish the genomic locations of the integrated constructs. Also m-FISH is used to analyze translocation formation in greater detail.

An inducible I-SceI system to overcome limitations arising from the requirement of transfection for I-SceI protein expression did not prove feasible in these cells. Extension to human systems will also be a major advance.

So finally to summarize this work we can conclude by saying:

"The presence of DSB clusters impairs both HRR and c-NHEJ thereby resulting in initiation of error prone alt-EJ and Rad52 mediated like repair mechanisms".

Zusammenfassung

Die in dieser Dissertation vorgestellten Ergebnisse zeigen, dass mit zunehmender DSB-Clusterbildung und damit zunehmender Komplexität des DSBs die Nutzung von CtIP-abhängigen DNA-Prozessierungswegen verstärkt in Anspruch genommen wird. Allerdings können ebenso CtIP-unabhängige DSB-Reparaturwege, die bisher noch nicht charakterisiert wurden, eine Rolle spielen. DSB-Clustering und die damit erhöhte Komplexität von DSBs führt zu einer größeren Abhängigkeit von "fehleranfälligen" DSB-Reparaturwegen wie Alt-EJ und SSA. Vor diesem Hintergrund scheinen das resektionsunabhängige c-NHEJ und die resektionsabhängige und fehlerfreie HRR eine weniger wichtige Rolle bei der Reparatur komplexerer DSB-Cluster zu spielen.

Eine verstärkte Beteiligung der HRR an der Reparatur komplexer DSBs, die durch hoch-LET-IR induziert wurden, wurde in der Literatur zwar vorgeschlagen, jedoch noch nicht in biologischen Systemen, in denen definierte Formen komplexer DSBs erzeugt wurden, bestätigt; welche aber in dieser Dissertation genutzt wurden. Eine offensichtliche Diskrepanz in dieser Annahme besteht darin, dass HRR ein fehlerfreier Reparaturpfad ist und damit im Widerspruch zu dem vermehrten Auftreten von Chromosomenaberrationen steht, die sich nach Bestrahlung mit hoch-LET-IR bilden. Es ist daher möglich, dass die HRR, obwohl sie aktiv ist, die Verarbeitung nicht abschließen kann und daher andere, durch Resektion vermittelte fehleranfällige Pfade die beobachteten Translokationen verursachen.

Das biologische System, das in dieser Arbeit verwendet wurde, ist ein einzigartiges Werkzeug, mit dem wir „saubere“ DSBs und Cluster von DSBs auf kontrollierte Weise erzeugen können. Die Fülle an Klonen, die uns mit diesen Integrationen zur Verfügung stehen, gibt uns einen vielfältigen Bereich an DSB-Komplexität, der von einfachen DSBs über DSB-Paare bis hin zu DSB-Quadruplets im CHO-Wildtyp und in Mutanten (defizient in DNA-PKcs, Ku80 und XRCC3) reicht. Diese Klone ermöglichen die Untersuchung, welche Reparaturpfade mit zunehmender Komplexität des DSBs in Kraft treten und wie dies das vermehrte Auftreten von chromosomalen Translokationen verursacht. Die wichtigsten Ergebnisse dieser Experimente sind nachstehend zusammengefasst:

Die Hemmung von Parp1-abhängigem alt-EJ führt zu der erwarteten Abnahme der Translokationsbildung, wobei die Abnahme bei Klonen mit DSB-Clustern signifikanter ist. Diese erwartete Abnahme wird bei DNA-PKcs-Klonen mit inkompatiblen DSB-Enden nicht beobachtet, und stattdessen wird eine signifikante Zunahme der Translokationen beobachtet. Andererseits ist in DNA-PKcs-Klonen, die DSB-Cluster mit kompatiblen Enden enthalten, eine Abnahme der Translokationen nach Hemmung von Parp1 zu beobachten. Diese Ergebnisse legen nahe, dass die Endverarbeitung eine wichtige Rolle bei der Reparatur komplexer DSB-Cluster spielt und dass dies erheblich zur Bildung von Translokationen beiträgt. Der entgegengesetzte Trend bei dem DNA-PKcs-Klon mit fehlender "R"-Orientierung beobachteten Klon weist darauf hin, dass die Bildung von Translokationen auf einem anderen Weg als auf Alt-EJ beruht - dies wurde in der Tat nach Abreicherung von Rad52 bestätigt.

Die Ku80-Mutation inhibiert ebenfalls c-NHEJ und zeigt eine ähnliche Sensibilisierung für das Überleben wie der DNA-PKcs-Mutanten- "R" -Orientierungsklon. Bemerkenswerterweise führte die Ku80-Mutation jedoch zu einer Abnahme der Chromosomenaberrationsbildung aus DSB-Clustern. Der im xrs6 2xS.R11-Klon beobachtete Effekt konnte auch im CHO 2xS.R14-Klon und im XRC1-3 2xS.R10-Klon überprüft werden und die Ergebnisse legen nahe, dass, während in der DNA-PKcs-Mutante kein zusätzlicher Effekt auf die Translokationsbildung beobachtet wird, eine Abnahme derer im CHO 2 × S. R14-Klon beobachtet werden kann.

Überdies legen Experimente zum Überleben der Zellen, zur Immunfluoreszenz und zur Zytogenetik in den CHO-Klonen, die einfache und komplexe DSBs ausbilden, nahe, dass mit zunehmender DSB-Komplexität die Beteiligung der HRR abnimmt. Überraschenderweise verringerte die chemische Hemmung von Rad51 die Anzahl der Translokationen im CHO 2xS.R14-Klon, obwohl das genetische Herunterregulieren einen Anstieg bewirkte. Überlebensexperimente, die mit dem RAD51-Inhibitor BO2 durchgeführt wurden, zeigten auch eine stärkere Reduktion mit einfachen DSBs.

Schließlich zeigen die in dieser Arbeit vorgestellten Ergebnisse auch, dass DSB-Cluster im Vergleich zu einfachen DSBs eine stärkere Auslastung von Rad52 für die Verarbeitung aufweisen. Wir sehen eine stärkere Abnahme nach Rad52-Knockdown in Klonen, die DSB-Cluster beherbergen als in Klonen, die einfache DSBs beherbergen.

References:

1. https://www.nature.com/subjects/double-strand-dna-breaks. *https://www.nature.com/subjects/double-strand-dna-breaks*.
2. Jackson, S.P. and J. Bartek, *The DNA-damage response in human biology and disease.* Nature, 2009. **461**(7267): p. 1071.
3. Khan, F.A. and S.O. Ali, *Physiological Roles of DNA Double-Strand Breaks.* Journal of nucleic acids, 2017. **2017**: p. 6439169-6439169.
4. Chu, G., *Double-Strand Break Repair*. 2014. 1-15.
5. Hesslein, D.G. and D.G. Schatz, *Factors and forces controlling V (D) J recombination.* Advances in immunology, 2001. **78**: p. 169-232.
6. Tonegawa, S., *Somatic generation of antibody diversity.* Nature, 1983. **302**(5909): p. 575-81.
7. Stavnezer, J., J.E. Guikema, and C.E. Schrader, *Mechanism and regulation of class switch recombination.* Annu Rev Immunol, 2008. **26**: p. 261-92.
8. https://www.nature.com/subjects/class-switch-recombination. *https://www.nature.com/subjects/class-switch-recombination*.
9. Khan, F.A. and S.O. Ali, *Physiological Roles of DNA Double-Strand Breaks.* Journal of nucleic acids, 2017. **2017**: p. 20.
10. Held, K.D., *Radiobiology for the Radiologist, 6th ed., by Eric J. Hall and Amato J. Giaccia.* Radiation Research, 2006. **166**(5): p. 816-817.
11. Goel, D.M.W.a.D.A. *https://radiopaedia.org/articles/photoelectric-effect*.
12. Schipler, A. and G. Iliakis, *DNA double-strand-break complexity levels and their possible contributions to the probability for error-prone processing and repair pathway choice.* Nucleic Acids Res, 2013. **41**(16): p. 7589-605.
13. Mladenov, E. and G. Iliakis, *Induction and repair of DNA double strand breaks: the increasing spectrum of non-homologous end joining pathways.* Mutat Res, 2011. **711**(1-2): p. 61-72.
14. https://www.mun.ca/biology/scarr/Specific_Ionization_&_LET.html.
15. Lomax, M.E., L.K. Folkes, and P. O'Neill, *Biological consequences of radiation-induced DNA damage: relevance to radiotherapy.* Clin Oncol (R Coll Radiol), 2013. **25**(10): p. 578-85.
16. https://ce4rt.com/rad-tech-talk/explaining-linear-energy-transfer/.
17. Ward, J.F., *The Yield of DNA Double-strand Breaks Produced Intracellularly by Ionizing Radiation: A Review.* International Journal of Radiation Biology, 1990. **57**(6): p. 1141-1150.
18. Iliakis, G., T. Murmann, and A. Soni, *Alternative end-joining repair pathways are the ultimate backup for abrogated classical non-homologous end-joining and homologous recombination repair: Implications for the formation of chromosome translocations.* Mutat Res Genet Toxicol Environ Mutagen, 2015. **793**: p. 166-75.
19. Goodhead, D.T., *Initial Events in the Cellular Effects of Ionizing Radiations: Clustered Damage in DNA.* International Journal of Radiation Biology, 1994. **65**(1): p. 7-17.
20. O'Neill, P. and P. Wardman, *Radiation chemistry comes before radiation biology.* International Journal of Radiation Biology, 2009. **85**(1): p. 9-25.
21. Iliakis, G., et al., *Backup Pathways of Nonhomologous End Joining May Have a Dominant Role in the Formation of Chromosome Aberrations.* 2007: p. 67-85.
22. Sage, E. and N. Shikazono, *Radiation-induced clustered DNA lesions: Repair and mutagenesis.* Free Radical Biology and Medicine, 2017. **107**: p. 125-135.
23. Sage, E. and N. Shikazono, *Radiation-induced clustered DNA lesions: Repair and mutagenesis.* Free Radic Biol Med, 2017. **107**: p. 125-135.

References

24. Timm, S., et al., *Clustered DNA damage concentrated in particle trajectories causes persistent large-scale rearrangements in chromatin architecture.* Radiother Oncol, 2018. **129**(3): p. 600-610.
25. Mavragani, I.V., et al., *Ionizing Radiation and Complex DNA Damage: From Prediction to Detection Challenges and Biological Significance.* Cancers, 2019. **11**(11): p. 1789.
26. Mladenova, V., E. Mladenov, and G. Iliakis, *Novel Biological Approaches for Testing the Contributions of Single DSBs and DSB Clusters to the Biological Effects of High LET Radiation.* Frontiers in Oncology, 2016. **6**(163).
27. Ward, J.F., *Biochemistry of DNA Lesions.* Radiation Research, 1985. **104**(2s): p. S103-S111.
28. Rydberg, B., *Clusters of DNA Damage Induced by Ionizing Radiation: Formation of Short DNA Fragments. II. Experimental Detection.* Radiation Research, 1996. **145**(2): p. 200-209.
29. Hayes, D.P., *Non-problematic risks from low-dose radiation-induced DNA damage clusters.* Dose-response : a publication of International Hormesis Society, 2008. **6**(1): p. 30-52.
30. Hagiwara, Y., et al., *Clustered DNA double-strand break formation and the repair pathway following heavy-ion irradiation.* Journal of Radiation Research, 2019. **60**(1): p. 69-79.
31. Rydberg, B., *Radiation-induced DNA Damage and Chromatin Structure.* Acta Oncologica, 2001. **40**(6): p. 682-685.
32. Barendsen, G.W., *RBE—LET Relationships for Different Types of Lethal Radiation Damage in Mammalian Cells: Comparison with DNA Dsb and an Interpretation of Differences in Radiosensitivity.* International Journal of Radiation Biology, 1994. **66**(5): p. 433-436.
33. Mladenova, V., E. Mladenov, and G. Iliakis, *Novel Biological Approaches for Testing the Contributions of Single DSBs and DSB Clusters to the Biological Effects of High LET Radiation.* Frontiers in Oncology, 2016. **6**: p. 163-163.
34. Johnston, P.J. and P.E. Bryant, *A Component of DNA Double-strand Break Repair Is Dependent on the Spatial Orientation of the Lesions within the Higher-order Structures of Chromatin.* International Journal of Radiation Biology, 1994. **66**(5): p. 531-536.
35. Bryant, P.E. and P.J. Johnston, *Restriction-endonuclease-induced DNA double-strand breaks and chromosomal aberrations in mammalian cells.* Mutat Res, 1993. **299**(3-4): p. 289-96.
36. Johnston, P.J., P.L. Olive, and P.E. Bryant, *Higher-order chromatin structure-dependent repair of DNA double-strand breaks: modeling the elution of DNA from nucleoids.* Radiat Res, 1997. **148**(6): p. 561-7.
37. Bryant, P. and P. J. Johnston, *Restriction-endonuclease-induced DNA double-strand breaks and chromosomal aberrations in mammalian cells.* 1993. **299**: p. 289-96.
38. Gruen, M., et al., *An In Vivo Selection System for Homing Endonuclease Activity.* 2002. **30**: p. e29.
39. Belfort, M. and R.J. Roberts, *Homing endonucleases: keeping the house in order.* Nucleic Acids Res, 1997. **25**(17): p. 3379-88.
40. Jasin, M., *Genetic manipulation of genomes with rare-cutting endonucleases.* Trends Genet, 1996. **12**(6): p. 224-8.
41. Chevalier, B.S. and B.L. Stoddard, *Homing endonucleases: structural and functional insight into the catalysts of intron/intein mobility.* Nucleic Acids Res, 2001. **29**(18): p. 3757-74.
42. Honma, M., et al., *Non-homologous end-joining for repairing I-SceI-induced DNA double strand breaks in human cells.* DNA Repair (Amst), 2007. **6**(6): p. 781-8.
43. https://www.rcsb.org/structure/1R7M.
44. Bindra, R.S., et al., *Development of an assay to measure mutagenic non-homologous end-joining repair activity in mammalian cells.* Nucleic Acids Res, 2013. **41**(11): p. e115.
45. *DNA Damage and Repair. Volume 3: Advances from Phage to Humans. Contemporary Cancer Research. Edited by Jac A Nickoloff and Merl F Hoekstra.* The Quarterly Review of Biology, 2002. **77**(2): p. 244-244.

References

46. Laramore, G.E., et al., *Relative Biological Effectiveness (RBE)*, in *Encyclopedia of Radiation Oncology*, L.W. Brady and T.E. Yaeger, Editors. 2013, Springer Berlin Heidelberg: Berlin, Heidelberg. p. 748-748.
47. Schipler, A., *Homing endonuclease-based model systems for the study of DNA double strand break induced cell signaling and repair*, in *Fakultät für Biologie*. 2013, University of Duisburg-Essen: Essen.
48. Hada, M. and B.M. Sutherland, *Spectrum of complex DNA damages depends on the incident radiation.* Radiat Res, 2006. **165**(2): p. 223-30.
49. Gulston, M., et al., *Processing of clustered DNA damage generates additional double-strand breaks in mammalian cells post-irradiation.* Nucleic Acids Res, 2004. **32**(4): p. 1602-9.
50. Boboila, C., F.W. Alt, and B. Schwer, *Classical and alternative end-joining pathways for repair of lymphocyte-specific and general DNA double-strand breaks.* Adv Immunol, 2012. **116**: p. 1-49.
51. Stephens, P.J., et al., *Massive genomic rearrangement acquired in a single catastrophic event during cancer development.* Cell, 2011. **144**(1): p. 27-40.
52. Holley, W.R. and A. Chatterjee, *Clusters of DNA Damage Induced by Ionizing Radiation: Formation of Short DNA Fragments. I. Theoretical Modeling.* Radiation Research, 1996. **145**(2): p. 188-199.
53. Zhou, B.B. and S.J. Elledge, *The DNA damage response: putting checkpoints in perspective.* Nature, 2000. **408**(6811): p. 433-9.
54. Khanna, K.K. and S.P. Jackson, *DNA double-strand breaks: signaling, repair and the cancer connection.* Nature Genetics, 2001. **27**(3): p. 247-254.
55. Sulli, G., R. Di Micco, and F. d'Adda di Fagagna, *Crosstalk between chromatin state and DNA damage response in cellular senescence and cancer.* Nat Rev Cancer, 2012. **12**(10): p. 709-20.
56. d'Adda di Fagagna, F., *Living on a break: cellular senescence as a DNA-damage response.* Nat Rev Cancer, 2008. **8**(7): p. 512-22.
57. Rogakou, E.P., et al., *DNA double-stranded breaks induce histone H2AX phosphorylation on serine 139.* J Biol Chem, 1998. **273**(10): p. 5858-68.
58. Podhorecka, M., A. Skladanowski, and P. Bozko, *H2AX Phosphorylation: Its Role in DNA Damage Response and Cancer Therapy.* J Nucleic Acids, 2010. **2010**.
59. Bonner, W.M., et al., *GammaH2AX and cancer.* Nature reviews. Cancer, 2008. **8**(12): p. 957-967.
60. Kinner, A., et al., *Gamma-H2AX in recognition and signaling of DNA double-strand breaks in the context of chromatin.* Nucleic Acids Res, 2008. **36**(17): p. 5678-94.
61. Shibata, A. and P.A. Jeggo, *DNA double-strand break repair in a cellular context.* Clin Oncol, 2014. **26**(5): p. 243-9.
62. Rodier, F., J. Campisi, and D. Bhaumik, *Two faces of p53: aging and tumor suppression.* Nucleic acids research, 2007. **35**(22): p. 7475-7484.
63. Campisi, J. and F. d'Adda di Fagagna, *Cellular senescence: when bad things happen to good cells.* Nat Rev Mol Cell Biol, 2007. **8**(9): p. 729-40.
64. van Attikum, H. and S.M. Gasser, *Crosstalk between histone modifications during the DNA damage response.* Trends Cell Biol, 2009. **19**(5): p. 207-17.
65. Shiloh, Y., *ATM and related protein kinases: safeguarding genome integrity.* Nat Rev Cancer, 2003. **3**(3): p. 155-68.
66. Deckbar, D., P.A. Jeggo, and M. Lobrich, *Understanding the limitations of radiation-induced cell cycle checkpoints.* Crit Rev Biochem Mol Biol, 2011. **46**(4): p. 271-83.
67. Murmann-Konda, T.T.Y., *The contribution of DNA DSB repair pathways to the repair of chromosome breaks throughout the cell cycle.* 2017, Medizinische Fakultät, Universitätsklinikum Essen, Institut für Medizinische Strahlenbiologie.
68. Iliakis, G., et al., *DNA damage checkpoint control in cells exposed to ionizing radiation.* Oncogene, 2003. **22**(37): p. 5834-47.

References

69. Shaltiel, I.A., et al., *The same, only different - DNA damage checkpoints and their reversal throughout the cell cycle.* J Cell Sci, 2015. **128**(4): p. 607-20.
70. Sancar, A., et al., *Molecular mechanisms of mammalian DNA repair and the DNA damage checkpoints.* Annu Rev Biochem, 2004. **73**: p. 39-85.
71. Lobrich, M. and P.A. Jeggo, *The impact of a negligent G2/M checkpoint on genomic instability and cancer induction.* Nat Rev Cancer, 2007. **7**(11): p. 861-9.
72. Murakami, H. and S. Keeney, *Regulating the formation of DNA double-strand breaks in meiosis.* Genes & development, 2008. **22**(3): p. 286-292.
73. DiBiase, S.J., et al., *DNA-dependent Protein Kinase Stimulates an Independently Active, Nonhomologous, End-Joining Apparatus.* Cancer Research, 2000. **60**(5): p. 1245-1253.
74. Fell, V.L. and C. Schild-Poulter, *The Ku heterodimer: function in DNA repair and beyond.* Mutat Res Rev Mutat Res, 2015. **763**: p. 15-29.
75. Britton, S., J. Coates, and S.P. Jackson, *A new method for high-resolution imaging of Ku foci to decipher mechanisms of DNA double-strand break repair.* J Cell Biol, 2013. **202**(3): p. 579-95.
76. Hammel, M., et al., *Ku and DNA-dependent protein kinase dynamic conformations and assembly regulate DNA binding and the initial non-homologous end joining complex.* J Biol Chem, 2010. **285**(2): p. 1414-23.
77. Jiang, W., et al., *Differential phosphorylation of DNA-PKcs regulates the interplay between end-processing and end-ligation during nonhomologous end-joining.* Molecular cell, 2015. **58**(1): p. 172-185.
78. Lieber, M.R., *The mechanism of double-strand DNA break repair by the nonhomologous DNA end-joining pathway.* Annu Rev Biochem, 2010. **79**: p. 181-211.
79. Iliakis, G., E. Mladenov, and V. Mladenova, *Necessities in the Processing of DNA Double Strand Breaks and Their Effects on Genomic Instability and Cancer.* Cancers (Basel), 2019. **11**(11).
80. Liu, T. and J. Huang, *DNA End Resection: Facts and Mechanisms.* Genomics, proteomics & bioinformatics, 2016. **14**(3): p. 126-130.
81. Sartori, A.A., et al., *Human CtIP promotes DNA end resection.* Nature, 2007. **450**(7169): p. 509-14.
82. Takata, M., et al., *Homologous recombination and non-homologous end-joining pathways of DNA double-strand break repair have overlapping roles in the maintenance of chromosomal integrity in vertebrate cells.* The EMBO journal, 1998. **17**(18): p. 5497-5508.
83. Paull, T.T. and R.A. Deshpande, *The Mre11/Rad50/Nbs1 complex: recent insights into catalytic activities and ATP-driven conformational changes.* Experimental cell research, 2014. **329**(1): p. 139-147.
84. Grindley, N.D.F., *Resolvase*, in *Encyclopedia of Genetics*, S. Brenner and J.H. Miller, Editors. 2001, Academic Press: New York. p. 1687-1688.
85. Mazin, A.V., et al., *Rad54, the motor of homologous recombination.* DNA repair, 2010. **9**(3): p. 286-302.
86. Heyer, W.-D., K.T. Ehmsen, and J. Liu, *Regulation of homologous recombination in eukaryotes.* Annual review of genetics, 2010. **44**: p. 113-139.
87. San Filippo, J., P. Sung, and H. Klein, *Mechanism of Eukaryotic Homologous Recombination.* Annual Review of Biochemistry, 2008. **77**(1): p. 229-257.
88. Wang, H., et al., *DNA ligase III as a candidate component of backup pathways of nonhomologous end joining.* Cancer Res, 2005. **65**(10): p. 4020-30.
89. Zhang, Y. and M. Jasin, *An essential role for CtIP in chromosomal translocation formation through an alternative end-joining pathway.* Nature Structural &Amp; Molecular Biology, 2010. **18**: p. 80.
90. Chan, S.H., A.M. Yu, and M. McVey, *Dual roles for DNA polymerase theta in alternative end-joining repair of double-strand breaks in Drosophila.* PLoS Genet, 2010. **6**(7): p. e1001005.

References

91. Kent, T., et al., *Mechanism of microhomology-mediated end-joining promoted by human DNA polymerase theta.* Nat Struct Mol Biol, 2015. **22**(3): p. 230-7.
92. Howard, S.M., D.A. Yanez, and J.M. Stark, *DNA Damage Response Factors from Diverse Pathways, Including DNA Crosslink Repair, Mediate Alternative End Joining.* PLOS Genetics, 2015. **11**(1): p. e1004943.
93. Bhargava, R., D.O. Onyango, and J.M. Stark, *Regulation of Single-Strand Annealing and its Role in Genome Maintenance.* Trends in genetics : TIG, 2016. **32**(9): p. 566-575.
94. Mladenov, E., et al., *DNA double-strand-break repair in higher eukaryotes and its role in genomic instability and cancer: Cell cycle and proliferation-dependent regulation.* Semin Cancer Biol, 2016. **37-38**: p. 51-64.
95. Bhargava, R., D.O. Onyango, and J.M. Stark, *Regulation of Single-Strand Annealing and its Role in Genome Maintenance.* Trends Genet, 2016. **32**(9): p. 566-575.
96. Mansour, W.Y., et al., *Hierarchy of nonhomologous end-joining, single-strand annealing and gene conversion at site-directed DNA double-strand breaks.* Nucleic acids research, 2008. **36**(12): p. 4088-4098.
97. Wu, W., et al., *Repair of radiation induced DNA double strand breaks by backup NHEJ is enhanced in G2.* DNA Repair (Amst), 2008. **7**(2): p. 329-38.
98. Wang, M., et al., *PARP-1 and Ku compete for repair of DNA double strand breaks by distinct NHEJ pathways.* Nucleic acids research, 2006. **34**(21): p. 6170-6182.
99. Ceccaldi, R., B. Rondinelli, and A.D. D'Andrea, *Repair Pathway Choices and Consequences at the Double-Strand Break.* Trends Cell Biol, 2016. **26**(1): p. 52-64.
100. Averbeck, N.B., et al., *DNA end resection is needed for the repair of complex lesions in G1-phase human cells.* Cell Cycle, 2014. **13**(16): p. 2509-16.
101. Biehs, R., et al., *DNA Double-Strand Break Resection Occurs during Non-homologous End Joining in G1 but Is Distinct from Resection during Homologous Recombination.* Mol Cell, 2017. **65**(4): p. 671-684 e5.
102. Shibata, A., et al., *Factors determining DNA double-strand break repair pathway choice in G2 phase.* EMBO J, 2011. **30**(6): p. 1079-92.
103. Kostyrko, K., et al., *A role for homologous recombination proteins in cell cycle regulation.* Cell Cycle, 2015. **14**(17): p. 2853-61.
104. Schipler, A., et al., *Chromosome thripsis by DNA double strand break clusters causes enhanced cell lethality, chromosomal translocations and 53BP1-recruitment.* Nucleic acids research, 2016. **44**: p. gkw487.
105. Iliakis, G., et al., *DEFINED BIOLOGICAL MODELS OF HIGH-LET RADIATION LESIONS.* Radiat Prot Dosimetry, 2019. **183**(1-2): p. 60-68.
106. Iliakis, G., et al., *Mechanisms of DNA double strand break repair and chromosome aberration formation.* Cytogenet Genome Res, 2004. **104**(1-4): p. 14-20.
107. Hromas, R., et al., *PREVENTING THE CHROMOSOMAL TRANSLOCATIONS THAT CAUSE CANCER.* Trans Am Clin Climatol Assoc, 2016. **127**: p. 176-195.
108. Bennardo, N., et al., *Alternative-NHEJ Is a Mechanistically Distinct Pathway of Mammalian Chromosome Break Repair.* PLOS Genetics, 2008. **4**(6): p. e1000110.
109. Makharashvili, N. and T.T. Paull, *CtIP: A DNA damage response protein at the intersection of DNA metabolism.* DNA Repair (Amst), 2015. **32**: p. 75-81.
110. Okayasu, R., *Repair of DNA damage induced by accelerated heavy ions—A mini review.* International Journal of Cancer, 2012. **130**(5): p. 991-1000.
111. Hagiwara, Y., et al., *Clustered DNA double-strand break formation and the repair pathway following heavy-ion irradiation.* Journal of Radiation Research, 2018. **60**(1): p. 69-79.

112. Ferguson, D.O., et al., *The nonhomologous end-joining pathway of DNA repair is required for genomic stability and the suppression of translocations.* Proceedings of the National Academy of Sciences, 2000. **97**(12): p. 6630-6633.
113. Krajewska, M., et al., *ATR inhibition preferentially targets homologous recombination-deficient tumor cells.* Oncogene, 2014. **34**: p. 3474.
114. Jackson, S.P., *The DNA-damage response: new molecular insights and new approaches to cancer therapy.* Biochemical Society transactions, 2009. **37**(Pt 3): p. 483-494.
115. Krajewska, M., et al., *ATR inhibition preferentially targets homologous recombination-deficient tumor cells.* Oncogene, 2015. **34**(26): p. 3474-81.
116. Ritter, S. and M. Durante, *Heavy-ion induced chromosomal aberrations: a review.* Mutat Res, 2010. **701**(1): p. 38-46.
117. Durante, M. and S.C. Formenti, *Radiation-Induced Chromosomal Aberrations and Immunotherapy: Micronuclei, Cytosolic DNA, and Interferon-Production Pathway.* Frontiers in Oncology, 2018. **8**(192).
118. George, K., et al., *Chromosome Aberrations in the Blood Lymphocytes of Astronauts after Space Flight.* Radiation research, 2002. **156**: p. 731-8.
119. Savage, J.R.K., *A brief survey of aberration origin theories.* Mutation Research/Fundamental and Molecular Mechanisms of Mutagenesis, 1998. **404**(1): p. 139-147.
120. Loucas, B.D., et al., *Chromosome damage in human cells by gamma rays, alpha particles and heavy ions: track interactions in basic dose-response relationships.* Radiat Res, 2013. **179**(1): p. 9-20.
121. Yu, X., et al., *The Ku-dependent non-homologous end-joining pathway contributes to low-dose radiation-stimulated cell survival.* J Cell Physiol, 2011. **226**(2): p. 369-74.
122. Okayasu, R., et al., *Repair of DNA Damage Induced by Accelerated Heavy Ions in Mammalian Cells Proficient and Deficient in the Non-homologous End-Joining Pathway.* Radiation Research, 2006. **165**(1): p. 59-67.
123. Wang, H., et al., *The Ku-dependent non-homologous end-joining but not other repair pathway is inhibited by high linear energy transfer ionizing radiation.* DNA Repair (Amst), 2008. **7**(5): p. 725-33.
124. Moore, S., F.K. Stanley, and A.A. Goodarzi, *The repair of environmentally relevant DNA double strand breaks caused by high linear energy transfer irradiation--no simple task.* DNA Repair (Amst), 2014. **17**: p. 64-73.
125. Yajima, H., et al., *The complexity of DNA double strand breaks is a critical factor enhancing end-resection.* DNA Repair (Amst), 2013. **12**(11): p. 936-46.
126. Lee, R., et al., *Chromosome aberration measurements in mitotic and G2-PCC lymphocytes at the standard sampling time of 48 h underestimate the effectiveness of high-LET particles.* Radiat Environ Biophys, 2011. **50**(3): p. 371-81.
127. Pannunzio, N.R., G.M. Manthey, and A.M. Bailis, *RAD59 and RAD1 cooperate in translocation formation by single-strand annealing in Saccharomyces cerevisiae.* Current Genetics, 2010. **56**(1): p. 87-100.
128. Pannunzio, N.R., G.M. Manthey, and A.M. Bailis, *RAD59 is required for efficient repair of simultaneous double-strand breaks resulting in translocations in Saccharomyces cerevisiae.* DNA Repair (Amst), 2008. **7**(5): p. 788-800.

References

Acknowledgement

First and foremost, I would like to express my gratitude to my supervisor, Prof. Dr. George Iliakis, for giving me the opportunity to pursue my doctoral studies under his supervision at Institute of Medical Radiation Biology, Essen. As a professor and a teacher he was always there and I could always count on him for his support. It has been a long journey with times when the going got tough but, his reassuring kind words and most importantly his generous support always made it easier.

My project was funded from BMBF [02NUK043B-COLLAR] and DFG [GRK1739]]. I am extremely grateful for their support that helped me to carry out my research.

I am extremely grateful to Dr. Emil Mladenov who was always patient with me in being my mentor during my PhD and taught me the techniques like transfection by nucleofaction, trained me in using Imaris software and Adobe illustrator, and most importantly the skills of organizing and presenting data.

A great support comes when your senior guides you as a friend and helps you out in every thick and thin. I am extremely thankful to Dr. Veronika Mladenova for she was always there especially when I needed her guidance the most.

I was extremely fortunate to find a great teacher in Dr. Aashish Soni. I started my training under him and I am thankful to him for he trained me in cytogenetic techniques, clonogenic survival assay, and most importantly he helped me to develop scientific way of thinking.

I was fortunate enough that under both my guides Dr. Emil Mladenov and Dr. Aashish Soni I was able to contribute and be a part of their published papers.

Dr. Lisa Marie Krieger special thanks goes to her for always helping me out with essentially every kind of problems. I would like to thank her specially for being a friend, for teaching me Immunofluorescence technique and later on with all the administrative help she essentially made my PhD journey a lot easier.

My heartfelt gratitude also goes to Tamara Mußfeldt, Malihe Mesbah and Christian Moellers, without their help in the lab it would have become extremely difficult to conduct experiments so smoothly.

Some people enter your life as strangers and along the journey become your best friends. I was fortunate enough to find best friends while doing my PhD, I would like to thank Sharif “Janko”

Acknowledgement

Mortoga Hassan, Vasiliki Tasiou, and Pelin Kucuk for being part of my happiness away from home. Their friendship is special! I would also like to sincerely thank Dr. Prabodha Meher, Christina Vasilieou, Dr. Mohd. Yasser and Gerasimos Pollakis for making every day happier. I would also like to thank Martha Garbos, Dr Tamara Murmann-Konda and Dr Rositsa Dueva for helping me out especially at the beginning of my PhD.

At the end I would like to thank my family and my all my loved ones for always being there. My parents always ensured that all my dreams come true. It is because of them that I never stopped "believing". Thank you Mom Dad for always being the best "Mom and Dad". My elder brother is my biggest strength and I would like to thank him for always being my biggest support system. I am extremely thankful to my sister in law for always being understanding of me and supporting me. Last but, not least I would like to thank my baby niece Vaidehi for coming into my life when smile was something I was missing the most. I would like to dedicate my work to my grandparents it is because of their blessings I am able to experience everything beautiful in my life.

Thank you all and I sign off for now! Until next time……Gratitude never ends…. It grows!

Curriculum Vitae

The Curriculum Vitae is not available in the online version due to data legal reasons.

Curriculum vitae

Declarations

Erklärung:

Hiermit erkläre ich, gem. §7 Abs. (2) d) + f) der Promotionsordnung der FaKultät für Biologie zur Erlangung des Dr. rer. nat., dass ich die vorliegende Dissertation selbstständig verfasst und mich keiner anderen als der angegebenen Hilfsmittel bedient, bei der Abfassung der Dissertation nur die angegebenen Hilfsmittel benutzt und alle wörtlich oder inhaltlich übernommenen Stellen als solche gekennzeichnet habe.

Jaipur, 10/01/2020 _____

Unterschrift der Doktorandin

Erklärung:

Hiermit erkläre ich, gem. § 7 Abs. (2) e) + g) der Promotionsordnung der FaKultät für Biologie zur Erlangung des Dr. rer. nat., dass ich keine anderen Promotionen bzw. Promotionsversuche in der Vergangenheit durchgeführt habe und dass diese Arbeit von keiner anderen FaKultät/Fachbereich abgelehnt worden ist.

Jaipur, 10/01/2020 _____

Unterschrift der Doktorandin

Erklärung:

Hiermit erkläre ich, gem. § 6 Abs. (2) g) der Promotionsordnung der FaKultät für Biologie zur Erlangung des Dr. rer. nat., dass ich das Arbeitsgebiet, dem das Thema „"DSB clusters impair the efficiency of both homologous recombination and c-NHEJ and initiate Rad52 dependent error prone processing" zuzuordnen ist, in Forschung und Lehre vertrete und den Antrag von Shipra Chaudhary befürworte und die Betreuung auch im Falle eines Weggangs, wenn nicht wichtige Gründe dem entgegenstehen, weiterführen werde.

Essen, / / _____

Unterschrift eines Mitgliedes der Universität Duisburg-Essen

Declarations